Weight function approach to studying perfect and imperfect interfaces in anisotropic and piezoelectric bimaterials

Author:

Lewis Pryce

Supervisor:

Prof. Gennady Mishuris

Thesis submitted in candidature for the degree of
Philosophiae Doctor

October 2015

DECLARATION

This work has not previously been accepted in substance for any degree and is not being concurrently submitted in candidature for any degree.

Signed ..... (candidate)

Date .....

STATEMENT 1

This thesis is the result of my own investigations, except where otherwise stated. Other sources are acknowledged by footnotes giving explicit references. A bibliography is appended.

Signed ..... (candidate)

Date .....

STATEMENT 2

I hereby give consent for my thesis, if accepted, to be available for photocopying and for inter-library loan, and for the title and summary to be made available to outside organisations.

Signed ..... (candidate)

Date .....

Acknowledgements

To begin with I would like to thank my supervisor, Professor Gennady Mishuris. The support he has given me over the past few years has been greatly appreciated and his enthusiasm for mathematics and development of young researchers is truly inspirational. I will always consider it an honour to have been given the opportunity to work with such an incredible mathematician.

Much appreciation is also given to my second supervisor, Professor Simon Cox, whose advice and support has also been of great use during my time in postgraduate study. Moreover, I would like to thank Dr. Lorenzo Morini, from Trento University, who is a co-author for the work presented in Chapters 3 and 5 of the thesis. My most sincere gratitude is also given to Dr. Adam Vellender and Dr. Alexander Zagnetko who are both co-authors on the content included in Chapter 4.

I have enjoyed every minute of my time in Aberystwyth since 2008, as both an undergraduate and postgraduate. Needless to say I would like to express my deepest thanks to all members of staff in the Department of Mathematics who have given their time to help me over the years. In particular, I would like to thank all members of the Mathematical Modelling of Structures, Solids and Fluids research group who have made my PhD years at the department such an amazing experience.

Many thanks go to all of my officemates over the past three years: Adam Vellender, Jennifer Wheatley, Piotr Kusmierczyk and Monika Perkowska. Their friendship has been a pillar of support and my time here would have been much less enjoyable without the many hours spent with all of them. I

extend this thanks to fellow PhD students Morgan Jones, Daria Andreeva and Daniel Peck who have also provided me with some unforgettable memories during my time in Aberystwyth. I must also mention Liam Davies-Jones and Jeremy Lloyd whose invaluable friendship has been of great comfort for many years.

Last but definitely not least, I must thank my family who have always believed in me and have given me much needed encouragement over the years. This thesis would never have been finished without the support given to me by Mum, Dad, Bethan, Sian, Owen and Dave. Finally, I must pay tribute to my late Grandmother, Sybil Pryce, who passed away in October 2013. She supported me in everything I did and is sorely missed but will always be an inspiration.

Abstract

The focus of the thesis is interfacial crack problems in anisotropic and piezoelectric bimaterials. We seek to solve a variety of problems using weight function techniques and singular integral equations.

We begin by studying a dynamic crack along a perfectly bonded interface in an anisotropic bimaterial. Using a weight function derived from a mirrored problem it is possible to derive important material parameters which govern the crack propagation. Following this a static crack is considered. However, in this case the materials are not bonded perfectly, an imperfect interface is present instead. A method is derived where singular integral equations for the imperfect interface problem are derived through use of perfect interface weight functions. The weight functions are then extended to fracture in piezoelectric bimaterials which allows equivalent integral equations to be derived relating the mechanical and electrical fields. In past literature a number of results have been found which can only be used when considering a symmetric load system on the crack faces. All of the problems considered here have asymmetric loading.

Firstly, a steady-state formulation is used to derive asymptotic coefficients of the crack displacement and interfacial tractions for a dynamic crack along a perfect interface. The method can be used to find many asymptotic coefficients but the one of most importance here is the stress intensity factor which therefore enables the calculation of energy release rate at the crack tip. As an example an orthotropic bimaterial with two different loading configurations is used to examine the importance of crack speed and load asymmetry on the properties of the crack propagation.

We proceed to study imperfect interface conditions for an anisotropic bimaterial. Usually when looking at such a problem it is necessary to derive new weight functions which correspond to the imperfect interface. An innovative method which makes use of the Betti formula and existing weight functions for the analogous perfect interface problem is derived. This procedure is used to obtain singular integral equations which relate the crack loading, which is assumed to be known, to the displacement jump over both the crack and interface and tractions along the bonded area between the materials. Examples of the results obtained through solving the integral equations numerically are given.

Finally, we extend the weight functions used previously in the thesis to a piezoelectric setting. The general form of the weight function for any piezoelectric bimaterial is given before two specific examples are studied in depth. The examples are chosen in such a way to illustrate the effect that the poling direction of the bimaterial can have on both the mechanical and electrical fields. For both examples explicit expressions are derived for the weight functions which are then used to derive singular integral equations which can be used to study the effect of both mechanical loading and electrical charges being applied to the crack faces. To finish we present some examples for both poling directions to illustrate the use of the derived equations.

Contents

Chapter 1

Introduction and literature review

The work presented in this thesis consists of a number of problems concerning crack propagation along interfaces in bimaterials with complex properties. When considering such problems both the mechanical properties of the bimaterial and the nature of the interface separating them must be taken into account. The problems we analyse in the thesis concern both anisotropic and piezoelectric bimaterials and also consider perfect and imperfect transmission conditions along the bonded section between the materials. The work seen in Chapters 3, 4 and 5 can be found in Pryce et al. (2013, 2014, 2015) respectively.

Throughout the thesis we make use of weight functions, defined as singular, non-trivial solutions of homogeneous traction-free crack problems which are used in the derivation of important parameters in fracture mechanics. Weight functions are an efficient tool for studying the behaviour of certain physical fields in the region of the crack tip.

This chapter presents a historical review of some of the previous work in fracture mechanics which will be used in the analysis presented in the remainder of the thesis. Specific attention will be given to advances in the field of stress intensity factors, weight functions and imperfect interfaces. We then proceed to give a deeper study of anisotropic materials and results concerning interfacial fracture for these materials. Finally, piezoelectric materials will be reviewed and the extension of existing concepts for anisotropic materials to piezoelectric materials will be discussed. To conclude this chapter of the thesis we will discuss the room for further development in the field and give an outline of the remaining chapters.

1.1 Literature review

Early studies of elasticity saw the development of Hooke's law in the late 17th century. However, it was not until the early 1900s that study in fracture mechanics began to truly flourish. The first major developments were seen in Inglis (1913) where an elliptical hole in glass was considered. It was found that applying a perpendicular, tensile load to the ellipse resulted in the vertices being subjected to the highest level of mechanical stress. Following the work of Inglis (1913), Griffith (1920) replaced the ellipse with a crack due to contrasting results between theoretical work and experimental results. Griffith discovered that the potential energy of the system, Ω, was dependent on the crack length. If the crack was extended there would be an increase in crack surface area and, at a microscopic level, a certain amount of work per unit area was expended in the creation of that additional area. This work per unit area was given the name surface energy, denoted Ω_s. Using

the equilibrium principle of minimum potential energy gave

$$\frac{\partial}{\partial l}(\Omega + \Omega_s) = 0, \tag{1.1}$$

where l is the crack length. Griffith stated that a crack was at a *critical state of incipient growth* if the microscopic increase of the work per unit area was the same as the decrease in overall potential energy when the crack was extended and new surface area formed.

It was in 1948 that Mott attempted to extend the work of Griffith to a moving crack. Mott (1948) adopted a steady-state approach to a crack moving at a constant speed, where the system was independent of time if the observer was moving at the same speed as the crack. Finding an approximation for the total kinetic energy T_{tot}, as a function of the crack length and velocity, Mott also applied the equilibrium principle of minimum potential energy to give:

$$\frac{\partial}{\partial l}(\Omega + \Omega_s + T_{tot}) = 0. \tag{1.2}$$

It was believed that this formula could be used to find the velocity at which the Griffith crack would propagate through a material. However, the assumption of Mott that the derivative of the combined total energy of the system (with respect to the length of the fracture) vanishes was not correct. Therefore, the conclusions drawn from this work are widely seen as being invalid. In spite of this the work performed in Mott (1948) was still of great importance to the field.

The next step of major importance in the study of fracture mechanics was that of Irwin (1957). It was here that Irwin introduced the stress intensity factor, K, commonly shortened to SIF. The stress intensity factor is a key parameter in studying the behaviour of physical fields in the vicinity

of the crack tip. K depends on a number of features of the geometry being considered, including material parameters, crack properties and the applied loading on the crack faces. Irwin also introduced the notion of crack opening modes: Modes I, II and III. Mode I fracture opening is that which is perpendicular to the crack faces and parallel to the crack front. Mode II refers to the shear opening of the crack perpendicular to the crack front and parallel to the crack face. Finally, Mode III opening is parallel to both the crack front and the crack surface. The three types of crack opening are illustrated in Figure 1.1. When considering two-dimensional geometries it is often said that the Mode I and II openings are the in-plane fields whereas Mode III describes the out-of-plane (or antiplane) fields.

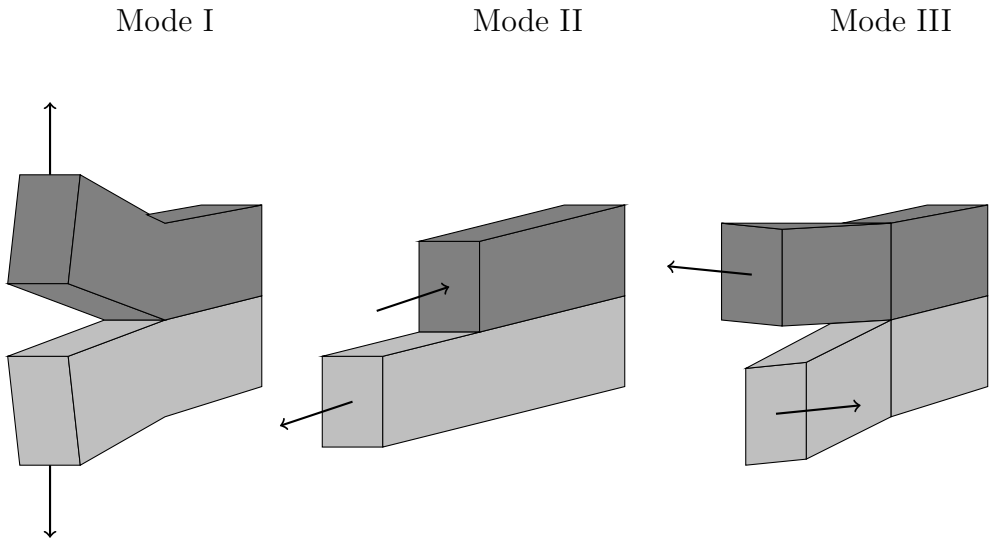

Figure 1.1: Crack opening modes

In his analysis, Irwin considered the energy release rate at the crack tip, which is often thought as the energy released from the crack tip when the fracture propagates and more surface area is created. For a Mode I crack a

relationship relating the energy release rate to the Young's modulus, E, and stress intensity factor for the material was found

$$G = \frac{K^2}{E}. \tag{1.3}$$

Irwin (1957) also discovered a critical value of the stress intensity factor at which the fracture will begin to propagate, often referred to as fracture toughness. As a direct result of this and equation (1.3), and considering conservation of energy, it is possible to find a minimum energy required for a crack to propagate.

The next major breakthrough in the analysis of energy release rates came courtesy of Cherepanov (1967) and Rice (1968) in the form of the J-integral. The J-integral is defined as a path-independent contour integral around the crack tip which can be used to find the energy released through the crack tip during crack propagation. It was shown that the energy release rate obtained by using the J-integral is the same as that found using the equation derived by Irwin (1957) for a quasistatic crack in a brittle material.

Another area of great interest is when you have a crack lying along an interface between two bonded materials. The case of a crack between dissimilar isotropic media was considered by Williams (1959). It was found that the Mode III stress fields had a square-root singularity at the crack tip, whereas the in-plane fields had a similar square-root behaviour with an additional oscillatory effect. Work on fracture was extended to a homogeneous anisotropic body by Stroh (1958) and Hoenig (1982). Hoenig found that the square-root behaviour of the physical fields at the crack tip was also present for the crack in an anisotropic material. It was also found that the angular variation of the fields surrounding the crack tip was more complex due to the

anisotropy of the material.

Work on a crack propagating along an interface in an anisotropic bi-material was not as clear as that for the corresponding isotropic problem, with some problems arising in finding the properties of the stresses and displacements in the vicinity of the crack tip. Willis (1971) defined a stress concentration vector, containing three complex numbers, for use in the evaluation of the near-tip stresses. However, these results led to complications in the derivation of the stress intensity factors and therefore progression in the manner of Irwin (1957) was not possible.

A number of advancements in the field were found in the work of Qu and Bassani (1989) where they derived conditions for the near-tip fields to be non-oscillatory. It was found in this case that the fields corresponding to the three Modes of crack opening could be separated and that the stress intensity factors took only real values. The work was studied further for a Griffith crack by Bassani and Qu (1989). Following this work by Qu and Bassani, significant breakthroughs were made by Suo (1990). Making use of the formalisms developed by Lekhnitskii (1963) and Eshelby et al. (1953), Suo constructed near-tip solutions for both non-oscillatory and oscillatory fields. It was shown that for non-oscillatory fields the structure of the stresses and displacements at the crack tip were the same for those in a homogeneous anisotropic body due to the real-valued stress intensity factors. However, when considering oscillatory fields the in-plane fields were seen to be governed by one complex valued stress intensity factor whereas the antiplane components were still derived using a real-valued constant.

The work of Suo (1990) was extended to a dynamic crack by Yang et al.

(1991). A steady-state crack was considered and the formalisms used by Suo were adapted accordingly for the new, moving coordinate system. The results found hold up to the Rayleigh-wave speed of the more compliant of the two bonded materials, that is the lowest of the two Rayleigh-wave speeds. In the moving coordinate system it was found that the behaviour of the near-tip fields were identical to those for a static crack and the oscillations still occurred for the in-plane fields, with the oscillation index becoming infinite at the crack limiting speed.

Further studies into fracture in both isotropic and anisotropic bimaterials have made significant use of weight functions. Originally introduced by Bueckner (1970) and Rice (1968), weight functions are defined as functions which can be used in conjunction with the loading on crack faces to obtain integral expressions for the stress intensity factors. Bueckner (1985) used weight function techniques to find SIF for a penny shaped crack and a half-plane crack. A number of results on the relationship between weight functions and stress intensity factors are found in Wu and Carlsson (1991) and Fett and Munz (1997). Many other examples of weight functions can be found in existing literature, including for Mode I fracture (Glinka and Shen, 1991), a 3-dimensional semi-infinite crack in an infinite body (Kassir and Sih, 1973), a crack lying perpendicular to an interface in a thin surface layer (Fett et al., 1996) and a corner crack in a plate of finite thickness (Zheng et al., 1996). A special weight function was found in Willis and Movchan (1995) for a semi-infinite crack in an infinite homogeneous, isotropic medium. Defined as a singular displacement field to a traction free interfacial crack problem, this weight function was used in the derivation of a reciprocal identity con-

necting the weight function to the physical fields, often referred to as the Betti identity. The Betti identity has been used in a number of studies, including that of a 3-dimensional interfacial crack (Bercial-Velez et al., 2005) and the derivation of stress intensity factors in an isotropic (Piccolroaz et al., 2007) and anisotropic bimaterial (Morini et al., 2013b).

All of the work discussed up to this point for bimaterial fracture has involved perfect transmission conditions over the area of adhesion between the two materials, that is continuity of both tractions and displacements. A more realistic concept was developed by Atkinson (1977) where a thin layer of soft adhesive was placed between the materials. This thin layer can then be replaced by suitable transmission conditions, provided that the bonding agent is soft enough. A number of studies into these transmission conditions were performed, in the early 2000's,(Antipov et al., 2001; Lenci, 2001; Mishuris, 2001), where it was found that it was suitable to replace the thin layer by continuity of tractions and a discontinuous displacement, directly proportional to the traction, over the interface. When considering such interfaces the behaviour of the physicals fields in the vicinity of the crack tip are altered significantly. The work of Mishuris and Kuhn (2001) found that the square-root singularity found for a perfect interface was not present for imperfect interfaces; a logarithmic singularity was present at the crack tip in its place. Imperfect transmission conditions were studied more generally by Benveniste and Miloh (2001) for a thin curved isotropic layer of constant thickness whereas Benveniste (2006) considered the 3-dimensional problem of two anisotropic materials separated by an arbitrarily curved layer of anisotropic material.

With the differing behaviour of physical fields at the crack tip, and therefore the lack of stress intensity factors, a more general definition of weight functions was developed. The new definition said that weight functions were used in the derivation of key asymptotic constants at the crack tip, which in the case of a perfect interface agrees with the definition of the stress intensity factor. However, for imperfect interfaces weight functions are used to find the asymptotic constants required to find the crack tip opening displacement, which was originally proposed as a key parameter for studying fracture criteria by Cottrell (1962) and Wells (1961). The importance of the displacement at the crack tip was further justified by Rice and Sorenson (1978), Kanninen et al. (1979) and Shih et al. (1979). Recently, weight functions have been used to look at waves in thin waveguides containing imperfect interfaces (Vellender et al., 2011; Vellender and Mishuris, 2012) and the effect of material defects on the propagation of a semi-infinite crack along an imperfect interface in an infinitely large isotropic bimaterial (Vellender et al., 2013).

Recent developments for semi-infinite cracks in an infinite bimaterial have seen the implementation of singular integral equations. Making use of weight functions and the Betti formula, expressions for crack and interface displacement jumps and interfacial tractions have been found for a perfect interface in an isotropic bimaterial (Piccolroaz and Mishuris, 2013), a perfect interface in an anisotropic bimaterial (Morini et al., 2013a) and an imperfect interface in an isotropic bimaterial (Mishuris et al., 2013). Historically singular integral equations have played a large role in the study of cracks in elastic media since being introduced by Muskhelishvili (1963). Using the linear singular operator theory of Gohberg and Krein (1960), Duduchava (1979) analysed

singular integral equations with fixed point singularities. They were also used by Mishuris (1997a,b) in the analysis of layers and wedges separated by imperfect interfaces.

The study of cracks in piezoelectric materials has also seen some important developments. In order to formulate the problem suitable boundary conditions on the crack faces are required. Parton (1976) suggested using the continuity of both electrical potential and displacements over the crack, However, these conditions are unrealistic due to the vast difference between permeability of the materials and the space separating the crack faces. As an alternative, Pak (1990) used the zero electric displacement condition on the crack face instead. With these conditions Kuo and Barnett (1991) performed asymptotic analysis of the behaviour at the crack tip in a piezoelectric material. This work showed that the singularity present at the crack tip was similar to that in a non-piezoelectric material apart from an additional real-valued constant which is involved in the asymptotics of the out-of-plane and electrical fields at the crack tip.

A major breakthrough in piezoelectric fracture mechanics was that of Suo et al. (1992). Similar to his work in Suo (1990), a perfect interface in a bimaterial was considered and the Stroh formalism was extended to the piezoelectric setting. Full field expressions for both mechanical and electrical fields in the vicinity of the crack tip were found and the results agreed with those of Kuo and Barnett (1991) with the existence of the additional constant governing the out-of-plane and piezoelectric asymptotics. Following from this work Gao and Wang (2001) used an alternative method based on Green's functions to formulate singular integral equations to derive the

fields. However, as reported by Pan and Yuan (2000) and Pan (2003), these formulations usually result in the need of complicated schemes in order to calculate the integrals numerically. The further restriction of all of the results reported so far is that they were restricted to symmetrical loading on the crack faces.

The derivation of the general, extended Stroh matrices for piezoelectric materials usually results in the need to numerically solve a highly complex octic equation. As an alternative to this Hwu (2008) extended the Lekhnitskii formalism to piezoelectric materials and made use of this to formulate the Stroh matrices for piezoelectric materials with transversely isotropic behaviour. In recent years another significant development was that of Hadjesfandiari (2013) where the Betti reciprocal identity was also extended to a piezoelectric setting to relate two sets of mechanical and electrical components over the same geometry.

1.2 Thesis structure

It is clear from the review of the literature that the breadth of knowledge in the field of fracture mechanics is already vast but there are some areas that still require further investigation. The remainder of the thesis will consider three separate problems concerning different material and interfacial properties.

Chapter 2 will give more information on the background knowledge required for further analysis. This will include an in depth study of anisotropic materials, the Stroh formalism and interfacial fracture in anisotropic bimaterials. We also give more mathematical detail on piezoelectric materials and

how the existing methods for anisotropic bimaterials have been extended to include the added electrical effects. Finally, an insight into some of the mathematical techniques used in this thesis will be given.

The third Chapter sees the beginning of the new research. The work presented concerns the derivation of stress intensity factors for a moving semi-infinite crack along a perfect interface in an anisotropic bimaterial. The analysis here extends the approach of Morini et al. (2013b) for a stationary crack to the steady-state moving crack with an arbitrary load on the crack face. A method for computing further asymptotic terms, which can be used in perturbation analysis, is also developed. The newly derived stress intensity factors are then used to find the variation in energy release rate as the crack velocity is changed. Moreover, the effect of the crack speed on the oscillatory behaviour of the near-tip fields is also considered.

Chapter 4 proceeds to study a crack along an imperfect interface in an anisotropic bimaterial. In the same vein as Piccolroaz and Mishuris (2013), Morini et al. (2013a) and Mishuris et al. (2013), singular integral equations are found which are then used to find the displacement jump over both the crack and interface. However, a variation in approach is used here. Previously, corresponding material properties and interfacial transmission conditions have been used in the derivation of the weight functions required to obtain the integral equations. Here, we use an approach where weight functions formed using perfect interface transmission conditions are used to obtain the physical fields for the imperfect interface problem. Finite element simulations are also performed and their results compared to those obtained through numerically solving the integral equations.

Piezoelectric materials are the main focus of Chapter 5. We introduce a weight function similar to that of Willis and Movchan (1995) for a perfect interface in a transversely isotropic piezoelectric bimaterial. Following this, singular integral equations are derived which relate the components of both the mechanical and electrical fields in the material. Two specific poling directions are considered: firstly we consider when the piezoelectric effect couples with the in-plane fields and therefore has no effect on the antiplane deformations and secondly the opposite case, where the piezoelectricity decouples from the in-plane fields and affects only the antiplane deformations.

The final Chapter of the thesis will summarise the main results from Chapters 3, 4 and 5. We also discuss the possibilities of extending the work further and possible applications of the new results to other fields of research.

Chapter 2

Background

In this chapter we present a detailed summary of some of the important results used in the remainder of the thesis. We begin by looking at the mathematical models used when considering displacement and traction fields in anisotropic materials before proceeding to look at known results for fractures along perfect interfaces in anisotropic bimaterials. The extension of these results to piezoelectric materials is also discussed in detail. The final part of the chapter will consider some of the mathematical techniques which are used extensively in Chapters 3, 4 and 5 of the thesis.

2.1 Anisotropic materials

Anisotropic materials are classed as those with physical properties that are directionally dependent, as opposed to isotropic materials which have identical properties in all directions. Hooke's law for anisotropic materials was developed in the 17th century and relates stresses and strains:

$$\sigma_{ij} = C_{ijkl}\varepsilon_{kl}, \qquad \varepsilon_{ij} = S_{ijkl}\sigma_{kl}, \quad \text{for } i,j,k,l = 1,2,3, \tag{2.1}$$

where σ and ε are the stress and strain respectively. C_{ijkl} and S_{ijkl} are the components of the fourth-order stiffness tensor, $\mathbf{C}$, and compliance tensor, $\mathbf{S}$. It is immediately clear from (2.1) that $\mathbf{S} = \mathbf{C}^{-1}$.

Due to the symmetry of the stiffness tensor, σ_{ij}, it is possible to reduce the fourth-order tensor, C_{ijkl}, to a second-order tensor, C_{ij}. In order to do this Voigt notation is introduced, that is $11 \to 1, 22 \to 2, 33 \to 3, 23(\text{or } 32) \to 4, 13(\text{or } 31) \to 5$ and $12(\text{or } 21) \to 6$. Through use of this notation the first part of (2.1) can be rewritten in matrix form

$$\begin{pmatrix} \sigma_1 \\ \sigma_2 \\ \sigma_3 \\ \sigma_4 \\ \sigma_5 \\ \sigma_6 \end{pmatrix} = \begin{pmatrix} C_{11} & C_{12} & C_{13} & C_{14} & C_{15} & C_{16} \\ C_{12} & C_{22} & C_{23} & C_{24} & C_{25} & C_{26} \\ C_{13} & C_{23} & C_{33} & C_{34} & C_{35} & C_{36} \\ C_{14} & C_{24} & C_{34} & C_{44} & C_{45} & C_{46} \\ C_{15} & C_{25} & C_{35} & C_{45} & C_{55} & C_{56} \\ C_{16} & C_{26} & C_{36} & C_{46} & C_{56} & C_{66} \end{pmatrix} \begin{pmatrix} \varepsilon_1 \\ \varepsilon_2 \\ \varepsilon_3 \\ \varepsilon_4 \\ \varepsilon_5 \\ \varepsilon_6 \end{pmatrix}. \tag{2.2}$$

For general anisotropic materials the stiffness and compliance matrices both contain 21 independent components.

In this thesis, certain subclasses of anisotropic materials will be considered. One such material is an orthotropic material which has three mutually orthogonal planes of symmetry. In such a case the stiffness matrix reduces further and only relies on 9 independent components. Another type of material that can be considered is a transverse isotropic material which has symmetrical material properties about an axis which is also normal to a plane of isotropy. As a result of this further restriction the stiffness matrix for transverse isotropic materials depends only on 5 parameters. For perfectly isotropic materials only two parameters are required in order to classify the

entire material: Young's modulus and Poisson's ratio.

2.1.1 The Stroh formalism

In the 1950s the study of anisotropic materials was evolved by the results introduced in Eshelby et al. (1953) for calculating stress and displacement fields for two-dimensional geometries in the (x_1, x_2) plane. The complex variable formalism introduced by Eshelby is commonly referred to as the Stroh formalism after its appearance in Stroh (1958). The method used was developed form the governing equations of linear anisotropy

$$\sigma_{ij,j} = 0, \qquad \varepsilon_{ij} = \frac{1}{2}(u_{i,j} + u_{j,i}) \qquad i, j, k, l = 1, 2, 3, \tag{2.3}$$

where u is the displacement field. When combined with Hooke's law, (2.1), the following second order partial differential equations were obtained

$$\sigma_{ij} = C_{ijkl} u_{k,l} \qquad C_{ijkl} u_{k,lj} = 0. \tag{2.4}$$

A solution to (2.4) was found as a linear combination of the two co-ordinates, x_1 and x_2,

$$u_k = a_k f_k(z), \qquad \text{where } z = x_1 + \mu x_2, \tag{2.5}$$

where μ is a complex constant. When considering fracture mechanics with interfaces this form of the solution is of great use if the geometry is oriented sensibly to the coordinate system. Specifically, if the crack and interface are said to lie along the x_1 axis then the displacement along them is a function of x_1 only.

Using the desired form of the solution, (2.5), along with the second part of (2.4) yields an eigenvalue problem which can be solved to find μ and a_k:

$$[\mathbf{Q} + \mu(\mathbf{R} + \mathbf{R}^T) + \mu^2 \mathbf{T}]\mathbf{A} = 0 \tag{2.6}$$

where $\mathbf{Q}_{ik} = C_{i1k1}, \mathbf{R}_{ik} = C_{i1k2}$ and $\mathbf{T}_{ik} = C_{i2k2}$. In general, for anisotropic materials the six eigenvalues of (2.6) are found to be three pairs of distinct complex conjugate numbers. This gives a final result for the displacement field as

$$\mathbf{u} = \begin{pmatrix} u_1 \\ u_2 \\ u_3 \end{pmatrix} = 2\mathrm{Re}\mathbf{A}\mathbf{f}(z) = 2\mathrm{Re} \begin{pmatrix} A_{11} & A_{12} & A_{13} \\ A_{21} & A_{22} & A_{23} \\ A_{31} & A_{32} & A_{33} \end{pmatrix} \begin{pmatrix} f_1(z_1) \\ f_2(z_2) \\ f_3(z_3) \end{pmatrix}, \tag{2.7}$$

where the columns of the matrix $\mathbf{A}$ consist of the three eigenvectors, a_k, for the three solutions of (2.6) which have real positive imaginary part (μ_k where $k = 1, 2, 3$) and $z_k = x_1 + \mu_k x_2$. The methods used for the degenerate cases of (2.6) have been discussed in detail by Ting (1996).

Following a similar procedure an expression for stresses in the materials were also found to be

$$\sigma_{2i} = 2\mathrm{Re}\mathbf{L}\mathbf{f}'(z), \quad \text{where} \quad L_{i\mu} = (C_{i2k1} + \mu C_{i2k2})A_{k\mu}. \tag{2.8}$$

At a similar time to the work performed by Eshelby another method for finding displacement and stresses in anisotropic materials was developed by Lekhnitskii (1963). Despite a great difference in the approach of Lekhnitskii it was later realised that the resulting matrices, $\mathbf{A}$ and $\mathbf{L}$, obtained from his work gave a specific normalisation for the eigenvalue problem given in Eshelby et al. (1953). Further details on the methods used by Lekhnitskii will be seen later in this chapter where their extension to piezoelectric materials is discussed in detail.

2.1.2 Results for a perfect interface in an anisotropic bimaterial

The work presented here is that of Suo (1990) where a semi-infinite crack along a perfect interface in an anisotropic bimaterial was considered. The static crack is said to occupy the region $\{x_1 < 0, x_2 = 0\}$ with the interface bonding the two materials lying along the region $\{x_1 > 0, x_2 = 0\}$. The material in the upper half-plane ($x_2 > 0$) and lower half-plane ($x_2 < 0$) are referred to as materials I and II respectively. The transmission conditions along the interface, given as continuity of displacement and tractions, are represented mathematically as

$$[\![\mathbf{u}]\!](x_1) = \mathbf{u}(x_1, 0^+) - \mathbf{u}(x_1, 0^-) = 0, \quad [\![\sigma_{2i}]\!](x_1) = 0, \quad \text{for } x_1 > 0, \quad (2.9)$$

where the superscript $\pm$ refers to the approach from above or below the x_1-axis respectively. Using this information Suo (1990) found expressions for the near-tip displacement and tractions when a symmetric loading system was applied on the crack faces. Expressions for energy release rate and stress intensity factor at the crack tip were also found.

In order to proceed further the single material matrix $\mathbf{B} = i\mathbf{A}\mathbf{L}^{-1}$, commonly called the surface admittance tensor, was introduced. The bimaterial matrix $\mathbf{H} = \mathbf{B}_I + \mathbf{B}_{II}^{\star}$ is also defined, where the subscript is used to notify which material the matrix is associated with and $\star$ denotes complex conjugation. It was shown by Stroh (1958) that $\mathbf{B}$ is positive-definite Hermitian. It follows that $\mathbf{H}$ is also positive-definite Hermitian and is therefore invertible.

Making use of the transmission conditions (2.9) for a traction free crack face problem, the following Riemann-Hilbert problem was found along the

crack for the unknown function $\mathbf{h}(z)$ (Suo, 1990):

$$\mathbf{h}^{+}(x_1) + (\mathbf{H}^{\star})^{-1}\mathbf{H}\mathbf{h}^{-}(x_1) = 0, \quad -\infty < x_1 < 0. \tag{2.10}$$

The branch cut of $\mathbf{h}$ is situated along the negative x_1-axis and the superscript $\pm$ refers to the limiting value of the function as the branch cut is approached from above and below.

The method used by Suo (1990) found a solution in the form $\mathbf{h}(z) = \mathbf{w}z^{-\frac{1}{2}+i\epsilon}$. The real valued parameter ϵ is known as the oscillatory index of the bimaterial. When inserted into equation (2.10) the following eigenvalue problem is obtained

$$\mathbf{H}^{\star}\mathbf{w} = e^{2\pi\epsilon}\mathbf{H}\mathbf{w}. \tag{2.11}$$

The three sets of eigenvalues and eigenvectors which solve (2.11) are given by: $(\epsilon, \mathbf{w}), (-\epsilon, \mathbf{w}^{\star}), (0, \mathbf{w_3})$, where $\mathbf{w}$ is a complex valued vector and $\mathbf{w}_3$ is purely real-valued.

Using the solutions of the eigenvalue problem (2.11) it was found in Suo (1990) that the interfacial traction is given by

$$\sigma_{2i}(x_1) = \frac{1}{\sqrt{2\pi x_1}}\left[Kx_1^{i\epsilon}\mathbf{w} + K^{\star}x_1^{-i\epsilon}\mathbf{w}^{\star} + K_3\mathbf{w}_3\right] \quad \text{for } 0 < x_1 < \infty, \tag{2.12}$$

where $K = K_1 + iK_2$ is the stress intensity factor associated with the Mode I and II fields and K_3 is the Mode III SIF. The jump in displacement over the crack face was also found:

$$[\![\mathbf{u}]\!](x_1) = (\mathbf{H} + \mathbf{H}^{\star})\sqrt{\frac{(-x_1)}{2\pi}}\left[\frac{K(-x_1)^{i\epsilon}\mathbf{w}}{(1+2i\epsilon)\cosh\pi\epsilon} + \frac{K^{\star}(-x_1)^{-i\epsilon}\mathbf{w}^{\star}}{(1-2i\epsilon)\cosh\pi\epsilon} + K_3\mathbf{w}_3\right], \quad \text{for } -\infty < x_1 < 0. \tag{2.13}$$

In order to find the energy release rate at the crack tip, G, the relationship

developed in Irwin (1957) was used:

$$G = \frac{1}{2\Delta}\int_0^{\Delta} \sigma_{2i}^T(\Delta - r)[\![\mathbf{u}]\!](r)\mathrm{d}r, \tag{2.14}$$

where Δ is an arbitrary length scale. Using equations (2.12), (2.13) and (2.14) Suo (1990) found the following expression for G

$$G = \frac{\mathbf{w}^{\star T}(\mathbf{H} + \mathbf{H}^{\star})\mathbf{w}|K|^2}{4\cosh^2 \pi\epsilon} + \frac{\mathbf{w}_3^T(\mathbf{H} + \mathbf{H}^{\star})\mathbf{w}_3 K_3^2}{8}. \tag{2.15}$$

The final result needed from Suo (1990) is the formulae used to derive the stress intensity factors when a symmetric loading, $\mathbf{p} = (p_1, p_2, p_3)^T$, is applied on the crack faces. The expressions found for K and K_3 were found to be

$$K = -\left(\frac{2}{\pi}\right)^{\frac{1}{2}} \cosh \pi\epsilon \int_{-\infty}^{0} (-x_1)^{-\frac{1}{2}-i\epsilon} p_1 \mathrm{d}x_1, \quad K_3 = -\left(\frac{2}{\pi}\right)^{\frac{1}{2}} \int_{-\infty}^{0} (-x_1)^{-\frac{1}{2}} p_{31} \mathrm{d}x_1, \tag{2.16}$$

where

$$p_1 = \frac{\mathbf{w}^{\star T}\mathbf{H}\mathbf{p}}{\mathbf{w}^{\star T}\mathbf{H}\mathbf{w}}, \quad p_{31} = \frac{\mathbf{w}_3^T\mathbf{H}\mathbf{p}}{\mathbf{w}_3^T\mathbf{H}\mathbf{w}_3}.$$

2.2 Piezoelectric materials

We now proceed to study the mathematical framework used when considering piezoelectric materials. The definition of a piezoelectric material is one that produces an electric charge when subjected to a stress field. These materials also deform when an electric charge is run through them (commonly referred to as the inverse piezoelectric effect and illustrated in Figure 2.1). There are many uses for piezoelectric materials in modern industry; for example they are commonly used in cars in both the collision detection system which

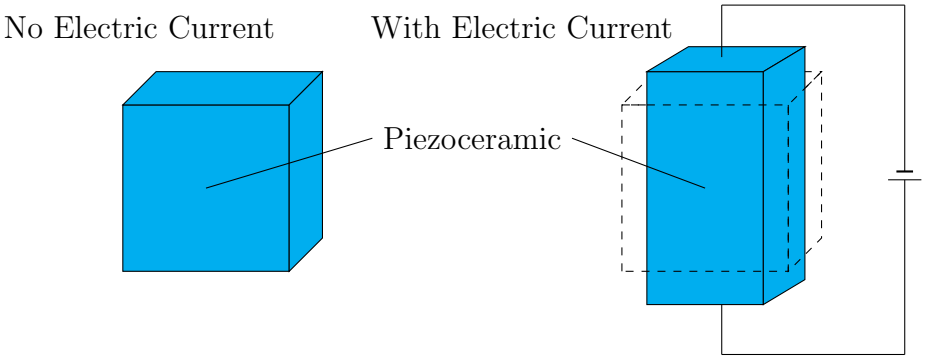

Figure 2.1: Inverse piezoelectric effect

activates airbags for safety and also in actuators in diesel engines which control the fuel flow in the vehicle.

To study piezoelectric materials it is necessary to find expressions relating the mechanical and electrical fields in the material. Using an energy based argument Suo et al. (1992) found the following governing equations for piezoelectric materials

$$\sigma_{ij} = C_{ijkl}\varepsilon_{kl} - e_{lji}E_l, \quad D_i = \omega_{il}E_l + e_{ikl}\varepsilon_{kl}, \tag{2.17}$$

where E is the electrical field, D is the electrical displacement, ω is the material permittivity tensor and e is the piezoelectric tensor of the material. Similarly to the results for anisotropic materials the Voigt notation is used

to give the following matrix expressions

$$\begin{pmatrix}\sigma_1\\ \sigma_2\\ \sigma_3\\ \sigma_4\\ \sigma_5\\ \sigma_6\end{pmatrix} = \begin{pmatrix}C_{11} & C_{12} & C_{13} & C_{14} & C_{15} & C_{16}\\ C_{12} & C_{22} & C_{23} & C_{24} & C_{25} & C_{26}\\ C_{13} & C_{23} & C_{33} & C_{34} & C_{35} & C_{36}\\ C_{14} & C_{24} & C_{34} & C_{44} & C_{45} & C_{46}\\ C_{15} & C_{25} & C_{35} & C_{45} & C_{55} & C_{56}\\ C_{16} & C_{26} & C_{36} & C_{46} & C_{56} & C_{66}\end{pmatrix}\begin{pmatrix}\varepsilon_1\\ \varepsilon_2\\ \varepsilon_3\\ \varepsilon_4\\ \varepsilon_5\\ \varepsilon_6\end{pmatrix} - \begin{pmatrix}e_{11} & e_{21} & e_{31}\\ e_{12} & e_{22} & e_{32}\\ e_{13} & e_{23} & e_{33}\\ e_{14} & e_{24} & e_{34}\\ e_{15} & e_{25} & e_{35}\\ e_{16} & e_{26} & e_{36}\end{pmatrix}\begin{pmatrix}E_1\\ E_2\\ E_3\end{pmatrix} \tag{2.18}$$

$$\begin{pmatrix}D_1\\ D_2\\ D_3\end{pmatrix} = \begin{pmatrix}e_{11} & e_{12} & e_{13} & e_{14} & e_{15} & e_{16}\\ e_{21} & e_{22} & e_{23} & e_{24} & e_{25} & e_{26}\\ e_{31} & e_{32} & e_{33} & e_{34} & e_{35} & e_{36}\end{pmatrix}\begin{pmatrix}\varepsilon_1\\ \varepsilon_2\\ \varepsilon_3\\ \varepsilon_4\\ \varepsilon_5\\ \varepsilon_6\end{pmatrix} + \begin{pmatrix}\omega_{11} & \omega_{12} & \omega_{13}\\ \omega_{21} & \omega_{22} & \omega_{23}\\ \omega_{31} & \omega_{32} & \omega_{33}\end{pmatrix}\begin{pmatrix}E_1\\ E_2\\ E_3\end{pmatrix}. \tag{2.19}$$

The permittivity and piezoelectric tensors are also simplified when subclasses of anisotropic materials are used as the poling direction of the material would be changed. An example of this is a transverse isotropic piezoelectric material with poling direction parallel to one of the cartesian axes. This will be discussed in more detail in Chapter 5.

2.2.1 Extended Stroh formalism for piezoelectricity

As seen previously in this chapter the Stroh formalism is a very effective tool to use in the study of anisotropic materials. With this in mind it was extended to piezoelectric material in Suo et al. (1992) in order to find the electric potential, ϕ, and electrical displacement in addition to the physical

displacement and traction fields. Here we present a summary of the results from that paper.

In order to obtain the desired results the following definitions for the electrical fields are required

$$D_{i,i} = 0, \qquad E_i = -\phi_{,i}\,. \tag{2.20}$$

Inserting equations (2.3) and (2.20) into equation (2.17) yields

$$(C_{ijkl}u_k + e_{lji}\phi)_{,li} = 0, \quad (-\omega_{il}\phi + e_{ikl}u_k)_{,li} = 0. \tag{2.21}$$

The extended displacement field, $\mathbf{u} = (u_1, u_2, u_3, \phi)^T$, was introduced by Suo et al. (1992) and a solution was once again found in the form $\mathbf{u} = \mathbf{a}f_k(z)$ where z is the same linear combination of x_1 and x_2 used in the Stroh formalism for anisotropic materials. This yields the following eigenvalue problem which has the same form as that for anisotropic materials

$$[\mathbf{Q} + \mu(\mathbf{R} + \mathbf{R}^T) + \mu^2\mathbf{T}]\mathbf{A} = 0. \tag{2.22}$$

Despite looking similar to the previous results for non-piezoelectric materials this problem is significantly different as 4×4 matrices are now involved to incorporate the additional piezoelectric effects. For general anisotropic piezoceramics the matrices have the following form:

$$\mathbf{Q} = \begin{pmatrix} C_{11} & C_{16} & C_{15} & e_{11} \\ C_{16} & C_{66} & C_{56} & e_{16} \\ C_{15} & C_{56} & C_{55} & e_{15} \\ e_{11} & e_{16} & e_{15} & -\omega_{11} \end{pmatrix}, \quad \mathbf{R} = \begin{pmatrix} C_{16} & C_{12} & C_{14} & e_{16} \\ C_{66} & C_{26} & C_{46} & e_{12} \\ C_{56} & C_{25} & C_{45} & e_{14} \\ e_{21} & e_{26} & e_{25} & -\omega_{12} \end{pmatrix},$$

$$\mathbf{T} = \begin{pmatrix} C_{66} & C_{26} & C_{46} & e_{26} \\ C_{26} & C_{22} & C_{24} & e_{22} \\ C_{46} & C_{24} & C_{44} & e_{24} \\ e_{26} & e_{22} & e_{24} & -\omega_{22} \end{pmatrix}.$$

The eight eigenvalues of (2.22) are found to be four pairs of complex conjugate numbers and therefore the extended displacement field is given by

$$\begin{pmatrix} u_1 \\ u_2 \\ u_3 \\ \phi \end{pmatrix} = 2\mathrm{Re} \begin{pmatrix} A_{11} & A_{12} & A_{13} & A_{14} \\ A_{21} & A_{22} & A_{23} & A_{24} \\ A_{31} & A_{32} & A_{33} & A_{34} \\ A_{41} & A_{42} & A_{43} & A_{44} \end{pmatrix} \begin{pmatrix} f_1(z_1) \\ f_2(z_2) \\ f_3(z_3) \\ f_4(z_4) \end{pmatrix}, \tag{2.23}$$

where $z_k = x_1 + \mu_k x_2$ (for $k = 1, 2, 3, 4$) with μ_k once again being taken as the four eigenvalues of (2.22) with positive imaginary part.

When considering the tractions and electrical displacements Suo et al. (1992) introduced the extended traction field $\mathbf{t} = (\sigma_{2i}, D_2)^T$. Using the same method as used for anisotropic materials this extended traction vector was found to be given by

$$\mathbf{t}(x_1) = 2\mathrm{Re}\mathbf{L}\mathbf{f}'(z). \tag{2.24}$$

The components of the 4×4 matrix, $\mathbf{L}$, are given by

$$L_{jk} = \sum_{r=1}^{3} [(C_{2jr1} + \mu_k C_{2jr2}) A_{rk}] + (e_{1j2} + \mu_k e_{2j2}) A_{4k}, \quad \text{for } j = 1, 2, 3,$$

$$L_{4k} = \sum_{r=1}^{3} [(e_{2r1} + \mu_k e_{2r2}) A_{rk}] - (\omega_{12} + \mu_k \omega_{22}) A_{4k}.$$

2.2.2 Fracture in piezoelectric bimaterials

The paper of Suo et al. (1992) considered the same geometry previously considered for anisotropic materials earlier in this Chapter. The transmission

conditions used had continuity of displacements and tractions over the interface but to incorporate the piezoelectric effect both the electric potential and electric displacement fields were also considered to be continuous over the bonded portion of the interface. Following the same procedure as Suo (1990) for anisotropic bimaterials the following eigenvalue problem was obtained

$$\mathbf{H}^{\star}\mathbf{w} = e^{2\pi\epsilon}\mathbf{H}\mathbf{w}. \tag{2.25}$$

Despite being similar in appearance to equation (2.11) the bimaterial matrix $\mathbf{H}$ is now the 4×4 matrix resulting from the matrices $\mathbf{A}$ and $\mathbf{L}$ obtained when extending the Stroh formalism to piezoelectric materials.

The solution to (2.25) consists of four pair of eigenvalues and eigenvectors. These are given by: $(\epsilon, \mathbf{w}), (-\epsilon, \mathbf{w}^{\star}), (-i\kappa, \mathbf{w}_3)$ and $(i\kappa, \mathbf{w}_4)$. Once again $\mathbf{w}$ is a complex valued vector whereas $\mathbf{w}_3$ and $\mathbf{w}_4$ are real-valued vectors. With these results the extended traction field $\mathbf{t}$ was found along the interface:

$$\mathbf{t}(x_1) = \frac{1}{\sqrt{2\pi x_1}}\left[K x_1^{i\epsilon}\mathbf{w} + K^{\star} x_1^{-i\epsilon}\mathbf{w}^{\star} + K_3 x_1^{\kappa}\mathbf{w}_3 + K_4 x_1^{-\kappa}\mathbf{w}_4\right], \tag{2.26}$$

where K_4 is the electric intensity factor, introduced by Suo et al. (1992) as the equivalent of the stress intensity factors for the electrical fields. The following results for the jump in the extended displacement, $\mathbf{u} = (u_1, u_2, u_3, \phi)$,over the crack and energy release rate at the crack tip were also found:

$$\begin{aligned}[\![\mathbf{u}]\!](x_1) = (\mathbf{H} + \mathbf{H}^{\star})\sqrt{\frac{(-x_1)}{2\pi}}\Bigg[&\frac{K(-x_1)^{i\epsilon}\mathbf{w}}{(1+2i\epsilon)\cosh\pi\epsilon} + \frac{K^{\star}(-x_1)^{-i\epsilon}\mathbf{w}^{\star}}{(1-2i\epsilon)\cosh\pi\epsilon} \\ &+ \frac{K_3(-x_1)^{\kappa}\mathbf{w}_3}{(1+2\kappa)\cos\pi\kappa} + \frac{K_4(-x_1)^{-\kappa}\mathbf{w}_4}{(1-2\kappa)\cos\pi\kappa}\Bigg],\end{aligned} \tag{2.27}$$

$$G = \frac{\bar{\mathbf{w}}^T(\mathbf{H} + \bar{\mathbf{H}})\mathbf{w}|K|^2}{4\cosh^2\pi\epsilon} + \frac{\mathbf{w}_3^T(\mathbf{H} + \bar{\mathbf{H}})\mathbf{w}_4 K_3 K_4}{4\cos^2\pi\kappa}. \tag{2.28}$$

2.2.3 The Lekhnitskii formalism for piezoelectric materials

When finding the fields for a crack propagating along a piezoelectric bimaterial interface it is clear that the single material matrices $\mathbf{A}$ and $\mathbf{L}$ are of utmost importance. While it is possible to use the extended Stroh formalism, as seen in Suo et al. (1992), to find these matrices it often leads to a very complicated eigenvalue problem (2.22) which is not easily numerically solvable. It is therefore helpful to use another method to find the matrices. For anisotropic materials Lekhnitskii (1963) provided an alternate method to find $\mathbf{A}$ and $\mathbf{L}$. The results presented here are the extension of this approach to piezoelectric materials, as seen in Hwu (2008), which results in the need to numerically solve a sextic equation as opposed to the octic equation obtained through the extended Stroh formalism.

When using the Lekhnitskii formalism the plane strain and short circuit conditions are imposed, that is $\varepsilon = 0$ and $E_3 = 0$. The inverse of equations (2.18) and (2.19) can then be written as follows:

$$\varepsilon_p = \mathbf{S}_p \sigma_p, \tag{2.29}$$

where $\varepsilon_p = (\varepsilon_1, \varepsilon_2, \varepsilon_4, \varepsilon_5, \varepsilon_6, -E_1, -E_2)^T$, $\sigma_p = (\sigma_1, \sigma_2, \sigma_4, \sigma_5, \sigma_6, D_1, D_2)^T$ and $\mathbf{S}_p$ is a 7×7 matrix constructed using the compliance tensor, dielectric non-permittivities and piezoelectric strain/voltage tensor of the material (Hwu, 2008). We note here that the expression is simplified by the plane strain and short circuit conditions mentioned previously. For the general case, where ε_3 and E_3 are not equal to 0, the full 9×9 matrix representation of $\mathbf{S}_p$ would be required.

The stress function $\psi_i = l_i f(z)$ is introduced where the l_i are the unknown vectors required to construct the material matrix $\mathbf{L}$ and z is the same linear combination of the coordinates x_1 and x_2 as used for the Stroh formalism. The function ψ is related to the stress fields by the equations: $\sigma_{i1} = -\psi_{i,2}$ and $\sigma_{i2} = \psi_{i,1}$ where $\sigma_{4j} = D_j$. Using this definition of ψ along with equations (2.3) and (2.20) gives

$$\mathbf{D}_\varepsilon \mathbf{u} = \mathbf{S}_p \mathbf{D}_\sigma \psi, \tag{2.30}$$

where the operator matrices are given by

$$\mathbf{D}_\varepsilon = \begin{pmatrix} \frac{\partial}{\partial x_1} & 0 & 0 & 0 \\ 0 & \frac{\partial}{\partial x_2} & 0 & 0 \\ 0 & 0 & \frac{\partial}{\partial x_2} & 0 \\ 0 & 0 & \frac{\partial}{\partial x_1} & 0 \\ \frac{\partial}{\partial x_2} & \frac{\partial}{\partial x_1} & 0 & 0 \\ 0 & 0 & 0 & \frac{\partial}{\partial x_1} \\ 0 & 0 & 0 & \frac{\partial}{\partial x_2} \end{pmatrix}, \quad \mathbf{D}_\sigma = \begin{pmatrix} -\frac{\partial}{\partial x_2} & 0 & 0 & 0 \\ 0 & \frac{\partial}{\partial x_1} & 0 & 0 \\ 0 & 0 & \frac{\partial}{\partial x_1} & 0 \\ 0 & 0 & -\frac{\partial}{\partial x_2} & 0 \\ \frac{\partial}{\partial x_1} & 0 & 0 & 0 \\ 0 & 0 & 0 & -\frac{\partial}{\partial x_2} \\ 0 & 0 & 0 & -\frac{\partial}{\partial x_1} \end{pmatrix}. \tag{2.31}$$

To continue with deriving the matrices Hwu (2008) used the compatibility equations for two-dimensional problems, given as

$$\varepsilon_{11,22} + \varepsilon_{22,11} - 2\varepsilon_{12,12} = 0, \quad -\varepsilon_{23,1} + \varepsilon_{13,2} = 0, \quad E_{1,2} - E_{2,1} = 0. \tag{2.32}$$

Combining these three relationships gives the equation $\mathbf{D}_C \varepsilon_p = 0$, where $\mathbf{D}_C$ is the matrix differential operator:

$$\mathbf{D}_C = \begin{pmatrix} \frac{\partial^2}{\partial x_2^2} & \frac{\partial^2}{\partial x_1^2} & 0 & 0 & -\frac{\partial^2}{\partial x_1 x_2} & 0 & 0 \\ 0 & 0 & -\frac{\partial}{\partial x_1} & \frac{\partial}{\partial x_2} & 0 & 0 & 0 \\ 0 & 0 & 0 & 0 & 0 & \frac{\partial}{\partial x_2} & -\frac{\partial}{\partial x_1} \end{pmatrix}. \tag{2.33}$$

From equation (2.30) it follows immediately that $\mathbf{D}_C\mathbf{S}_p\mathbf{D}_\sigma\psi = 0$. Substituting in $\psi_i = l_i f(z)$ and recalling $z = x_1 + \mu x_2$, where the unknown complex number μ is required to find $\mathbf{A}$ and $\mathbf{L}$, yields the equation

$$\mathbf{\Gamma}_C\mathbf{S}_p\mathbf{\Gamma}_\sigma\mathbf{l} = 0, \tag{2.34}$$

where

$$\mathbf{\Gamma}_C = \begin{pmatrix} \mu^2 & 1 & 0 & 0 & -\mu & 0 & 0 \\ 0 & 0 & -1 & \mu & 0 & 0 & 0 \\ 0 & 0 & 0 & 0 & 0 & \mu & -1 \end{pmatrix}, \quad \mathbf{\Gamma}_\sigma = \begin{pmatrix} -\mu & 0 & 0 & 0 \\ 0 & 1 & 0 & 0 \\ 0 & 0 & 1 & 0 \\ 0 & 0 & -\mu & 0 \\ 1 & 0 & 0 & 0 \\ 0 & 0 & 0 & -\mu \\ 0 & 0 & 0 & 1 \end{pmatrix}. \tag{2.35}$$

This is a system of three equations, however, there are four unknowns, l_i, to be found. In order to find all four components of $\mathbf{l}$ the symmetry of the stress tensor must also be considered. This gives us $\sigma_{12} = \sigma_{21}$, which in turn gives that $\psi_{1,1} = -\psi_{2,2}$. From here it is seen that l_1 and l_2 are related by the additional constraint

$$l_1 = -\mu l_2. \tag{2.36}$$

With these four relationships it was possible for Hwu (2008) to proceed to find the vectors $\mathbf{l}$.

Making use of (2.36) the equation (2.34) is reduced to

$$\mathbf{\Gamma}_C\mathbf{S}_p\mathbf{\Gamma}_\sigma^-\mathbf{l}_{-1} = 0, \tag{2.37}$$

where

$$\mathbf{l}_{-1} = \begin{pmatrix} l_2 \\ l_3 \\ l_4 \end{pmatrix}, \qquad \mathbf{\Gamma}_{\sigma}^{-} = \begin{pmatrix} \mu^2 & 0 & 0 \\ 1 & 0 & 0 \\ 0 & 1 & 0 \\ 0 & -\mu & 0 \\ -\mu & 0 & 0 \\ 0 & 0 & -\mu \\ 0 & 0 & 1 \end{pmatrix}. \tag{2.38}$$

Solving this eigenvalue problem Hwu (1993) once again found that the eight values obtained for μ were four sets of complex conjugate numbers. Once again taking those values of μ with positive imaginary part it is possible to find four distinct vectors, $\mathbf{l}_{-}$, which can then be used to find $\mathbf{l} = (-\mu l_2, l_2, l_3, l_4)^T$. These eigenvectors are then used to construct the required matrix $\mathbf{L}$.

With the matrix $\mathbf{L}$ now found Hwu (2008) made use of equation (2.30) in order to find $\mathbf{A}$. Substituting $u_i = a_i f(z)$ along with $\psi_i = l_i f(z)$ into equation (2.30) gives

$$\mathbf{\Gamma}_{\varepsilon}\mathbf{a} = \mathbf{S}_p\mathbf{\Gamma}_{\sigma}\mathbf{l}, \tag{2.39}$$

where

$$\mathbf{\Gamma}_{\varepsilon} = \begin{pmatrix} 1 & 0 & 0 & 0 & \mu & 0 & 0 \\ 0 & \mu & 0 & 0 & 1 & 0 & 0 \\ 0 & 0 & \mu & 1 & 0 & 0 & 0 \\ 0 & 0 & 0 & 0 & 0 & 1 & \mu \end{pmatrix}^T. \tag{2.40}$$

In order to find the vectors $\mathbf{a}$ a matrix, $\mathbf{\Gamma}_{\varepsilon}^{-}$, which satisfies the relationship $\mathbf{\Gamma}_{\varepsilon}^{-}\mathbf{\Gamma}_{\varepsilon} = \mathbf{I}$ is required. It was found in Hwu (2008) that the matrix which

satisfies this condition is given by

$$\mathbf{\Gamma}_{\varepsilon}^{-} = \begin{pmatrix} 1 & 0 & 0 & 0 & 0 & 0 & 0 \\ 0 & \frac{1}{\mu} & 0 & 0 & 0 & 0 & 0 \\ 0 & 0 & \frac{1}{\mu} & 0 & 0 & 0 & 0 \\ 0 & 0 & 0 & 0 & 0 & 1 & 0 \end{pmatrix}. \tag{2.41}$$

This means that it is now possible to write an expression for $\mathbf{a}$:

$$\mathbf{a} = \mathbf{\Gamma}_{\varepsilon}^{-}\mathbf{S}_{p}\mathbf{\Gamma}_{\sigma}\mathbf{l}. \tag{2.42}$$

Using the four vectors, $\mathbf{l}$, found from the eigenvalue problem (2.38) it is now possible to use equation (2.42) to find the four corresponding vectors $\mathbf{a}$ which are then used as the four columns of the matrix $\mathbf{A}$.

With the matrices $\mathbf{A}$ and $\mathbf{L}$ found the single material matrix $\mathbf{B}$ can once again be constructed and in the context of a bimaterial it is then possible to find $\mathbf{H}$. The decision over which formalism to choose out of Stroh and Lekhnitskii is dependent on the preferred method of the author as both give the same results. In this thesis we use the Stroh formalism when considering anisotropic materials in Chapters 3 and 4 whereas we use the Lekhnitskii formalism when considering piezoelectric bimaterials in Chapter 5.

2.3 Mathematical concepts

Here we present a number of mathematical techniques that will be used throughout the remainder of the thesis. To begin we define an analytic function in the complex plane before proceeding to look at the Cauchy integral formula and its inversion. We then define the Fourier transform of a function and discuss the many useful properties associated with these transforms

that make them such an efficient tool when solving partial differential equations. Finally, Green's second identity is presented and its application to displacement and traction fields in a half-plane are introduced.

2.3.1 Analyticity

When using functions of complex variables analyticity is an important property of said function. A function $f(z)$ of a complex variable $z = x + iy$ is said to be analytic at z if f is infinitely differentiable with respect to z at that point. For an open and connected region of the complex plane, Γ, it is said that f is analytic on Γ if it is analytic for every point $z \in \Gamma$. If f is analytic on the region Γ then it will satisfy the Cauchy-Riemann equations which state that if f is written in the form $f(z) = u(x, y) + iv(x, y)$:

$$\frac{\partial u}{\partial x} = \frac{\partial v}{\partial y}, \qquad \frac{\partial u}{\partial y} = -\frac{\partial v}{\partial x}, \tag{2.43}$$

for every point $z \in \Gamma$. As a direct result of the Cauchy-Riemann equations it is clear that if f is analytic on the region Γ then both u and v are harmonic in Γ.

2.3.2 Cauchy integrals

Throughout the remainder of the thesis we will consider integrals on closed domains and contours in the complex plane. Here we demonstrate some important results which will be of use when solving such problems.

If a function $f(z)$ is analytic on the track and inside of a closed Jordan contour, Γ, then the Cauchy integral theorem states that

$$\int_{\Gamma} f(z)\mathrm{d}z = 0. \tag{2.44}$$

Under the same conditions, if a is a point inside of Γ then the Cauchy integral formula is given by

$$f(a) = \frac{1}{2\pi i} \int_{\Gamma} \frac{f(z)}{z-a} \mathrm{d}z. \tag{2.45}$$

A more generalised Cauchy integral formula can be written as

$$f^{(n)}(a) = \frac{n!}{2\pi i} \int_{\Gamma} \frac{f(z)}{(z-a)^{n+1}} \mathrm{d}z, \tag{2.46}$$

where (2.45) is obtained when $n = 0$.

A number of the problems seen later in the thesis are of the form

$$f(z) = \frac{1}{2\pi i} \int_{L} \frac{g(t)}{t-z} \mathrm{d}t, \tag{2.47}$$

where L is the union of smooth arcs and closed contours. When considering such problems it is often desirable that the function, g, satisfies the Hölder condition on each arc or contour of L. The function is said to satisfy the Hölder condition along an arc, T, if for any $t_1, t_2 \in T$ the following condition holds: $|g(t_2) - g(t_1)| \leq A|t_2 - t_1|^c$. A and c are both positive constants called the Hölder constant and index respectively. If $0 < c \leq 1$ then g is a Hölder continuous function and in the specific case where $c = 1$ it is said that g satisifes the Lipschitz condition.

When integrating over arcs it is common convention to refer to the positive and negative side of the arc as the left and right sides relative to the direction of traversal respectively. Closed contours are traversed in a counter-clockwise direction so that the positive side is the enclosed region inside the contour and the negative side is the outer region. The limit of a function, f, from the positive and negative directions shall be denoted f^+ and f^- respectively. Making use of this notation, the Plemelj formulae state that for

the problem considered in (2.47):

$$f^+(z) = \frac{1}{2}g(z) + \frac{1}{2\pi i}\int_L \frac{g(t)}{t-z}\mathrm{d}t, \tag{2.48}$$

$$f^-(z) = -\frac{1}{2}g(z) + \frac{1}{2\pi i}\int_L \frac{g(t)}{t-z}\mathrm{d}t. \tag{2.49}$$

In turn these equations can be use to derive equations relating the approach of the functions f^+ and f^- along L. Firstly by subtracting (2.49) from (2.48):

$$\begin{aligned} f^+(z) - f^-(z) &= \frac{1}{2}g(z) + \frac{1}{2\pi i}\int_L \frac{g(t)}{t-z}\mathrm{d}t + \frac{1}{2}g(z) - \frac{1}{2\pi i}\int_L \frac{g(t)}{t-z}\mathrm{d}t, \\ &= g(z). \end{aligned} \tag{2.50}$$

Additionally, if (2.48) and (2.49) are added together the following important relationship is obtained:

$$\begin{aligned} f^+(z) + f^-(z) &= \frac{1}{2}g(z) + \frac{1}{2\pi i}\int_L \frac{g(t)}{t-z}\mathrm{d}t - \frac{1}{2}g(z) + \frac{1}{2\pi i}\int_L \frac{g(t)}{t-z}\mathrm{d}t, \\ &= \frac{1}{\pi i}\int_L \frac{g(t)}{t-z}\mathrm{d}t. \end{aligned} \tag{2.51}$$

Muskhelishvili (1963) made use of all of these properties to invert the following problem:

$$f(z) = \frac{1}{\pi i}\int_L \frac{\phi(t)}{t-z}\mathrm{d}t, \tag{2.52}$$

where L is the union of a finite number of non-closed arcs, ϕ is an unknown function and f is known and satisfies the Hölder condition along L. The inversion of this problem will be useful for the remainder of the thesis, in particular Chapter 5.

Muskhelishvili (1963) introduced the holomorphic function $\Phi(z)$ which vanishes at ∞, given by:

$$\Phi(z) = \frac{1}{2\pi i}\int_L \frac{\phi(t)}{t-z}\mathrm{d}t. \tag{2.53}$$

It then follows immediately from (2.51) that

$$\Phi^+(z) + \Phi^-(z) = \frac{1}{\pi i}\int_L \frac{\phi(t)}{t-z}\mathrm{d}t = f(z), \tag{2.54}$$

which can be used to find Φ. Once Φ is known (2.50) can then be used in order to find ϕ.

Muskhelishvili (1963) solved for $\Phi(z)$:

$$\Phi(z) = \frac{\sqrt{R_1(z)}}{2\pi i\sqrt{R_2(z)}}\int_L \frac{\sqrt{R_2(t)}f(t)}{\sqrt{R_1(t)}(t-z)}\mathrm{d}t + \frac{Q_{p-1}(z)}{\sqrt{R(z)}}, \tag{2.55}$$

where Q_{p-1} is an arbitrary polynomial with degree less than or equal to $p-1$ and p is the number of arcs contained in L. The remaining terms in the solution are given by:

$$R_1(z) = \prod_{k=1}^{q}(z-c_k), \quad R_2(z) = \prod_{k=q+1}^{2p}(z-c_k),$$

$$R(z) = R_1(z)R_2(z) = \prod_{k+1}^{2p}(z-c_k).$$

Here, c_k are the end points of the arcs contained in L and $c_1, ..., c_q$ are all the endpoints at which the solution is bounded.

Using the Plemelj formula Muskhelishvili (1963) found that

$$\phi(z) = \frac{\sqrt{R_1(z)}}{\pi i\sqrt{R_2(z)}}\int_L \frac{\sqrt{R_2(t)}f(t)}{\sqrt{R_1(t)}(t-z)}\mathrm{d}t + \frac{P_{p-1}(z)}{\sqrt{R(z)}}, \tag{2.56}$$

where P_{p-1} is an arbitrary polynomial defined in a similar manner to Q_{p-1}.

The types of problems in this thesis concern cracks along the negative real-axis along which we'll need to integrate. We now consider the specific example when L consist of of one arc along this portion of the real axis: $\{x_1 < 0, x_2 = 0\}$. To do this we first consider the region $\{-a < x_1 < 0, x_2 = 0\}$ then take the limit as a goes to ∞. The problem to invert is therefore

$$f(z) = \frac{1}{\pi i}\int_{-a}^{0} \frac{\phi(t)}{t-z}\mathrm{d}t. \tag{2.57}$$

For the problems in this thesis the solution is required to be bounded at $-a$ but unbounded at 0. With these additional constraints the equation found by Muskhelishvili (1963) yields the following expression for $\phi(z)$:

$$\phi(z) = \frac{\sqrt{z+a}}{\pi i\sqrt{z}} \int_{-a}^{0} \frac{\sqrt{t} f(t)}{\sqrt{t+a}(t-z)} \mathrm{d}t + \frac{P_0}{\sqrt{z(z+a)}}, \tag{2.58}$$

where P_0 is an arbitrary constant. Taking the limit as a goes to ∞ gives

$$\phi(z) = \frac{1}{\pi i} \int_{-\infty}^{0} \sqrt{\frac{t}{z}} \frac{f(t)}{t-z} \mathrm{d}t. \tag{2.59}$$

2.3.3 Fourier transforms

When working with partial differential equations it is often useful to use Fourier transforms in order to solve them. The Fourier transform of an integrable function $f(x_1)$ is defined as

$$\mathcal{F}\left[f(x_1)\right] = \bar{f}(\xi) = \int_{-\infty}^{\infty} f(x_1) e^{i\xi x_1} \mathrm{d}x_1. \tag{2.60}$$

If the Fourier transform of f is also integrable it is possible to reobtain the original function using the inverse Fourier transform, given by:

$$\mathcal{F}^{-1}\left[\bar{f}(\xi)\right] = f(x_1) = \frac{1}{2\pi} \int_{-\infty}^{\infty} \bar{f}(\xi) e^{-i\xi x_1} \mathrm{d}\xi. \tag{2.61}$$

We now present some of the properties of Fourier transforms that make them such an effective tool for the solving of partial differential equations:

LINEARITY. For two integrable functions f and g and two constants $\alpha, \beta \in \mathcal{R}$ the following result holds:

$$\mathcal{F}\left[\alpha f(x_1) + \beta g(x_1)\right] = \alpha \bar{f}(\xi) + \beta \bar{g}(\xi). \tag{2.62}$$

CONVOLUTION. The Fourier transform of the convolution of two integrable functions f and g is:

$$\mathcal{F}\left[f * g(x_1)\right] = \bar{f}(\xi)\bar{g}(\xi). \tag{2.63}$$

DERIVATIVE. The Fourier transform of the derivative of a differentiable function f is:

$$\mathcal{F}\left[f'(x_1)\right] = -i\xi\bar{f}(\xi). \tag{2.64}$$

2.3.4 Green's second identity

In this final section of this chapter we give Green's second identity and show how it can be used in solid mechanics to relate displacement and traction fields.

Green's second identity. For two functions ψ, ϕ which are both continuous and differentiable on a volume, V, Green's second identity states that:

$$\int_V (\psi\Delta\phi - \phi\Delta\psi)\mathrm{d}V = \int_{\partial V} \left(\psi\frac{\partial\phi}{\partial\mathbf{n}} - \phi\frac{\partial\psi}{\partial\mathbf{n}}\right)\mathrm{d}S, \tag{2.65}$$

where ∂V is the surface of the volume, V. The derivative terms are taken with respect to $\mathbf{n}$, the normal of the surface, and can also be written in the form: $\partial f/\partial\mathbf{n} = \nabla f \cdot \mathbf{n}$.

We now consider a simple example of Mode III fields in a two-dimensional, infinite, homogeneous, isotropic body. Two displacement fields over the same body will be denoted $u^{(1)}, u^{(2)}$ with both disappearing at infinity. In an isotropic material both of these displacement fields must satisfy Laplace's equation ($\Delta u^{(1)} = \Delta u^{(2)} = 0$) and therefore

$$\int_V \left[u^{(2)}\Delta u^{(1)} - u^{(1)}\Delta u^{(2)}\right]\mathrm{d}V = 0, \tag{2.66}$$

for any volume V. Making use of Green's second identity:

$$\int_{\partial V} \left[u^{(2)}\nabla u^{(1)}\cdot\mathbf{n} - u^{(1)}\nabla u^{(2)}\cdot\mathbf{n}\right]\mathrm{d}S = 0. \tag{2.67}$$

In isotropic materials $\mu\nabla u = \sigma_{i3}$ where μ is the shear modulus of the material. This gives

$$\int_{\partial V} \left[\frac{u^2 \sigma_{i3}^{(1)} \cdot \mathbf{n}}{\mu} - \frac{u^1 \sigma_{i3}^{(2)} \cdot \mathbf{n}}{\mu} \right] \mathrm{d}S = 0. \tag{2.68}$$

which then simplifies to

$$\int_{\partial V} \left[u^{(2)} \sigma_{i3}^{(1)} \cdot \mathbf{n} - u^{(1)} \sigma_{i3}^{(2)} \cdot \mathbf{n} \right] \mathrm{d}S = 0. \tag{2.69}$$

As an example of the direct application of this type of equation the volume, V, is taken to be the semi-circular domain of radius r in the upper-half plane with flat edge along the x_1-axis. If we denote the curved portion of the domain as R then the integral can be split in the following manner:

$$\int_{-r}^{r} \left[u^{(2)} \sigma_{i3}^{(1)} \cdot \mathbf{n} - u^{(1)} \sigma_{i3}^{(2)} \cdot \mathbf{n} \right] \mathrm{d}x_1 + \int_{R} \left[u^{(2)} \sigma_{i3}^{(1)} \cdot \mathbf{n} - u^{(1)} \sigma_{i3}^{(2)} \cdot \mathbf{n} \right] \mathrm{d}S = 0. \tag{2.70}$$

Taking this integral over the whole upper half-plane, that is as r tends to infinity:

$$\int_{x_2=0^+} \left[u^{(2)} \sigma_{i3}^{(1)} \cdot \mathbf{n} - u^{(1)} \sigma_{i3}^{(2)} \cdot \mathbf{n} \right] \mathrm{d}x_1 = 0, \tag{2.71}$$

with the second terms disappearing as a result of both displacement fields vanishing at infinity. This then simplifies to

$$\int_{x_2=0^+} \left[u^{(2)} \sigma_{23}^{(1)} - u^{(1)} \sigma_{23}^{(2)} \right] \mathrm{d}x_1 = 0. \tag{2.72}$$

A similar equation can be found using the lower half-plane

$$\int_{x_2=0^-} \left[u^{(2)} \sigma_{23}^{(1)} - u^{(1)} \sigma_{23}^{(2)} \right] \mathrm{d}x_1 = 0. \tag{2.73}$$

In the problems considered in this thesis we consider bimaterials with a semi-infinite crack and interface situated along the x_1-axis. By taking linear combinations of equations (2.72) and (2.73), or similar equations for Mode

I and Mode II fields, it is possible to find relationships between the average and jump in displacement and stresses of the two fields. Explicit examples of how weight functions are used to find physical fields using similar expressions to (2.72) and (2.73) will be seen in the remaining chapters.

Chapter 3

Weight function approach to derive stress intensity factors and energy release rates for a dynamic semi-infinite crack lying along a perfect interface in an anisotropic bimaterial

This chapter sees the beginning of the new work for the thesis. We begin by looking at a dynamic semi-infinite crack propagating at a constant speed along a perfect interface in an anisotropic bimaterial. For the purpose of this chapter only the in-plane (Modes I and II) fields are considered as Mode III fields are non-oscillatory and we seek to examine the effect of the velocity

on the oscillations at the crack tip. The main focus here is to find a method which can be used to derive stress intensity factors for arbitrary loads acting on the crack faces. Making use of these stress intensity factors it is then possible to calculate the energy release rate and see the effect that the forces acting on the crack faces and the velocity have on the propagation. Further to this, we also present a method which can be used to derive further asymptotic coefficients for any loading configuration.

The analogous problem for a static crack has been studied previously for isotropic and anisotropic bimaterials in Piccolroaz et al. (2009) and Morini et al. (2013b) respectively. Both papers employed Betti's reciprocal theorem and the weight function developed in Willis and Movchan (1995) in their analysis. The same method is used here with suitable changes being made to incorporate the crack speed.

The chapter is organised as follows: Chapter 3.1 sees the mathematical formulation of the problem and gives some extended background specific to the work in this chapter. The incorporation of the crack velocity to the Stroh formalism (Stroh, 1962) seen in Chapter 2 is given. The method shown is that of Yang et al. (1991) which is based on the previously discussed results seen in Suo (1990). A full definition of the Willis and Movchan (1995) weight function, and its incorporation in the Betti identity (which is the matricial extension of the results reported in Chapter 2.3.4), is also given. Chapter 3.2 sees the beginning of the new work with the derivation of weight function matrices for a semi-infinite crack propagating at constant speed at the interface between two dissimilar orthotropic materials under plane deformation. In Chapter 3.3, using the newly derived explicit weight functions together

with the Betti integral theorem, general formulae for stress intensity factors and higher order asymptotic terms are obtained. By means of the developed approach, both symmetric and skew-symmetric loading configurations acting on the crack faces can be considered, and higher order asymptotic terms can also be computed for non-smooth loading functions. The derived stress intensity factors are then used to evaluate the energy release rate. Two illustrative examples of numerical computations for a specific asymmetric load are presented in Chapter 3.4. To conclude, the effects of the loadings asymmetry on the energy release rate and the dependence of stress intensity factors on the crack tip velocity are discussed, and possible physical implications of these results on the continuing propagation of the crack are explored.

3.1 Problem formulation

We now introduce the mathematical framework of the model used for the remainder of the chapter. Existing results regarding the extension of the Stroh formalism to a dynamic setting, weight functions and the Betti formula are also reported.

The model used consists of a semi-infinite crack propagating at a constant speed, v, along a perfect interface between two semi-infinite anisotropic materials. The crack is said to be occupying the region $x_1 - vt < 0, x_2 = 0$, as illustrated in Figure 3.1.

Considering the Cartesian coordinate system shown in Figure 3.1, the traction on the crack faces is defined as follows

$$\sigma_{2i}(x_1 - vt, 0^{\pm}) = p_i^{\pm}(x_1 - vt) \quad \text{for} \quad x_1 - vt < 0, \tag{3.1}$$

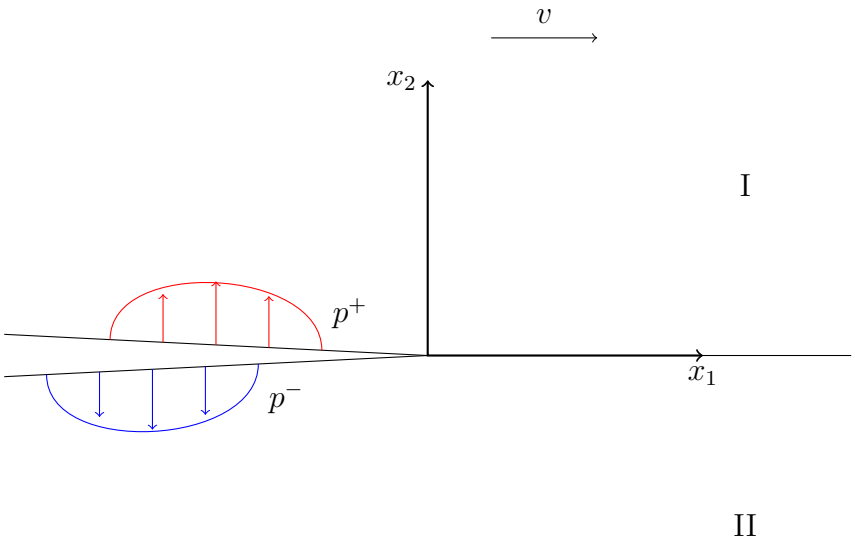

Figure 3.1: Geometry

and body forces are assumed to be zero. The only restriction on the loading considered in this chapter is that it must vanish within a region of the crack tip.

3.1.1 Extension of the Stroh formalism to a steady state interfacial crack

Here we present the changes to the Stroh formalism (seen in Chapter 2) when the crack is no longer static. We begin by recalling that for both anisotropic elastic media, occupying the upper and the lower half-planes in Figure 3.1, Hooke's law is given by

$$\sigma_{ij} = C_{ijkl}\epsilon_{kl} = C_{ijkl}\frac{\partial u_k}{\partial x_l}, \quad \text{for } i,j,k,l = 1,2, \tag{3.2}$$

where σ is the stress, ϵ is the strain and C is the stiffness tensor for the material. Furthermore, the following relationship relating the stress and

displacement is also used

$$\sum_{j=1}^{2} \frac{\partial \sigma_{ij}}{\partial x_j} = \rho \frac{\partial^2 u_i}{\partial t^2}, \tag{3.3}$$

where v is the crack speed and ρ is the material density. Combining (3.2) and (3.3) gives

$$C_{ijkl} \frac{\partial^2 u_k}{\partial x_j \partial x_l} = \rho \frac{\partial^2 u_i}{\partial t^2}. \tag{3.4}$$

A new coordinate system is now introduced: $(\tilde{x}_1 = x_1 - vt, \tilde{x}_2 = x_2)$. The following relationship is therefore found in this new coordinate system

$$\tilde{C}_{ijkl} \frac{\partial^2 u_k}{\partial \tilde{x}_j \partial \tilde{x}_l} = 0, \tag{3.5}$$

where $\tilde{C}_{ijkl} = C_{ijkl} - \rho v^2 \delta_{ik} \delta_{1j} \delta_{1l}$.

From this stage, for convenience, the steady state coordinates will be written as $\tilde{x}_1 = x$ and $\tilde{x}_2 = y$. Following the same procedure as was used for a static crack (Stroh, 1962), a solution is found in the form $u_i = A_i f(x + \mu y)$ to yield the eigenvalue problem

$$[\mathbf{Q} + \mu(\mathbf{R} + \mathbf{R}^T) + \mu^2 \mathbf{T}]\mathbf{A} = 0. \tag{3.6}$$

Despite looking identical to the eigenvalue problem seen for a static crack it is important to note that there is a fundamental change to one of the material matrices. The matrix $\mathbf{Q}$ is now given by $\mathbf{Q} = C_{i1k1} - \rho v^2 \delta_{ik}$, and therefore depends on both the material constants and the crack speed. However, $\mathbf{R} = C_{i1k2}$ and $\mathbf{T} = C_{i2k2}$ depend only on elastic constants of the material. This eigenvalue problem has previously been solved and general expressions for the traction and displacement fields can be found in Yang et al. (1991) and Ting (1996). At this stage we remind ourselves of the following single material

matrices:

$$\mathbf{L} = (\mathbf{R}^T + \mu\mathbf{T})\mathbf{A}, \qquad \mathbf{B} = i\mathbf{A}\mathbf{L}^{-1}.$$

It is also important, for further analysis, to re-introduce the bimaterial matrix $\mathbf{H} = \mathbf{B}_I + \mathbf{B}_{II}^{\star}$ and define the additional matrix $\mathbf{W} = \mathbf{B}_I - \mathbf{B}_{II}^{\star}$. It is important to note that, in the considered dynamic steady-state case, the matrices $\mathbf{A}, \mathbf{L}, \mathbf{B}, \mathbf{H}$ and $\mathbf{W}$ all depend on both the elastic constants for the materials and the crack speed, v.

The work seen in Suo (1990) has been extended to the steady-state crack by Yang et al. (1991) using the new coordinates x and y . Considering the traction-free condition, the following Riemann-Hilbert problem is satisfied along the negative portion of the real axis (Suo, 1990)

$$\mathbf{h}^{+}(x) + (\mathbf{H}^{\star})^{-1}\mathbf{H}\mathbf{h}^{-}(x) = 0, \quad -\infty < x < 0. \tag{3.7}$$

Once again the solution, $\mathbf{h}(z)$, is found in the form $\mathbf{h}(z) = \mathbf{w}z^{-\frac{1}{2}+i\epsilon}$, where $z = x + \mu y$ and the branch cut of $\mathbf{h}(z)$ is placed along the negative real axis. Combining this solution with (3.7) gives the eigenvalue problem

$$\mathbf{H}^{\star}\mathbf{w} = e^{2\pi\epsilon}\mathbf{H}\mathbf{w}, \tag{3.8}$$

which can be used to find ϵ and $\mathbf{w}$, both of which depend on the crack velocity (Yang et al., 1991). Making use of the results obtained from (3.8) expressions were found for the interfacial tractions and displacement jump over the crack faces by Yang et al. (1991). The expressions found once again look identical to those reported for the static case in Chapter 2 (Suo, 1990) but differ due to the incorporation of the moving crack into the material matrices and moving coordinate system.

For the physical problem with forces acting on the crack faces the asymptotic expansions of the physical traction and the jump in displacement across the interface, as $x \to 0$, can be written as follows (Morini et al., 2013b):

$$[\![\mathbf{u}]\!](x) = \frac{(-x)^{\frac{1}{2}}}{\sqrt{2\pi}}\boldsymbol{\mathcal{U}}(x)\mathbf{K} + \frac{(-x)^{\frac{3}{2}}}{\sqrt{2\pi}}\boldsymbol{\mathcal{U}}(x)\mathbf{Y}_2 + \frac{(-x)^{\frac{5}{2}}}{\sqrt{2\pi}}\boldsymbol{\mathcal{U}}(x)\mathbf{Y}_3 + \mathcal{O}((-x)^{\frac{7}{2}}), \quad (3.9)$$

$$\mathbf{t}(x) = \frac{x^{-\frac{1}{2}}}{2\sqrt{2\pi}}\boldsymbol{\mathcal{T}}(x)\mathbf{K} + \frac{x^{\frac{1}{2}}}{2\sqrt{2\pi}}\boldsymbol{\mathcal{T}}(x)\mathbf{Y}_2 + \frac{x^{\frac{3}{2}}}{2\sqrt{2\pi}}\boldsymbol{\mathcal{T}}(x)\mathbf{Y}_3 + \mathcal{O}(x^{\frac{5}{2}}), \quad (3.10)$$

where $\mathbf{K} = [K, K^\star]$ and $\mathbf{Y}_i = [Y_i, Y_i^\star]$. $K = K_1 + iK_2$ is the complex stress intensity factor and Y_i are constants derived in the same manner as the in order to find further terms in the asymptotic expansions. The matrices $\boldsymbol{\mathcal{U}}(x)$ and $\boldsymbol{\mathcal{T}}(x)$ are represented as follows

$$\boldsymbol{\mathcal{U}}(x) = \frac{2(\mathbf{H} + \mathbf{H}^\star)}{\cosh \pi\epsilon}\left[\frac{\mathbf{w}(-x)^{i\epsilon}}{1+2i\epsilon}, \frac{\mathbf{w}^\star(-x)^{-i\epsilon}}{1-2i\epsilon}\right], \qquad \boldsymbol{\mathcal{T}}(x) = 2\left[\mathbf{w}x^{i\epsilon}, \mathbf{w}^\star x^{-i\epsilon}\right]. \quad (3.11)$$

An explicit formula for computing the stress intensity factor for symmetric loading was given in Suo (1990). Whilst this expression is correct it is highly restricted as it is often desirable to use a non-symmetric loading configuration. In this chapter we will often split the stress intensity factor into two parts corresponding to the symmetric, $\mathbf{K}^S$, and asymmetric, $\mathbf{K}^A$, parts of the loading, given as $\langle\mathbf{p}\rangle$ and $[\![\mathbf{p}]\!]$ respectively. The expression found for the symmetric load (Suo, 1990) is written, using the notation of this chapter, below:

$$\mathbf{K}^S = -\left(\frac{2}{\pi}\right)^{\frac{1}{2}} \cosh \pi\epsilon \int_{-\infty}^{0} (-x)^{-\frac{1}{2}-i\epsilon}\langle\mathbf{p}_1\rangle(x)\mathrm{d}x, \quad (3.12)$$

where the vector $\langle\mathbf{p}_1\rangle(x)$ is related to the applied traction $\mathbf{p}(x)$ in the following way

$$\langle\mathbf{p}_1\rangle = \frac{\mathbf{w}^{\star T}\mathbf{H}\langle\mathbf{p}\rangle}{\mathbf{w}^{\star T}\mathbf{H}\mathbf{w}}.$$

Once the stress intensity factors are found it is possible to evaluate the energy release rate. The expression found by Irwin (1957) was for a static crack:

$$G = \frac{1}{2\Delta} \int_0^{\Delta} \mathbf{t}^T(\Delta - r)[\![\mathbf{u}]\!](r)\mathrm{d}r, \tag{3.13}$$

where Δ is an arbitrary length scale. However, it was stated in Yu and Suo (2000) that this equation can still be used with an arbitrary Δ as long as the crack is moving at subsonic speeds. In order to use the moving co-ordinate system introduced in this chapter only sub-Rayleigh wave speeds are considered. Therefore it is still possible to use equation (3.13) for our steady state formulation as sub-Rayleigh waves are always subsonic. As only the in-plane fields are being analysed in this chapter the portion of the energy release rate we seek to find is given by

$$G = \frac{\mathbf{w}^{\star T}(\mathbf{H} + \bar{\mathbf{H}})\mathbf{w}|K|^2}{4\cosh^2(\pi\epsilon)}. \tag{3.14}$$

The value of G will change as the crack moves at different speeds and this is one of the key features we seek to explore in this chapter, with the results being shown in Chapter 3.4.

3.1.2 Weight Functions

The weight function $\mathbf{U}$ is now defined in the same vein as Willis and Movchan (1995). $\mathbf{U} = (U_1, U_2)^T$ is the displacement field with a square root singularity at the crack tip that is obtained from the problem where the steady-state crack occupies the region of the x-axis with $x > 0$. Therefore $\mathbf{U}$ is discontinuous over the positive portion of the real axis. Despite being defined as a singular displacement field, the weight function is not a physical field and

is merely a function used to help solve the problem defined earlier in the chapter.

The symmetric and skew-symmetric parts of the weight function are given by the following expressions:

$$[\![\mathbf{U}]\!](x) = \mathbf{U}(x, 0^+) - \mathbf{U}(x, 0^-), \tag{3.15}$$

$$\langle \mathbf{U} \rangle(x) = \frac{1}{2}(\mathbf{U}(x, 0^+) + \mathbf{U}(x, 0^-)). \tag{3.16}$$

The traction field associated with the displacement field, $\mathbf{U}$, is denoted as $\mathbf{\Sigma} = (\Sigma_1, \Sigma_2)^T$ and is said to be continuous over the interface ($x < 0$) and the zero traction condition is imposed on the crack faces. Therefore, the following Riemann-Hilbert problem stands along the positive section of the real axis for this problem, as seen in Morini et al. (2013b)

$$\mathbf{h}_+(x) + (\mathbf{H}^\star)^{-1}\mathbf{H}\mathbf{h}_-(x) = 0, \qquad 0 < x < \infty, \tag{3.17}$$

A solution for $\mathbf{h}(z)$ is found in the form

$$\mathbf{h}(z) = \mathbf{v} z^{-\frac{3}{2}+i\epsilon}, \tag{3.18}$$

where the branch cut is now said to be along the positive x-axis. This gives the eigenvalue problem

$$\mathbf{H}^\star\mathbf{v} = e^{-2\pi\epsilon}\mathbf{H}\mathbf{v}. \tag{3.19}$$

$\mathbf{H}$ is positive definite hermitian and therefore it is clear, by comparing (3.19) with the solutions of (3.8), that $\mathbf{v} = \mathbf{w}^\star$.

An expression for $\mathbf{\Sigma}$ along the negative real axis is given by

$$\mathbf{\Sigma}(x) = \mathbf{h}_+(x) + (\mathbf{H}^\star)^{-1}\mathbf{H}\mathbf{h}_-(x), \qquad -\infty < x < 0. \tag{3.20}$$

Therefore the singular traction in the steady state has the form Morini et al. (2013b)

$$\mathbf{\Sigma}(x) = \frac{(-x)^{-\frac{3}{2}}}{\sqrt{2\pi}}\mathrm{Re}(R(-x)^{i\epsilon}\mathbf{w}^{\star}), \tag{3.21}$$

where $R = R_1 + iR_2$ is an arbitrary, complex number in a similar fashion to the stress intensity factor for the physical problem. By considering the results obtained for $\mathbf{\Sigma}$ when $\{R_1 = 1, R_2 = 0\}$ and $\{R_1 = 0, R_2 = 1\}$ it is possible to obtain two linearly independent vectors, and therefore a 2×2 matrix representing $\mathbf{\Sigma}$ (Piccolroaz et al., 2009).

Expressions relating the Fourier transform of the symmetric and skew-symmetric weight functions were found in Morini et al. (2013b) following from the work seen in Piccolroaz et al. (2007)

$$[\![\bar{\mathbf{U}}]\!]^{+}(\xi) = \frac{1}{|\xi|}(i\mathrm{sign}(\xi)\mathrm{Im}(\mathbf{H}) - \mathrm{Re}(\mathbf{H}))\bar{\Sigma}^{-}(\xi), \tag{3.22}$$

$$\langle\bar{\mathbf{U}}\rangle(\xi) = \frac{1}{2|\xi|}(i\mathrm{sign}(\xi)\mathrm{Im}(\mathbf{W}) - \mathrm{Re}(\mathbf{W}))\bar{\Sigma}^{-}(\xi). \tag{3.23}$$

Here the superscripts $\pm$ denotes whether the function is analytic in the upper or lower half plane respectively.

3.1.3 Betti Formula

It was mentioned previously that there are now two displacement fields to consider; the physical displacement, $\mathbf{u}$, and the singular displacement, $\mathbf{U}$. However, $\mathbf{U}$ is discontinuous across the x-axis for $x > 0$ whereas $\mathbf{u}$ is discontinuous across the x-axis for $x < 0$. Also considered is the traction associated with $\mathbf{U}$, given by $\mathbf{\Sigma}$, which is continuous when $x < 0$ and the traction $\mathbf{t}$ associated with $\mathbf{u}$ which is continuous when $x > 0$.

It was shown in Willis and Movchan (1995) that the Betti formula still holds for a crack moving with constant speed. Therefore, the following expressions are found along the upper and lower parts of the real axis, respectively

$$\int_{-\infty}^{\infty} \{\boldsymbol{\mathcal{R}}\mathbf{U}(x'-x,0^+)\cdot\boldsymbol{\sigma}(x,0^+) - \boldsymbol{\mathcal{R}}\boldsymbol{\Sigma}(x'-x,0^+)\cdot\mathbf{u}(x,0^+)\}\mathrm{d}x = 0, \tag{3.24}$$

$$\int_{-\infty}^{\infty} \{\boldsymbol{\mathcal{R}}\mathbf{U}(x'-x,0^-)\cdot\boldsymbol{\sigma}(x,0^-) - \boldsymbol{\mathcal{R}}\boldsymbol{\Sigma}(x'-x,0^-)\cdot\mathbf{u}(x,0^-)\}\mathrm{d}x = 0, \tag{3.25}$$

where

$$\boldsymbol{\mathcal{R}} = \begin{pmatrix} -1 & 0 \\ 0 & 1 \end{pmatrix}.$$

The homogeneous case of (3.7) is now considered. Combined with the applied traction on the crack faces, $\mathbf{p}(x)$, the following expressions for traction are obtained

$$\boldsymbol{\sigma}_{2i}(x,y=0^+) = \mathbf{p}^+(x) + \mathbf{t}(x), \qquad \boldsymbol{\sigma}_{2i}(x,y=0^-) = \mathbf{p}^-(x) + \mathbf{t}(x). \tag{3.26}$$

Subtracting (3.25) from (3.24) and using (3.26), along with the definition of the symmetric and skew-symmetric parts of the weight function, the following formula is obtained

$$\begin{aligned} &\int_{-\infty}^{\infty} \{\boldsymbol{\mathcal{R}}[\![\mathbf{U}]\!](x'-x)\cdot\mathbf{t}(x) - \boldsymbol{\mathcal{R}}\boldsymbol{\Sigma}(x'-x,0)\cdot[\![\mathbf{u}]\!](x)\}\mathrm{d}x \\ &= -\int_{-\infty}^{\infty} \{\boldsymbol{\mathcal{R}}[\![\mathbf{U}]\!](x'-x)\cdot\langle\mathbf{p}\rangle(x) + \boldsymbol{\mathcal{R}}\langle\mathbf{U}\rangle(x'-x)\cdot[\![\mathbf{p}]\!](x)\}\mathrm{d}x. \end{aligned} \tag{3.27}$$

Here, $\langle\mathbf{p}\rangle$ and $[\![\mathbf{p}]\!]$ refer to the symmetric and skew-symmetric parts of the loading respectively.

Using the Fourier convolution theorem the following identity, which relates the Fourier transforms of the weight functions and the solutions of the

physical problem, is obtained (Piccolroaz et al., 2007; Morini et al., 2013b)

$$[\![\bar{\mathbf{U}}]\!]^{+T}\boldsymbol{\mathcal{R}}\bar{\mathbf{t}}^{+} - \bar{\boldsymbol{\Sigma}}^{-T}\boldsymbol{\mathcal{R}}[\![\bar{\mathbf{u}}]\!]^{-} = -[\![\bar{\mathbf{U}}]\!]^{+T}\boldsymbol{\mathcal{R}}\langle\bar{\mathbf{p}}\rangle - \langle\bar{\mathbf{U}}\rangle^{T}\boldsymbol{\mathcal{R}}[\![\bar{\mathbf{p}}]\!], \tag{3.28}$$

where the $\pm$ once again denotes whether the transform is analytic in the upper or lower half plane.

Further work performed in Piccolroaz et al. (2007) and Morini et al. (2013b), combining (3.22), (3.23) and (3.28), found an explicit expression for finding the stress intensity factor, $\mathbf{K}$, using the weight functions and the loading applied on the crack faces. The following expression was obtained

$$\mathbf{K} = \frac{1}{2\pi i}\boldsymbol{\mathcal{Z}}_1^{-1}\int_{-\infty}^{\infty}[\![\bar{\mathbf{U}}]\!]^{+T}(\tau)\boldsymbol{\mathcal{R}}\langle\bar{\mathbf{p}}\rangle(\tau) + \langle\bar{\mathbf{U}}\rangle^{T}(\tau)\boldsymbol{\mathcal{R}}[\![\bar{\mathbf{p}}]\!](\tau)\mathrm{d}\tau, \tag{3.29}$$

where $\boldsymbol{\mathcal{Z}}_1$ is a constant matrix derived from the asymptotic representation of (3.28). It can be shown that both expressions for $\mathbf{K}$, (3.12) and (3.29), are equivalent when the loading considered is symmetric.

Following the method developed in Piccolroaz et al. (2007) and Morini et al. (2013b) an expression for further asymptotic coefficients can be found depending on whether the applied loading is smooth and has a Fourier transform that vanishes at a fast enough rate at infinity. If this is the case the general expression for the asymptotic coefficients can be found using the equation

$$\mathbf{Y}_j = \frac{1}{2\pi i}\boldsymbol{\mathcal{Z}}_j^{-1}\int_{-\infty}^{\infty}\tau^{j-1}\{[\![\bar{\mathbf{U}}]\!]^{+T}(\tau)\boldsymbol{\mathcal{R}}\langle\bar{\mathbf{p}}\rangle(\tau) + \langle\bar{\mathbf{U}}\rangle^{T}(\tau)\boldsymbol{\mathcal{R}}[\![\bar{\mathbf{p}}]\!](\tau)\}\mathrm{d}\tau. \tag{3.30}$$

Here, $\boldsymbol{\mathcal{Z}}_j$ is also derived from the asymptotic representation of (3.28). An example of finding $\boldsymbol{\mathcal{Z}}_2$ for orthotropic bimaterials is shown later in the chapter.

3.2 Steady-state weight functions for orthotropic bimaterials

In this section, expressions for the symmetric and skew-symmetric weight function matrices corresponding to a steady-state plane strain interfacial crack in orthotropic bimaterials are derived. Substituting the solution for $\mathbf{w}$ found in Yang et al. (1991), and shown in Appendix 1, into (3.21), and using the method used in Piccolroaz et al. (2009), yields the following linearly independent traction vectors for $-\infty < x < 0$

$$\boldsymbol{\Sigma}^1(x) = \frac{(-x)^{-\frac{3}{2}}}{2\sqrt{2\pi}} \begin{pmatrix} i[(-x)^{i\epsilon} - (-x)^{-i\epsilon}] \\ \sqrt{\frac{H_{11}}{H_{22}}}[(-x)^{i\epsilon} + (-x)^{-i\epsilon}] \end{pmatrix}, \tag{3.31}$$

$$\boldsymbol{\Sigma}^2(x) = \frac{(-x)^{-\frac{3}{2}}}{2\sqrt{2\pi}} \begin{pmatrix} -[(-x)^{i\epsilon} + (-x)^{-i\epsilon}] \\ i\sqrt{\frac{H_{11}}{H_{22}}}[(-x)^{i\epsilon} - (-x)^{-i\epsilon}] \end{pmatrix}, \tag{3.32}$$

where H_{11} and H_{22} are parameters depending on the crack tip speed and elastic constants of both considered materials. Explicit expressions for H_{11} and H_{22} have been introduced in Yang et al. (1991) and are given in Appendix 1. The branch cut for these vectors is situated along the positive real axis and polar coordinates with angle between -2π and 0 are taken. The Fourier transforms obtained are

$$\bar{\boldsymbol{\Sigma}}^{1-}(\xi) = \frac{(i\xi)^{\frac{1}{2}}\sqrt{2}}{(1+4\epsilon^2)\sqrt{\pi}} \begin{pmatrix} i\left[(-\frac{1}{2} - i\epsilon)\Gamma(\frac{1}{2} + i\epsilon)(i\xi)^{-i\epsilon} - (-\frac{1}{2} + i\epsilon)\Gamma(\frac{1}{2} - i\epsilon)(i\xi)^{i\epsilon}\right] \\ \sqrt{\frac{H_{11}}{H_{22}}}\left[(-\frac{1}{2} - i\epsilon)\Gamma(\frac{1}{2} + i\epsilon)(i\xi)^{-i\epsilon} + (-\frac{1}{2} + i\epsilon)\Gamma(\frac{1}{2} - i\epsilon)(i\xi)^{i\epsilon}\right] \end{pmatrix}, \tag{3.33}$$

$$\bar{\mathbf{\Sigma}}^{2-}(\xi) =$$

$$\frac{(i\xi)^{\frac{1}{2}}\sqrt{2}}{(1+4\epsilon^2)\sqrt{\pi}} \begin{pmatrix} -\left[(-\frac{1}{2}-i\epsilon)\Gamma(\frac{1}{2}+i\epsilon)(i\xi)^{-i\epsilon}+(-\frac{1}{2}+i\epsilon)\Gamma(\frac{1}{2}-i\epsilon)(i\xi)^{i\epsilon}\right] \\ i\sqrt{\frac{H_{11}}{H_{22}}}\left[(-\frac{1}{2}-i\epsilon)\Gamma(\frac{1}{2}+i\epsilon)(i\xi)^{-i\epsilon}-(-\frac{1}{2}+i\epsilon)\Gamma(\frac{1}{2}-i\epsilon)(i\xi)^{i\epsilon}\right] \end{pmatrix}, \tag{3.34}$$

where $\Gamma(\cdot)$ is the gamma function and the branch cut of $\bar{\mathbf{\Sigma}}^{-}$ is situated along the positive imaginary axis. Note that the expressions (3.33) and (3.34) are written using a different representation than was used in Morini et al. (2013b). The reason behind this will become clearer in Chapter 3.3.

The Fourier transforms (3.22) and (3.23) can now be computed, for $\xi \in \mathbb{R}$, with the expressions for $\mathbf{H}$ and $\mathbf{W}$ found in Yang et al. (1991) and Morini et al. (2013b) respectively

$$[\![\bar{\mathbf{U}}]\!]^{+}(\xi) = \frac{1}{|\xi|} \begin{pmatrix} -H_{11} & -i\beta\text{sign}(\xi)\sqrt{H_{11}H_{22}} \\ i\beta\text{sign}(\xi)\sqrt{H_{11}H_{22}} & -H_{22} \end{pmatrix} \bar{\mathbf{\Sigma}}^{-}(\xi), \tag{3.35}$$

$$\langle\bar{\mathbf{U}}\rangle(\xi) = \frac{1}{2|\xi|} \begin{pmatrix} -\delta_1 H_{11} & i\gamma\text{sign}(\xi)\sqrt{H_{11}H_{22}} \\ -i\gamma\text{sign}(\xi)\sqrt{H_{11}H_{22}} & -\delta_2 H_{22} \end{pmatrix} \bar{\mathbf{\Sigma}}^{-}(\xi), \tag{3.36}$$

where branch cuts are now situated along the negative imaginary axis. Here β, γ, δ_1 and δ_2 are all dimensionless parameters depending on the elastic coefficients of the bimaterial and the crack tip velocity (Yang et al., 1991). Full expressions for both matrices, $\mathbf{H}$ and $\mathbf{W}$, are stated in Appendix 1, including full expressions for the parameters β, γ, δ_1 and δ_2. It is clearly seen from the results of Yang et al. (1991) that β is of great importance when considering the oscillations near the crack tip as the oscillation index $\epsilon = 0$ when $\beta = 0$.

3.3 Evaluation of the Coefficients in the Asymptotic Expansion of the Displacement and Stress Fields for the Steady-State Crack

3.3.1 Determination of the Stress Intensity Factor

It is now possible to develop a method in order to find the stress intensity factor for an orthotropic bimaterial, similar to that seen for the static crack in Morini et al. (2013b). Making use of the eigenvalues, $\mathbf{w}$, found by Yang et al. (1991) for the case of orthotropic materials, the matrix $\boldsymbol{\mathcal{T}}(x)$ in equation (3.10) is given by

$$\boldsymbol{\mathcal{T}}(x) = \begin{pmatrix} -ix^{i\epsilon} & ix^{-i\epsilon} \\ \sqrt{\frac{H_{11}}{H_{22}}}x^{i\epsilon} & \sqrt{\frac{H_{11}}{H_{22}}}x^{-i\epsilon} \end{pmatrix}. \tag{3.37}$$

Note that this result is equivalent to (3.11) with the known value of $\mathbf{w}$ inserted. The Fourier transform of this expansion is computed in order to find the asymptotic expansion as $\xi \to \infty$, with $\mathrm{Im}(\xi) \in (0, \infty)$. The result is

$$\bar{\mathbf{t}}(\xi) = \frac{(-i\xi)^{-\frac{1}{2}}}{2\sqrt{2\pi}}\boldsymbol{\mathfrak{T}}_1(\xi)\mathbf{K} + \frac{(-i\xi)^{-\frac{3}{2}}}{2\sqrt{2\pi}}\boldsymbol{\mathfrak{T}}_2(\xi)\mathbf{Y}_2 + \mathcal{O}((\xi)^{-\frac{5}{2}}), \tag{3.38}$$

where

$$\boldsymbol{\mathfrak{T}}_1(\xi) = \begin{pmatrix} -i(-i\xi)^{-i\epsilon}\Gamma(\frac{1}{2}+i\epsilon) & i(-i\xi)^{i\epsilon}\Gamma(\frac{1}{2}-i\epsilon) \\ \sqrt{\frac{H_{11}}{H_{22}}}(-i\xi)^{-i\epsilon}\Gamma(\frac{1}{2}+i\epsilon) & \sqrt{\frac{H_{11}}{H_{22}}}(-i\xi)^{i\epsilon}\Gamma(\frac{1}{2}-i\epsilon) \end{pmatrix}, \tag{3.39}$$

$$\boldsymbol{\mathfrak{T}}_2(\xi) = \begin{pmatrix} -i(-i\xi)^{-i\epsilon}\Gamma(\frac{3}{2}+i\epsilon) & i(-i\xi)^{i\epsilon}\Gamma(\frac{3}{2}-i\epsilon) \\ \sqrt{\frac{H_{11}}{H_{22}}}(-i\xi)^{-i\epsilon}\Gamma(\frac{3}{2}+i\epsilon) & \sqrt{\frac{H_{11}}{H_{22}}}(-i\xi)^{i\epsilon}\Gamma(\frac{3}{2}-i\epsilon) \end{pmatrix}. \tag{3.40}$$

It is noted here that these expressions differ to those seen in Morini et al. (2013b) and Piccolroaz et al. (2007) to incorporate the different branch cut

used in this chapter. It is now possible to find the asymptotic expansion of the members of Betti's identity from equation (3.28), using expressions (3.35) and (3.36), as $\xi \to \infty$

$$[\![\bar{\mathbf{U}}]\!]^{+T}\boldsymbol{\mathcal{R}}\bar{\mathbf{t}}^{+} = \xi^{-1}\boldsymbol{\mathcal{Z}}_1\mathbf{K} + \xi^{-2}\boldsymbol{\mathcal{Z}}_2\mathbf{Y}_2 + \xi^{-3}\boldsymbol{\mathcal{Z}}_3\mathbf{Y}_3 + \mathcal{O}(\xi^{-4}), \quad \text{where } \mathrm{Im}(\xi) \in (0, \infty), \tag{3.41}$$

$$\bar{\boldsymbol{\Sigma}}^{-T}\boldsymbol{\mathcal{R}}[\![\bar{\mathbf{u}}]\!]^{-} = \xi^{-1}\boldsymbol{\mathcal{Z}}_1\mathbf{K} + \xi^{-2}\boldsymbol{\mathcal{Z}}_2\mathbf{Y}_2 + \xi^{-3}\boldsymbol{\mathcal{Z}}_3\mathbf{Y}_3 + \mathcal{O}(\xi^{-4}), \quad \text{where } \mathrm{Im}(\xi) \in (-\infty, 0). \tag{3.42}$$

The matrices $\boldsymbol{\mathcal{Z}}_1$ and $\boldsymbol{\mathcal{Z}}_2$ are given by

$$\boldsymbol{\mathcal{Z}}_1 = -\frac{H_{11}}{4s^+s^-(1+4\epsilon^2)}\begin{pmatrix} -\frac{(\beta-1)(1-2i\epsilon)}{E^2} & E^2(\beta+1)(1+2i\epsilon) \\ \frac{i(\beta-1)(1-2i\epsilon)}{E^2} & iE^2(\beta+1)(1+2i\epsilon) \end{pmatrix},$$

$$\boldsymbol{\mathcal{Z}}_2 = -\frac{H_{11}}{4(1+4\epsilon^2)}\begin{pmatrix} -\frac{(\beta-1)(1-2i\epsilon)}{g^+s^-E^2} & \frac{E^2(\beta+1)(1+2i\epsilon)}{s^+g^-} \\ \frac{i(\beta-1)(1-2i\epsilon)}{g^+s^-E^2} & \frac{iE^2(\beta+1)(1+2i\epsilon)}{s^+g^-} \end{pmatrix},$$

where

$$E = e^{\epsilon\frac{\pi}{2}}, \qquad s^{\pm} = \frac{(1+i)\sqrt{\pi}}{2\Gamma\left(\frac{1}{2} \pm i\epsilon\right)}, \qquad g^{\pm} = \frac{(1-i)\sqrt{\pi}}{2\Gamma\left(\frac{3}{2} \pm i\epsilon\right)}.$$

Following the method of Morini et al. (2013b), (3.28) is rewritten as

$$\boldsymbol{\psi}^{+}(\xi) - \boldsymbol{\psi}^{-}(\xi) = -[\![\bar{\mathbf{U}}]\!]^{+T}\boldsymbol{\mathcal{R}}\langle\bar{\mathbf{p}}\rangle - \langle\bar{\mathbf{U}}\rangle^{T}\boldsymbol{\mathcal{R}}[\![\bar{\mathbf{p}}]\!], \tag{3.43}$$

using the Plemelj formula it is possible to find $\boldsymbol{\psi}^{\pm}(\xi)$ using the formula

$$\boldsymbol{\psi}^{\pm}(\xi) = \frac{1}{2\pi i}\int_{-\infty}^{\infty}\frac{\boldsymbol{\psi}(\tau)}{\tau - \xi}\mathrm{d}\tau, \tag{3.44}$$

where $\boldsymbol{\psi}(\tau) = -[\![\bar{\mathbf{U}}]\!]^{+T}(\tau)\boldsymbol{\mathcal{R}}\langle\bar{\mathbf{p}}\rangle(\tau) - \langle\bar{\mathbf{U}}\rangle^{T}(\tau)\boldsymbol{\mathcal{R}}[\![\bar{\mathbf{p}}]\!](\tau)$. The solution of (3.43) is given by

$$[\![\bar{\mathbf{U}}]\!]^{+T}\boldsymbol{\mathcal{R}}\bar{\mathbf{t}}^{+} = \boldsymbol{\psi}^{+}, \qquad \text{where } \mathrm{Im}(\xi) \in (0,\infty),$$

$$\bar{\boldsymbol{\Sigma}}^{-T}\boldsymbol{\mathcal{R}}[\![\bar{\mathbf{u}}]\!]^{-} = \boldsymbol{\psi}^{-}, \qquad \text{where } \mathrm{Im}(\xi) \in (-\infty,0).$$

The asymptotic expansion of the Plemelj formula as $\xi \to \infty^{\pm}$ is given by

$$\boldsymbol{\psi}^{\pm}(\xi) = \frac{1}{2\pi i}\int_{-\infty}^{\infty}\frac{\boldsymbol{\psi}(\tau)}{\tau-\xi}\mathrm{d}\tau = \xi^{-1}\mathbf{V}_1^{\pm} + \xi^{-2}\mathbf{V}_2^{\pm} + \mathcal{O}(\xi^{-3}). \tag{3.45}$$

Comparing the terms of this asymptotic expansion with the terms of the expansions (3.41) and (3.42) it is clear that $\mathbf{V}_j^{\pm} = \boldsymbol{\mathcal{Z}}_j\mathbf{Y}_j$, where $\mathbf{Y}_1 = \mathbf{K}$. Using (3.45) it is easily seen that the stress intensity factor, $\mathbf{K}$, is given by

$$\mathbf{K} = \lim_{\xi\to\infty^{\pm}}\frac{1}{2\pi i}\boldsymbol{\mathcal{Z}}_1^{-1}\int_{-\infty}^{\infty}\frac{\xi\left(-[\![\bar{\mathbf{U}}]\!]^{+T}(\tau)\boldsymbol{\mathcal{R}}\langle\bar{\mathbf{p}}\rangle(\tau) - \langle\bar{\mathbf{U}}\rangle^{T}(\tau)\boldsymbol{\mathcal{R}}[\![\bar{\mathbf{p}}]\!](\tau)\right)}{\tau-\xi}\mathrm{d}\tau, \tag{3.46}$$

where the explicit expression for ${\boldsymbol{\mathcal{Z}}_{\mathbf{1}}}^{-1}$ is given by

$${\boldsymbol{\mathcal{Z}}_{\mathbf{1}}}^{-1} = \frac{2s^{+}s^{-}(1+4\epsilon^2)}{H_{11}}\begin{pmatrix} \frac{E^2}{(\beta-1)(1-2i\epsilon)} & \frac{iE^2}{(\beta-1)(1-2i\epsilon)} \\ -\frac{1}{(\beta+1)(1+2i\epsilon)E^2} & \frac{i}{(\beta+1)(1+2i\epsilon)E^2}\end{pmatrix}.$$

Assuming that the loading disappears in the region of the crack tip the limit in (3.46) exists and therefore the general expression for the stress intensity factor, $\mathbf{K}$, for the steady state is identical to that found in Morini et al. (2013b) (see equation (3.29)). For symmetric loading ($[\![\mathbf{p}]\!] = 0$) equation (3.46) yields the same expression for the stress intensity factors as (3.12).

Now that an expression for the stress intensity factor has been found it is possible to determine the energy release rate(ERR). Using (3.14) the following expression is obtained for the ERR in orthotropic materials

$$G = \frac{H_{11}(1-\beta^2)|K|^2}{4}. \tag{3.47}$$

The effect of crack speed on the energy release rate is explored in Chapter 3.4.

3.3.2 General Expression for the Coefficients of the Higher Order Terms

Using the asymptotic expansions (3.41), (3.42) and the corresponding terms of (3.45) a general expression for the jth coefficient of the asymptotic expansions, $\mathbf{Y}_i$, is found

$$\mathbf{V}_j^{\pm} = \lim_{\xi \to \infty^{\pm}} \left[\frac{\xi^j (-1)^{j-1}}{2\pi i (j-1)!} \int_{-\infty}^{\infty} \boldsymbol{\psi}(\tau) \frac{\mathrm{d}^{j-1}}{\mathrm{d}\xi^{j-1}} \left(\frac{\xi^{j-1}}{\tau - \xi} \right) \mathrm{d}\tau \right]. \tag{3.48}$$

This gives a general expression for the coefficients of the asymptotic expansion of the displacement and stress fields as

$$\mathbf{Y}_j = \lim_{\xi \to \infty^{\pm}} \frac{1}{2\pi i} \boldsymbol{\mathcal{Z}}_j^{-1} \int_{-\infty}^{\infty} \tau^{j-1} (\llbracket \bar{\mathbf{U}} \rrbracket^{+T}(\tau) \boldsymbol{\mathcal{R}} \langle \bar{\mathbf{p}} \rangle(\tau) + \langle \bar{\mathbf{U}} \rangle^{T}(\tau) \boldsymbol{\mathcal{R}} \llbracket \bar{\mathbf{p}} \rrbracket(\tau)) \left(\frac{\xi}{\xi - \tau} \right)^j \mathrm{d}\tau. \tag{3.49}$$

If the limit can be taken through the integral and the loading is applied in such a way that the limit exists it is clearly seen that equation (3.49) is identical to (3.30). The limit in (3.49) can be computed directly for $j \geq 2$ if the loading is given by a particularly smooth function which is therefore differentiable, otherwise it is computationally challenging. However, we wish to use a general asymmetric loading system in which case equation (3.30) cannot always be used. An example of loading for which (3.30) cannot be used is when point forces are applied on the crack faces (Piccolroaz et al., 2009). To find further asymptotic terms, for arbitrary loading, an alternate method must be used.

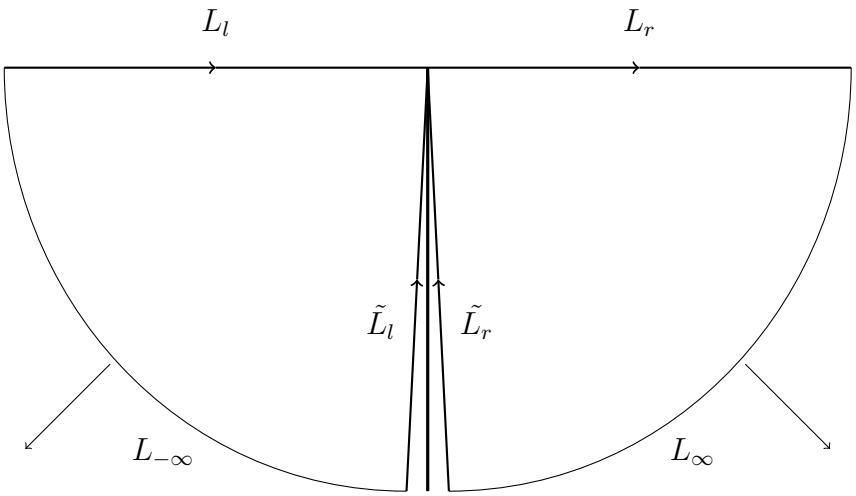

Figure 3.2: Integration Shift in the ξ-Plane

As the function $\mathbf{p}$ only exists on the negative real x-axis its Fourier transform is analytic in the lower half ξ-plane. Therefore, $[\![\bar{\mathbf{p}}]\!]$ and $\langle\bar{\mathbf{p}}\rangle$ are also analytic in the lower-half plane. As long as the applied loading $\mathbf{p}$ vanishes within a region of the crack tip it is clearly seen that $[\![\bar{\mathbf{p}}]\!]$ and $\langle\bar{\mathbf{p}}\rangle$ decay exponentially as ξ tends to $-i\infty$. It is also known that both $[\![\bar{\mathbf{U}}]\!]^+$ and $\langle\bar{\mathbf{U}}\rangle$ are analytic in the lower-half plane apart from the negative imaginary axis.

For computing $\mathbf{Y}_j$ the contour of integration shown in Figure 3.2 is used. However, as there is exponential decay as ξ goes to $-i\infty$, $L_{-\infty}$ and L_{∞} do not contribute to the total integral. Equation (3.49) now becomes

$$\mathbf{Y}_j = \lim_{\xi\to\infty^{\pm}} \left(-\frac{1}{2\pi i}\boldsymbol{\mathcal{Z}}_j^{-1} \left[\int_{\tilde{L}_l} \tau^{j-1}\boldsymbol{\psi}(\tau) \left(\frac{\xi}{\xi-\tau}\right)^j \mathrm{d}\tau - \int_{\tilde{L}_r} \tau^{j-1}\boldsymbol{\psi}(\tau) \left(\frac{\xi}{\xi-\tau}\right)^j \mathrm{d}\tau \right] \right). \tag{3.50}$$

The limit of (3.50) can be taken to give

$$\mathbf{Y}_j = -\frac{1}{2\pi i}\boldsymbol{\mathcal{Z}}_j^{-1}\int_{-i\infty}^{0}\tau^{j-1}[\![\boldsymbol{\psi}(\tau)]\!]\mathrm{d}\tau, \tag{3.51}$$

where $[\![\boldsymbol{\psi}(\tau)]\!]$ refers to the jump of the function $\boldsymbol{\psi}$ over the negative imaginary axis.

The expression (3.51) can be simplified further by considering the continuity of (3.22) and (3.23). The first term in both equations is analytic in the lower half-plane and therefore continuous over the negative imaginary axis. For this reason they do not contribute to the general expression for the asymptotic coefficients, (3.51). Therefore, equation (3.51) simplifies to give

$$\mathbf{Y}_j = -\frac{1}{2\pi i}\boldsymbol{\mathcal{Z}}_j^{-1}\int_{-i\infty}^{0}\tau^{j-1}[\![\boldsymbol{\phi}]\!](\tau)\mathrm{d}\tau, \tag{3.52}$$

where $\boldsymbol{\phi}(\tau)$ is given by

$$\boldsymbol{\phi}(\tau) = \frac{\mathrm{Re}(\mathbf{H})\{\bar{\boldsymbol{\Sigma}}^{-}(\tau)\boldsymbol{\mathcal{R}}\langle\bar{\mathbf{p}}\rangle(\tau)\}}{|\tau|} + \frac{\mathrm{Re}(\mathbf{W})\{\bar{\boldsymbol{\Sigma}}^{-}(\tau)\boldsymbol{\mathcal{R}}[\![\bar{\mathbf{p}}]\!](\tau)\}}{2|\tau|}.$$

3.4 Specific Examples

Specific examples for computing the stress intensity factors for orthotropic materials are now considered. Firstly, the loading on the crack faces is given by a point force of magnitude F acting perpendicular to the upper crack face a distance a behind the crack tip and two point forces, both of magnitude $F/2$, acting perpendicular to the lower crack face a distance b away from the point force acting upon the upper crack face. The loading moves at the same speed and in the same direction that the crack is propagating. This is shown in Figure 3.3. The forces are represented mathematically using the Dirac

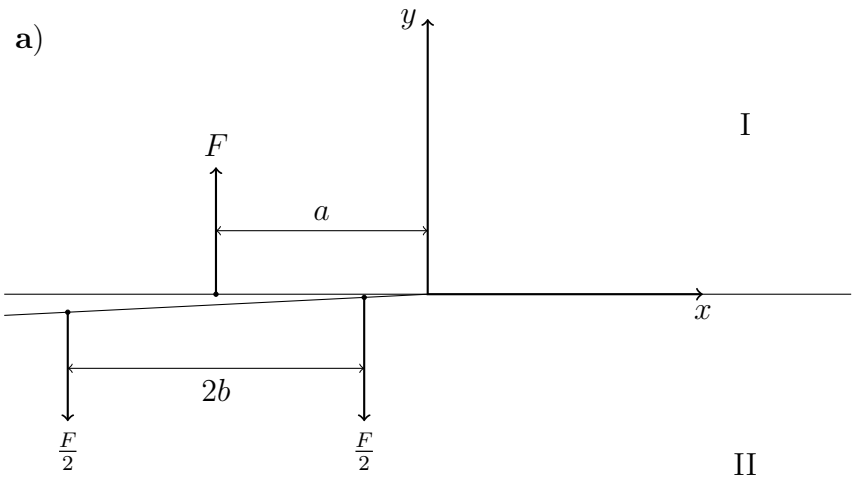

Figure 3.3: Mode I dominant loading

delta distribution (Piccolroaz et al., 2009)

$$p_+(x) = -F\delta(x+a), \qquad p_-(x) = -\frac{F}{2}\delta(x+a+b) - \frac{F}{2}\delta(x+a-b). \tag{3.53}$$

It is now possible to decompose the loading into its symmetric and skew-symmetric components

$$\begin{aligned} \langle p \rangle(x) &= \frac{1}{2}[p_+(x) + p_-(x)] = -\frac{F}{2}\delta(x+a) - \frac{F}{4}\delta(x+a-b) - \frac{F}{4}\delta(x+a-b), \\ [\![p]\!](x) &= p_+(x) - p_-(x) = -F\delta(x+a) + \frac{F}{2}\delta(x+a+b) + \frac{F}{2}\delta(x+a-b). \end{aligned} \tag{3.54}$$

In order to compute the stress intensity factors the Fourier transforms of the skew-symmetric and symmetric parts of the loading are required. These are given by

$$\langle \bar{p} \rangle(\xi) = -\frac{F}{2}e^{-i\xi a} - \frac{F}{4}e^{-i\xi(a+b)} - \frac{F}{4}e^{-i\xi(a-b)}, \tag{3.55}$$

$$[\![\bar{p}]\!](\xi) = -Fe^{-i\xi a} + \frac{F}{2}e^{-i\xi(a+b)} + \frac{F}{2}e^{-i\xi(a-b)}. \tag{3.56}$$

It is now possible to compute expressions for the first and second order asymptotic coefficients, $\mathbf{K}$ and $\mathbf{Y}_2$, using expressions (3.46) and (3.52) respectively.

To find an expression for $\mathbf{K}$ equation (3.46) is used, which is identical to using the dynamic equivalent of (3.29). The solution is split into the parts corresponding to the symmetric and anti-symmetric parts of the loading, denoted K^S and K^A respectively

$$K^S_{(a)} = F\frac{E^2}{(1-\beta)}\sqrt{\frac{H_{22}}{H_{11}}}\sqrt{\frac{2}{\pi}}\,\Lambda(1,a,b,\epsilon),$$

$$K^A_{(a)} = F\frac{E^2\delta_2}{(1-\beta)}\sqrt{\frac{H_{22}}{H_{11}}}\sqrt{\frac{2}{\pi}}\,\Xi(1,a,b,\epsilon). \tag{3.57}$$

where

$$\Lambda(c,a,b,\epsilon) = a^{-\frac{c}{2}-i\epsilon}\left[\frac{1}{2}+\frac{1}{4}(1+b/a)^{-\frac{c}{2}-i\epsilon}+\frac{1}{4}(1-b/a)^{-\frac{c}{2}-i\epsilon}\right],$$

$$\Xi(c,a,b,\epsilon) = a^{-\frac{c}{2}-i\epsilon}\left[\frac{1}{2}-\frac{1}{4}(1+b/a)^{-\frac{c}{2}-i\epsilon}-\frac{1}{4}(1-b/a)^{-\frac{c}{2}-i\epsilon}\right].$$

Regarding higher order asymptotic coefficients for the loading shown in Figure (3.3) the alternate method developed in Chapter 3.3.2 must be used. Once again the coefficient is split into symmetric and anti-symmetric parts. The second order term is given by

$$Y^S_{2(a)} = F\frac{E^2}{(\beta-1)}\sqrt{\frac{H_{22}}{H_{11}}}\sqrt{\frac{2}{\pi}}\,\Lambda(3,a,b,\epsilon),$$

$$Y^A_{2(a)} = F\frac{E^2\delta_2}{(\beta-1)}\sqrt{\frac{H_{22}}{H_{11}}}\sqrt{\frac{2}{\pi}}\,\Xi(3,a,b,\epsilon). \tag{3.58}$$

A different configuration has also been considered. This other point loading system consists of point forces acting on the crack faces at the same points as previously considered but the forces are now running parallel to

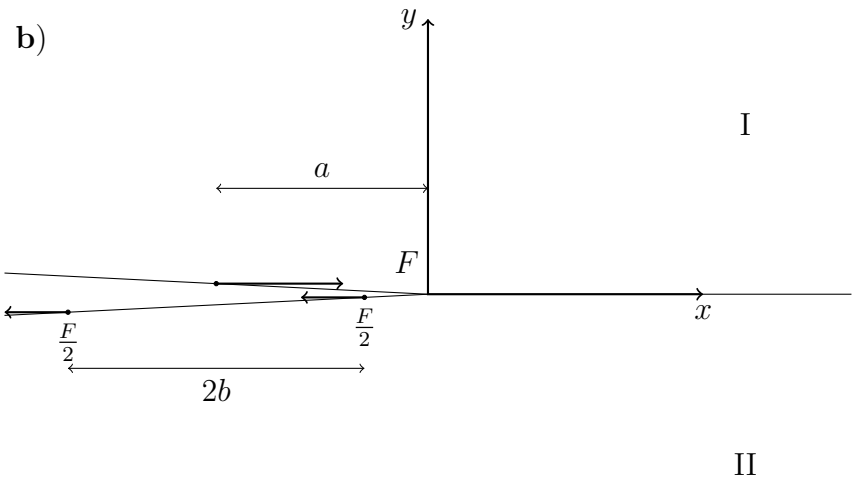

Figure 3.4: Mode II dominant loading

the crack as opposed to the perpendicular system shown in Figure 3.3. This different loading is shown in Figure 3.4.

For this loading the following expressions are found for the symmetric and antisymmetric part of the stress intensity factors

$$K^S_{(b)} = iF\frac{E^2}{(1-\beta)}\sqrt{\frac{2}{\pi}}\,\Lambda(1,a,b,\epsilon),$$

$$K^A_{(b)} = iF\frac{E^2\delta_1}{(1-\beta)}\sqrt{\frac{2}{\pi}}\,\Xi(1,a,b,\epsilon). \tag{3.59}$$

Using the method developed in Chapter 3.3.2, the symmetric and antisymmetric components of the second order asymptotic coefficient are found

$$Y^S_{2(b)} = iF\frac{E^2}{(\beta-1)}\sqrt{\frac{2}{\pi}}\,\Lambda(3,a,b,\epsilon),$$

$$Y^A_{2(b)} = iF\frac{E^2\delta_1}{(\beta-1)}\sqrt{\frac{2}{\pi}}\,\Xi(3,a,b,\epsilon). \tag{3.60}$$

Having computed expressions for the stress intensity factors it is now possible to calculate the energy release rate for two given materials. The

velocity is normalised by dividing by c_R, the lowest of the two Rayleigh wave speeds for the given materials. This is done because the Rayleigh wave speed is a limiting velocity for which the steady-state coordinate system can be used. In the results shown the energy release rate is normalised in the following manner: $GC_{66}^{(1)}/F^2$. Here, $C_{66}^{(1)}$ is taken as the value of C_{66} for the material above the crack. In all figures graphs labelled **a**) correspond to the Mode I dominant loading whereas those labelled **b**) refer to the case with Mode II dominant loading. For the purpose of calculations, a is set as 1.

In this chapter the material constants chosen for material I are those of Barium Titanate. Information on this material has been obtained from Geis et al. (2004) which states that the material is transverse isotropic, which is a subgroup of orthotropic materials. Material II is set as monocrystalline Aluminium, with a cubic structure, where material parameters have been obtained from Bower (2009). The properties of these materials are shown in Table 3.1. Using the method outlined in Appendix 1, it can be shown that the Rayleigh wave speed of Barium Titanate is $1,771$ ms^{-1} and for Aluminium it is $2,941$ ms^{-1}. Therefore the normalising velocity, c_R, used is that of Barium Titanate.

Material	C_{11}(GPa)	C_{22}(GPa)	C_{12}(GPa)	C_{66}(GPa)	ρ(kgm^{-3})
I. Barium Titanate	120.3	120.3	75.2	21.0	6,020
II. Aluminium	107.3	107.3	60.9	28.3	2,700

Table 3.1: Material properties

Figure 3.5 shows the variation of the normalised energy release rate, as a function of the velocity, for both loadings considered, whereas Figures 3.6

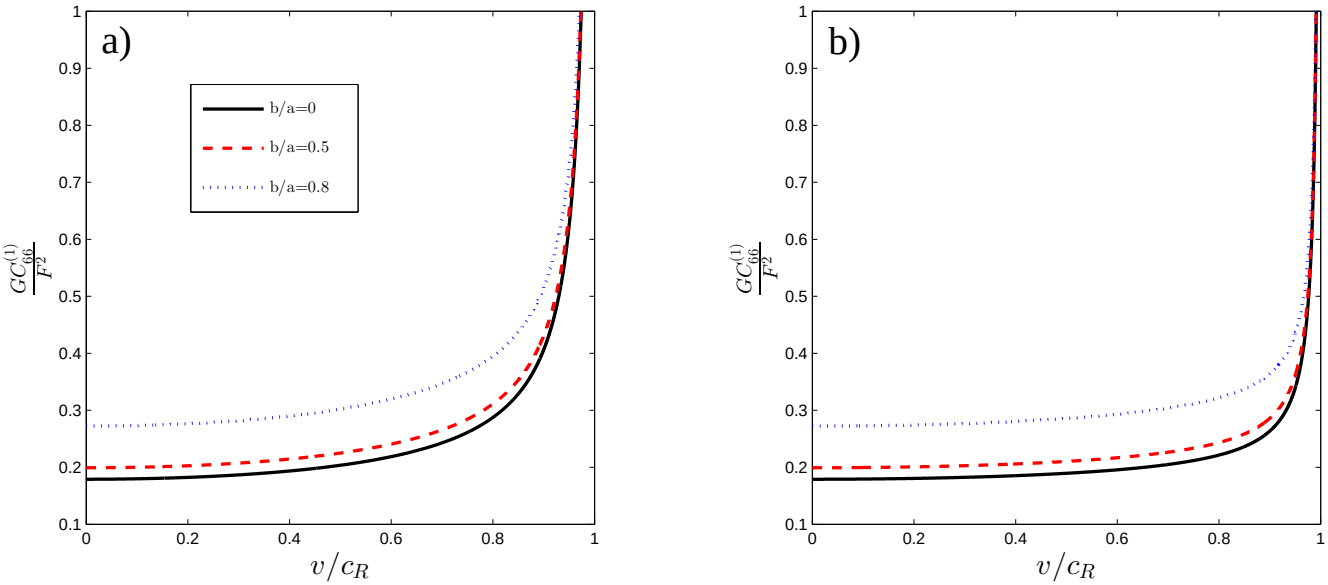

Figure 3.5: The normalised ERR, as a function of the velocity, for different positions of the self-balanced point forces applied to the crack surfaces, described by the ratio b/a.

and 3.7 illustrate the symmetric and antisymmetric contribution to the ERR, corresponding to K^S and K^A respectively. Both G^S and G^A are normalised by the total energy release rate G, associated with $K = K^S + K^A$.

It can be observed in Figure 3.5 that the energy release rate increases as the velocity increases and tends towards infinity as the velocity approaches the Rayleigh wave speed. This behaviour is observed regardless of the asymmetry of the loading acting on the crack faces. It is important to note that, as velocity increases, asymmetry gives a larger ERR, therefore it can be said that symmetric loading is more energetically beneficial than any asymmetric load.

Graphs in Figures 3.6 and 3.7 show that for $b/a = 0$, when both loadings

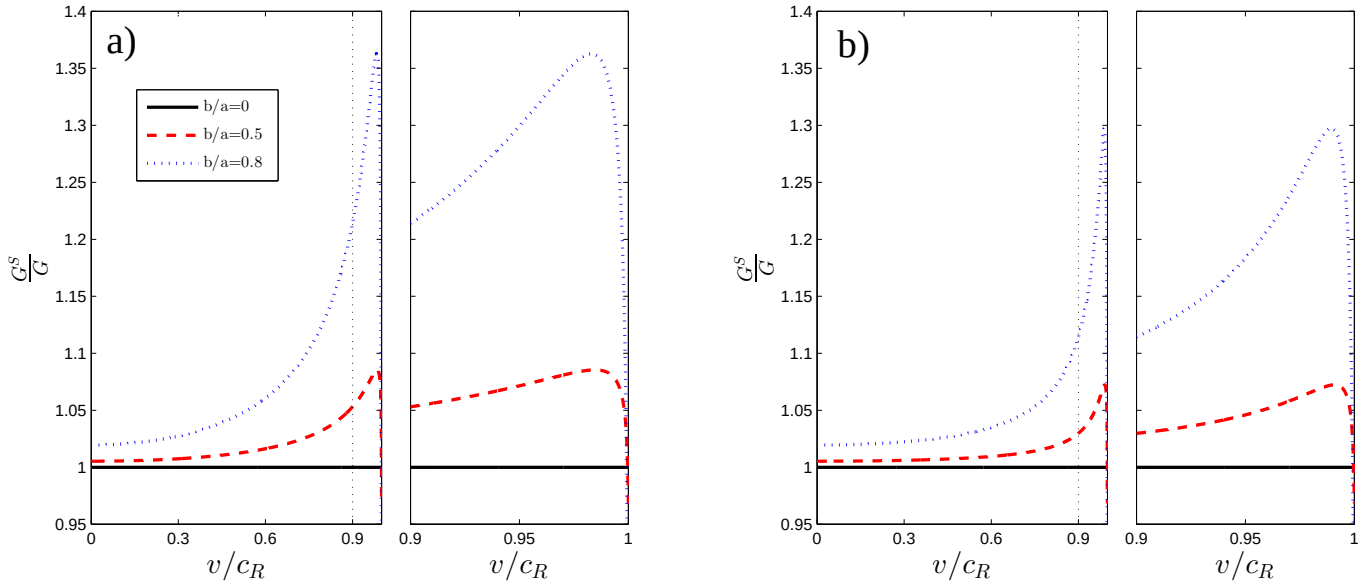

Figure 3.6: The normalised symmetric part of the ERR, as a function of the velocity, for different positions of the self-balanced point forces applied to the crack surfaces, described by the ratio b/a.

become symmetric, $G^S/G = 1$ and $G^A/G = 0$ therefore the energy release rate only consists of its symmetric part, regardless of velocity, which agrees with the results found for isotropic and anisotropic bimaterials in Piccolroaz et al. (2009) and Morini et al. (2013b). When asymmetry is introduced into the loading it is observed that the symmetric contribution to the energy release rate is higher than the total ERR and the ratio increases as the velocity increases. Upon approaching the Rayleigh wave speed there is an unexpected sharp decrease in the ratio G^S/G. This unexpected effect should be studied further by performing experiments studying crack propagation at near-Rayleigh speeds.

In comparison to the symmetric contribution shown in Figure 3.6, the

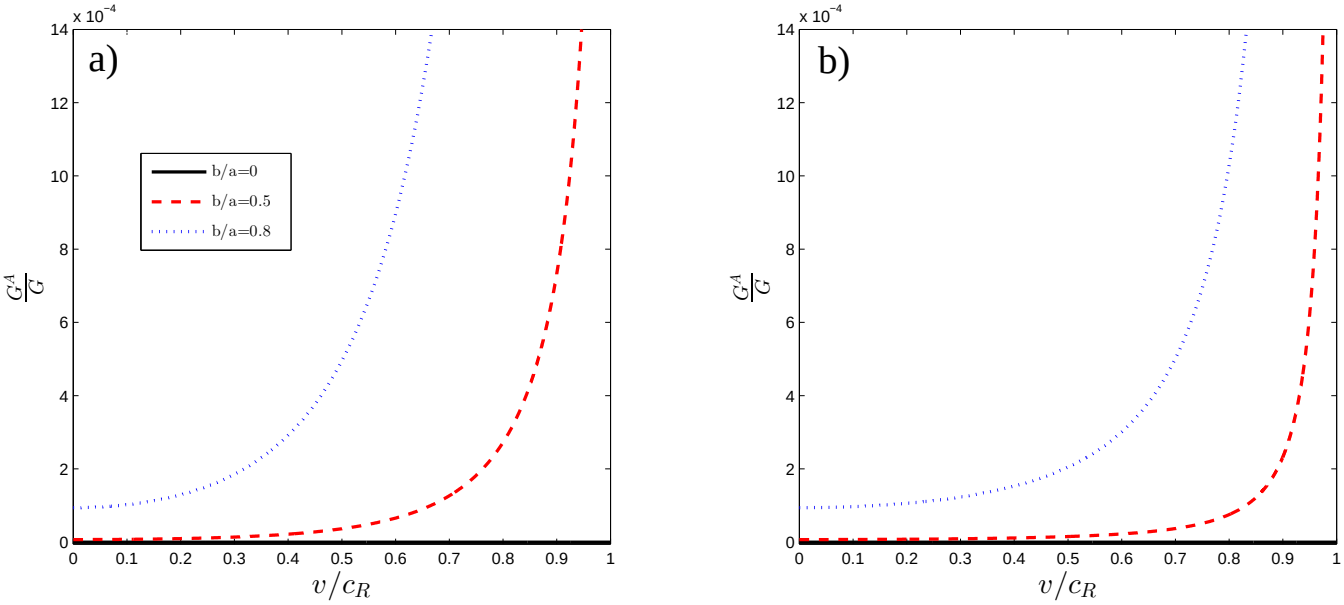

Figure 3.7: The normalised antisymmetric part of the ERR, as a function of the velocity, for different positions of the self-balanced point forces applied to the crack surfaces, described by the ratio b/a.

asymmetric part of the ERR, illustrated in Figure 3.7, is very small, in particular for low velocities. As the velocity starts to increase the asymmetric contribution to G becomes larger. This result is supported by Figure 3.8, showing the ratio G^A/G^S, which also shows an increased contribution by the asymmetric part of the loading at higher velocities.

The dependence of the stress intensity factor, K, on the normalised crack tip speed is illustrated in Figure 3.9. The first graph shows the ratio K_2/K_1 for the Mode I dominant loading. Here, K_1 and K_2 are the Mode I and II contributions to the SIF, respectively. For symmetric loading there is no Mode II contribution to K, due to the fact that there is only Mode I opening of the crack. It is important to observe that if asymmetry is introduced, for

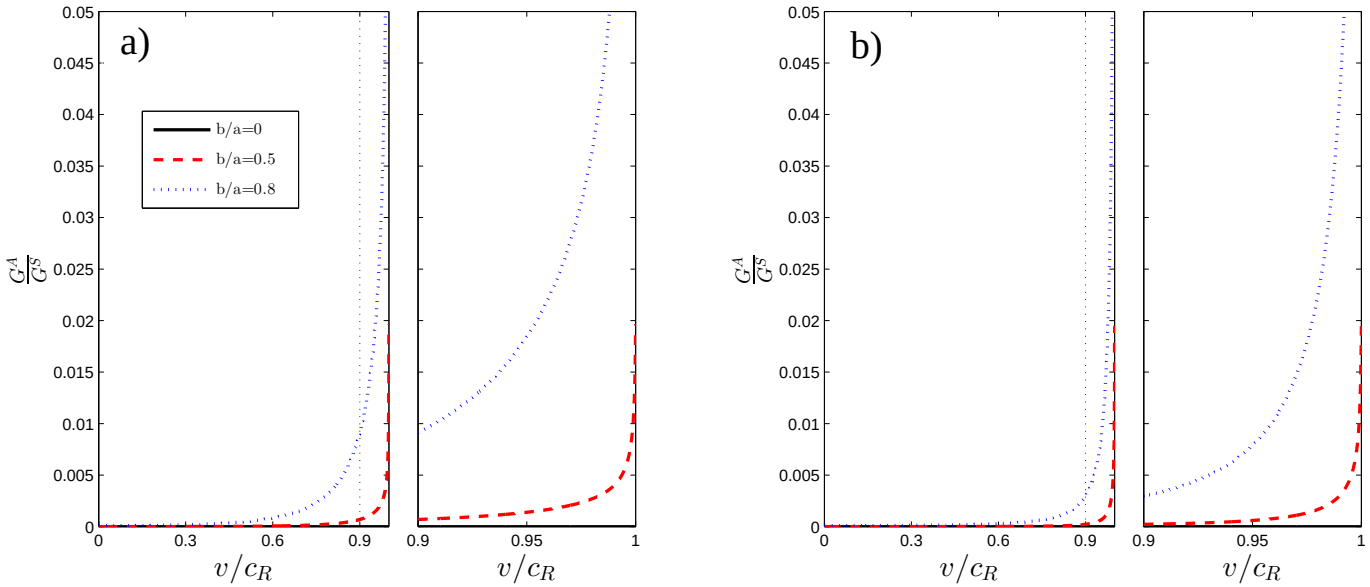

Figure 3.8: The ratio of antisymmetric and symmetric parts of the energy release rate, as a function of the velocity, for different positions of the self-balanced point forces applied to the crack surfaces, described by the ratio b/a.

all values of b/a, there exists a velocity at which K_2 changes sign. The second image in Figure 3.9 shows a similar result for the Mode II dominant loading when considering the ratio K_1/K_2. In this case, it is the K_1 component which changes sign. The velocity at which this change takes place is the same for both types of loading and does not depend on the asymmetry. This velocity corresponds to the value of the crack tip speed at which the Dundurs parameter, β, vanishes. This characteristic velocity can be found by solving the algebraic equation $\beta(v) = 0$ and depends only on the elastic properties of the materials and the speed at which the crack is propagating. Therefore it is clear that the asymmetry of the load does not affect the value at which

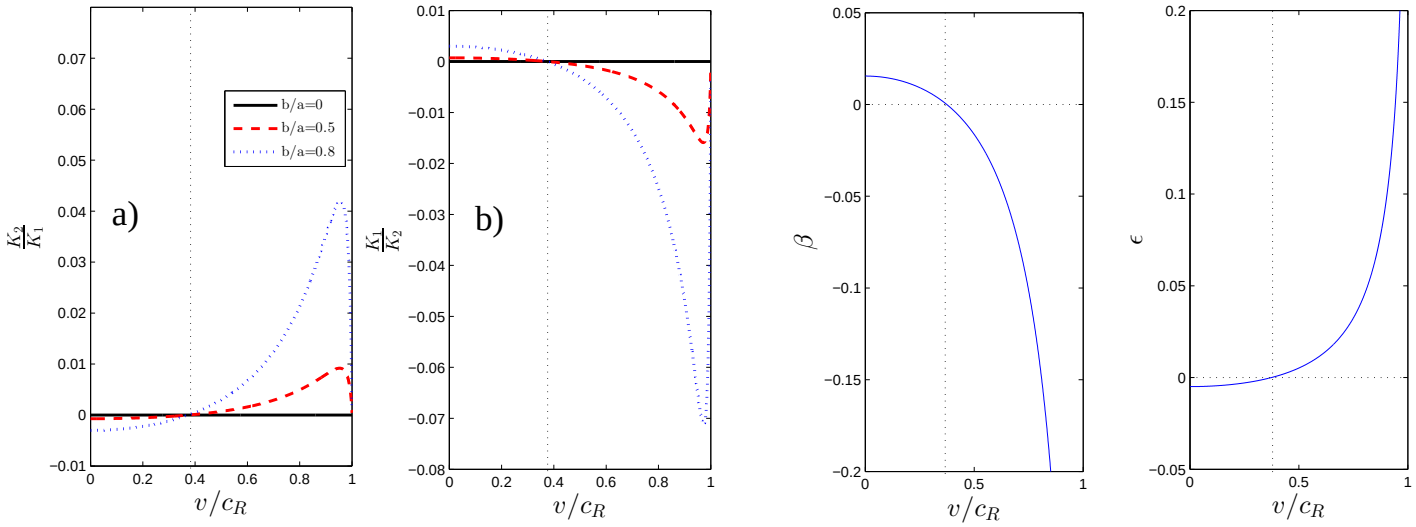

Figure 3.9: The ratios K_2/K_1 and K_1/K_2 for the Mode I and Mode II loadings respectively. The graphs of β and ϵ, as a function of velocity, are also shown.

the stress intensity factors have a change in sign. It is also clear from the results in Appendix 1 that when β vanishes the oscillatory term, ϵ, vanishes and this has also been shown in Figure 3.9. This agrees with the obtained results as, when $\epsilon = 0$, it can be observed that (3.57) consists only of real terms and (3.59) only has imaginary components.

It can be said that, when the crack tip speed reaches this characteristic value of the velocity, associated with $\beta = 0$, the propagation should continue along the interface in a straight line. Instead, when neither K_1 or K_2 are 0 there is a possibility of kinking or branching of the propagation. Increased magnitudes of the ratios considered in Figure 3.9 lead to an increased probability of crack redirection and as the velocity increases the ratios exhibit this behaviour which explains why straight propagation along the interface

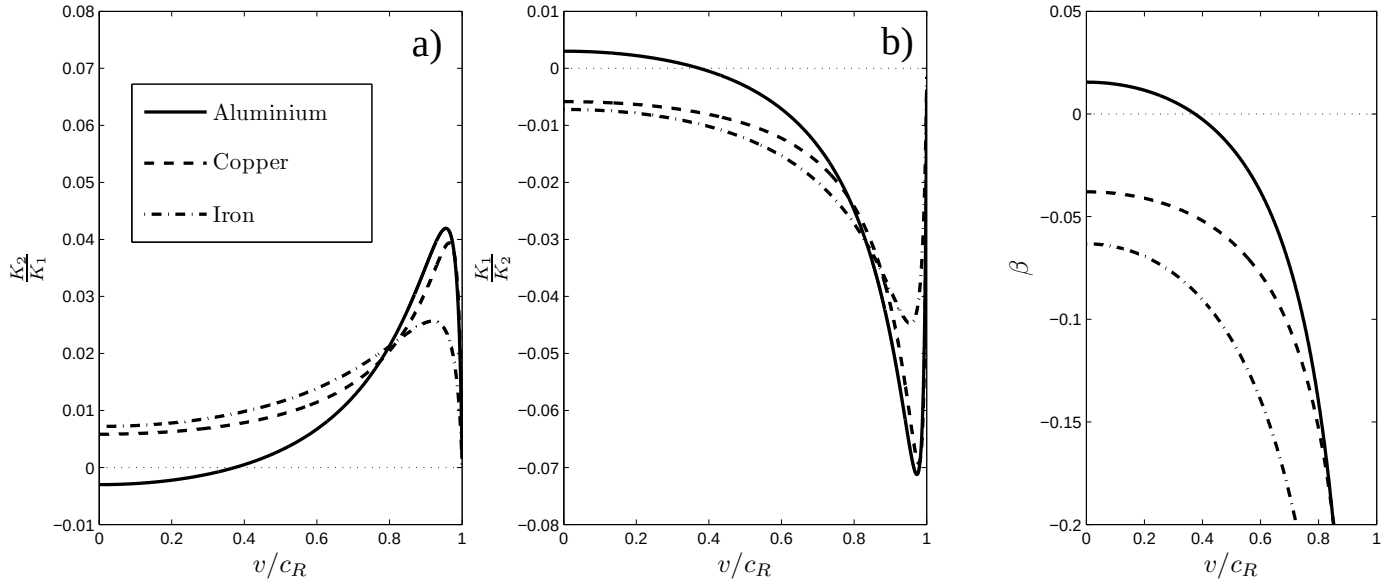

Figure 3.10: The change in behaviour of the crack propagation when the material below the crack is changed, for fixed asymmetry of the loading.

is unlikely for high crack speeds. These results are in agreement with many theoretical and experimental studies which have demonstrated that there exists a specific sub-Rayleigh velocity which is related to the stability of the crack propagation (Obrezanova et al., 2002a,b).

The behaviour of the stress intensity factor is also observed in Figure 3.10 for different materials in the lower half plane. The asymmetry of the load was fixed at $b/a = 0.8$. The results in these graphs show that the previously mentioned speed at which the direction of the crack propagation changes does not exist for all bimaterials. This is due to the fact that there does not always exist a velocity at which $\beta = 0$. For bimaterials which do not have this characteristic velocity the change of behaviour of the crack propagation would not be expected. However, the increased probability of

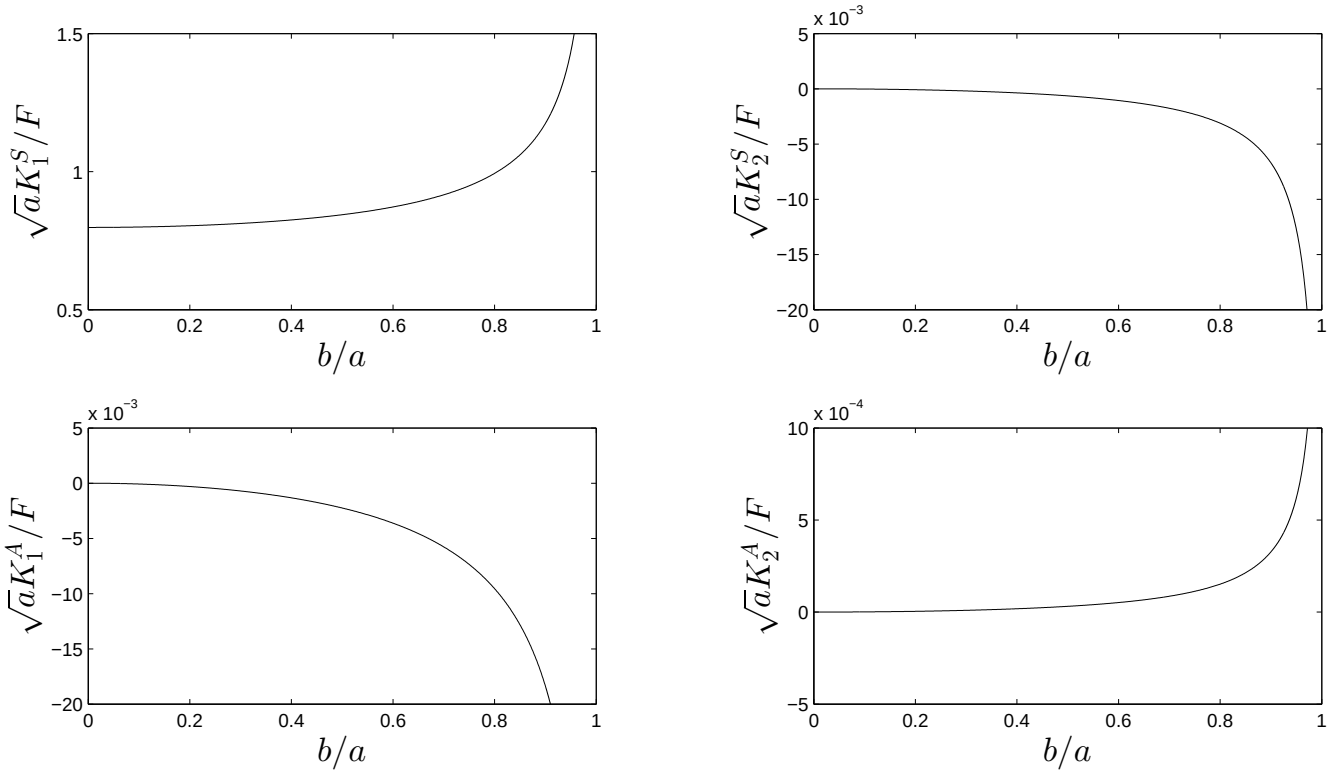

Figure 3.11: The normalised components of K^S and K^A for $v = 0$ with mode I dominant loading.

kinking/branching at higher velocities is still observed.

Figure 3.11 shows the variation in the real and imaginary parts of the normalised stress intensity factor when $v = 0$ and the asymmetry of the loading is varied. The loading considered here is the Mode I dominant loading so a comparison can be made to the results obtained for this system in Morini et al. (2013b). The behaviour of the results shown agree with those in Morini et al. (2013b) with only the real part of the symmetric stress intensity factor existing for symmetric loading and the magnitude of all components increases as the asymmetry becomes more profound. The behaviour is not identical to

that seen in Morini et al. (2013b) due to the different materials considered here.

3.5 Conclusions

A general method for calculating stress intensity factors and higher order terms in the asymptotic expansions of the displacement and stress fields for a dynamic steady-state crack at the interface between two dissimilar anisotropic materials has been developed. The proposed approach, based on weight functions and the Betti integral formula, can be applied to many crack problems in a wide range of materials, for example, several classes of anisotropic elastic media (monoclinic, orthotropic) and piezoceramics. As a particular case, a steady-state plane interfacial crack in orthotropic bimaterials has been studied. Expressions for the SIF and further higher order asymptotic coefficients have been found for two different configurations of loading acting on the crack faces.

It has been shown in our examples that greater asymmetry of the loading configuration leads to an increase in the energy release rate at the crack tip and has a particularly large effect for high crack velocities. Moreover, the analysis of the stress intensity factors for both loadings shows the existence of a sub-Rayleigh velocity at which the non-dominant part of the SIF changes sign which could lead to a change in direction in the crack propagation. This effect is only observable when asymmetric loading was applied and may give some explanation to the fact that kinking/branching is more probable at certain velocities. As different materials for the lower half-plane are considered, it has been shown that this characteristic velocity does not exist for every bi-

material and therefore experimental study is of great importance in order to clearly detect the presence of this critical value and its physical implications on crack propagation stability.

Chapter 4

Derivation of singular integral equations for an imperfect interface in an anisotropic bimaterial using perfect interface weight functions

This chapter sees the introduction of an imperfect interface in an anisotropic bimaterial. For the purpose of the work seen here only a static crack is considered and both the in-plane (Modes I and II) and out-of-plane (Mode III) fields are considered. The Mode III problem decouples from the in-plane problem to leave a scalar problem whereas Modes I and II are once again coupled, which lead to 2×2 matricial problems. The purpose of this chapter is to find singular integral equations which relate interfacial tractions and

crack displacements to the applied loadings on the crack faces.

Singular integral equations have been derived for the analogous problem with a perfect interface for both isotropic (Piccolroaz and Mishuris, 2013) and anisotropic (Morini et al., 2013a) bimaterials. Both papers made use of the Betti identity and the weight function of Willis and Movchan (1995) (introduced in the previous chapter) in their derivation. The incorporation of an imperfect interface was seen in Mishuris et al. (2013) where an imperfect interface in an isotropic bimaterial was considered. The weight function used here was similar to that of Willis and Movchan (1995) but with an imperfect interface as opposed to a perfect one. This means that it was necessary to derive the new weight function before proceeding to derive the integral equations. The approach seen in this chapter utilises the Betti identity in such a way that it is possible to use the weight function containing the perfect interface in order to find results for the imperfect physical problem, therefore negating the need to derive new weight functions.

The structure of the remainder of the chapter is as follows: Chapter 4.1 sees the introduction of the mathematical framework used for the remainder of the chapter. In Chapter 4.2 we report the Betti formula and begin the new work by combining perfect interface weight functions with imperfect interface physical fields in this reciprocal identity. We confirm the validity of this new method by verifying that it gives the same results for isotropic materials as those found in Mishuris et al. (2013). Once the relationship between the existing weight functions and sought solution has been established we then proceed to look at the out-of-plane and in-plane problems separately in Chapters 4.3 and 4.4 respectively. In both sections we first derive relationships

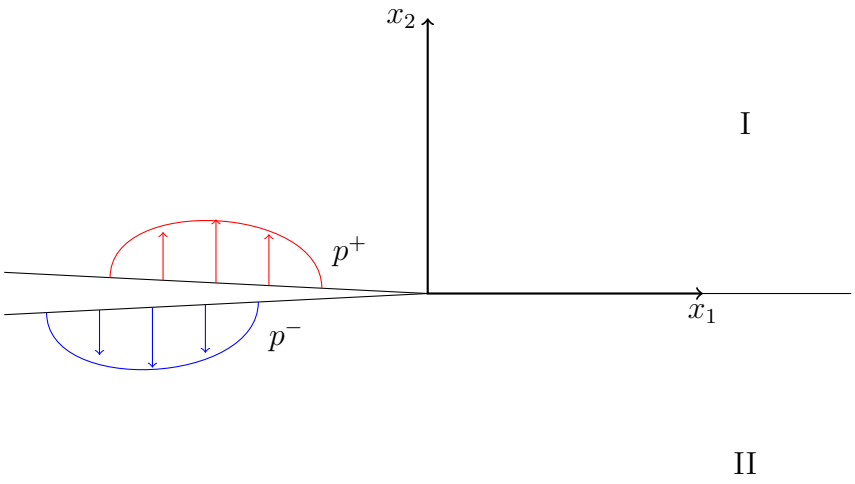

Figure 4.1: Geometry

between the Fourier transforms of the applied crack load (which is known) and the displacement jump over the crack and interfacial traction. Inverse Fourier transforms are then used to obtain the desired equations. We then present some numerical results for both cases to illustrate the implementation of our singular integral equations. For the Mode III solution we also show a comparison between results obtained from finite element solutions in COMSOL to those obtained from the equations we have derived.

4.1 Problem formulation

We consider an infinite anisotropic bimaterial with an imperfect interface and a semi-infinite interfacial crack respectively lying along the positive and negative x_1 semi-axes. The materials above and below the x_1-axis will be denoted materials I and II respectively.

The imperfect interface transmission conditions for $x_1 > 0$ are given by

$$\mathbf{t}(x_1, 0^+) = \mathbf{t}(x_1, 0^-), \tag{4.1}$$

$$\mathbf{u}(x_1, 0^+) - \mathbf{u}(x_1, 0^-) = \boldsymbol{\mathcal{K}}\mathbf{t}(x_1, 0^+), \tag{4.2}$$

where $\mathbf{t} = (t_1, t_2, t_3)^T = (\sigma_{21}, \sigma_{22}, \sigma_{23})^T$ is the traction vector and $\mathbf{u} = (u_1, u_2, u_3)^T$ is the displacement vector. The matrix $\boldsymbol{\mathcal{K}}$ quantifies the extent of imperfection of the interface, with $\boldsymbol{\mathcal{K}} = \mathbf{0}$ corresponding to the perfect interface. For an anisotropic bonding material, $\boldsymbol{\mathcal{K}}$ has the following structure:

$$\boldsymbol{\mathcal{K}} = \begin{pmatrix} K_{11} & K_{12} & 0 \\ K_{12} & K_{22} & 0 \\ 0 & 0 & \kappa \end{pmatrix}. \tag{4.3}$$

Expressions for the components of $\boldsymbol{\mathcal{K}}$, in terms of the material parameters of the bonding agent, were found by Antipov et al. (2001). In the case when a thin layer of isotropic material is used it was shown that $K_{12} = 0$.

The loading on the crack faces is considered known and given by

$$\mathbf{t}(x_1, 0^+) = \mathbf{p}^+(x_1), \quad \mathbf{t}(x_1, 0^-) = \mathbf{p}^-(x_1), \quad \text{for } x_1 < 0. \tag{4.4}$$

The geometry considered is illustrated in Figure 4.1. The only restriction imposed on $\mathbf{p}^{\pm}$ is that they must be self-balanced; note in particular that this allows for discontinuous and/or asymmetric loadings. The symmetric and skew-symmetric parts of the loading are given by $\langle\mathbf{p}\rangle$ and $[\![\mathbf{p}]\!]$ respectively, where the notation $\langle f\rangle$ and $[\![f]\!]$ respectively denote the average and jump of the argument function.

4.2 Application of existing weight functions

4.2.1 Weight functions and the Betti formula

In this section we introduce a method where integral identities for the physical problem with an imperfect interface are found using existing weight functions formulated in a *perfect* interface setting. Such weight functions can be found in the paper of Morini et al. (2013b). It is important to note that such weight functions play a role only as solutions to auxiliary problems and have no immediate physical interpretation.

The weight function used is that previously introduced in Chapter 3 with the crack occupying the positive x_1 axis with square-root singular displacement at the crack tip. The transmission conditions for the weight functions for $x_1 < 0$ are given as

$$\mathbf{\Sigma}(x_1, 0^+) = \mathbf{\Sigma}(x_1, 0^-), \tag{4.5}$$

$$\mathbf{U}(x_1, 0^+) = \mathbf{U}(x_1, 0^-). \tag{4.6}$$

Note in particular that condition (4.6) corresponds to a perfect interface weight function problem in contrast to the imperfect interface problem being physically considered.

It was shown in Morini et al. (2013b) that the following equations hold for the Fourier transforms of the symmetric and skew-symmetric parts of the weight function:

$$[\![\bar{\mathbf{U}}]\!]^+(\xi) = \frac{1}{|\xi|}(i\text{sign}(\xi)\text{Im}(\mathbf{H}) - \text{Re}(\mathbf{H}))\langle\bar{\mathbf{\Sigma}}\rangle^-(\xi); \tag{4.7}$$

$$\langle\bar{\mathbf{U}}\rangle(\xi) = \frac{1}{2|\xi|}(i\text{sign}(\xi)\text{Im}(\mathbf{W}) - \text{Re}(\mathbf{W}))\langle\bar{\mathbf{\Sigma}}\rangle^-(\xi), \tag{4.8}$$

where $\mathbf{H}$ and $\mathbf{W}$ are defined in the same manner seen previously in the thesis. We note here that for the work in this chapter the 3×3 matrices for $\mathbf{H}$ and $\mathbf{W}$ are required, as opposed to the 2×2 matrices used in Chapter 3. This is due to the Mode III fields also being analysed here.

The matrices $\mathbf{H}$ and $\mathbf{W}$ have the form

$$\mathbf{H} = \begin{pmatrix} H_{11} & -i\beta\sqrt{H_{11}H_{22}} & 0 \\ i\beta\sqrt{H_{11}H_{22}} & H_{22} & 0 \\ 0 & 0 & H_{33} \end{pmatrix}, \tag{4.9}$$

$$\mathbf{W} = \begin{pmatrix} \delta_1 H_{11} & i\gamma\sqrt{H_{11}H_{22}} & 0 \\ -i\gamma\sqrt{H_{11}H_{22}} & \delta_2 H_{22} & 0 \\ 0 & 0 & \delta_3 H_{33} \end{pmatrix}. \tag{4.10}$$

The entries of these matrices can be expressed in terms of the components of the material compliance tensors, $\mathbf{S}$. Explicit expressions for $\mathbf{H}$ and $\mathbf{W}$ for orthotropic bimaterials are given in Appendix 1.

The reciprocal identity introduced in Chapter 3 will once again be used heavily in this chapter. In convolution form the Betti identity is written as

$$\boldsymbol{\mathcal{R}}[\![\mathbf{U}]\!] * \langle \mathbf{t} \rangle^{(+)} - \boldsymbol{\mathcal{R}}\langle \boldsymbol{\Sigma} \rangle^{(-)} * [\![\mathbf{u}]\!] = -\boldsymbol{\mathcal{R}}[\![\mathbf{U}]\!] * \langle \mathbf{p} \rangle - \boldsymbol{\mathcal{R}}\langle \mathbf{U} \rangle * [\![\mathbf{p}]\!], \tag{4.11}$$

where the convolutions are taken with respect to x_1 and superscripts $^{(\pm)}$ denote the restriction of the preceding function to the respective semi-x_1-axis. The rotational matrix $\boldsymbol{\mathcal{R}}$ is now given as

$$\boldsymbol{\mathcal{R}} = \begin{pmatrix} -1 & 0 & 0 \\ 0 & 1 & 0 \\ 0 & 0 & -1 \end{pmatrix}.$$

Applying Fourier transforms then gives

$$[\![\bar{\mathbf{U}}]\!]^T \boldsymbol{\mathcal{R}} \langle \bar{\mathbf{t}} \rangle^+ - (\langle \bar{\boldsymbol{\Sigma}} \rangle^-)^T \boldsymbol{\mathcal{R}} [\![\bar{\mathbf{u}}]\!] = -[\![\bar{\mathbf{U}}]\!]^T \boldsymbol{\mathcal{R}} \langle \bar{\mathbf{p}} \rangle - \langle \bar{\mathbf{U}} \rangle^T \boldsymbol{\mathcal{R}} [\![\bar{\mathbf{p}}]\!], \tag{4.12}$$

which is the same as the result used in Chapter 3.

Note that the exact nature of the weight functions $\mathbf{U}$ and $\boldsymbol{\Sigma}$ used in the derivation of equations (4.11) and (4.12) have not been specified at this stage and therefore both are valid for a large class of weight functions. In particular, this is what enables us to use perfect interface weight functions for the imperfect interface physical setting. In the next section we show how this method could have been used to simplify the derivation of previous work in the field.

4.2.2 Verify method for isotropic materials

Here we show that the method discussed previously gives the same results for an imperfect interface in an isotropic bimaterial as those obtained in Mishuris et al. (2013). This is done to further illustrate that using the perfect interface weight functions yields the correct results.

Antiplane (Mode III)

In Mishuris et al. (2013) it was shown that the following expression holds relating the physical stresses and displacement with the physical loading on the crack faces

$$\overline{\langle t \rangle^{(+)}}(\xi) - F(\xi) \overline{[\![u]\!]^{(-)}}(\xi) = -(1+\kappa F(\xi)) \langle \bar{p} \rangle(\xi) + \frac{\mu_*}{2}(1+\kappa F(\xi)) [\![\bar{p}]\!](\xi), \tag{4.13}$$

where $t = t_3$ and $u = u_3$. Explicit expressions for $F(\xi)$ and μ_* are given in terms of the shear moduli of materials I and II, given by μ_1 and μ_2 respectively

$$F(\xi) = -\frac{|\xi|}{\kappa|\xi| + \kappa\xi_0}, \quad \xi_0 = \frac{\mu_1 + \mu_2}{\kappa\mu_1\mu_2}, \quad \mu_* = \frac{\mu_1 - \mu_2}{\mu_1 + \mu_2}.$$

For the Mode III case, equation (4.12) becomes

$$[\![\bar{U}]\!]\overline{\langle t\rangle^{(+)}} - \overline{\langle\Sigma\rangle^{(-)}}[\![\bar{u}]\!] = -[\![\bar{U}]\!]\langle\bar{p}\rangle - \langle\bar{U}\rangle[\![\bar{p}]\!]. \tag{4.14}$$

where $U = U_3$ and $\Sigma = \Sigma_3$. Inserting $[\![\bar{U}]\!] = \overline{[\![U]\!]^{(+)}} + \overline{[\![U]\!]^{(-)}}$ and $[\![\bar{u}]\!] = \overline{[\![u]\!]^{(+)}} + \overline{[\![u]\!]^{(-)}}$ into this expression and using the transmission conditions, $\overline{[\![U]\!]^{(-)}} = 0$ and $\overline{[\![u]\!]^{(+)}} = \kappa\langle\bar{t}\rangle$ yields the following expression

$$(\overline{[\![U]\!]^{(+)}} - \kappa\overline{\langle\Sigma\rangle^{(-)}})\overline{\langle t\rangle^{(+)}} - \overline{\langle\Sigma\rangle^{(-)}}\,\overline{[\![u]\!]^{(-)}} = -[\![\bar{U}]\!]\langle\bar{p}\rangle - \langle\bar{U}\rangle[\![\bar{p}]\!]. \tag{4.15}$$

Dividing through by $\overline{U^{(+)}} - \kappa\overline{\langle\Sigma\rangle^{(-)}}$ gives

$$\overline{\langle t\rangle^{(+)}} - F(\xi)\overline{[\![u]\!]^{(-)}} = -G(\xi)\langle\bar{p}\rangle - H(\xi)[\![\bar{p}]\!], \tag{4.16}$$

where

$$F(\xi) = \frac{\overline{\langle\Sigma\rangle^{(-)}}}{\overline{[\![U]\!]^{(+)}} - \kappa\overline{\langle\Sigma\rangle^{(-)}}}, \quad G(\xi) = \frac{[\![\bar{U}]\!]}{\overline{[\![U]\!]^{(+)}} - \kappa\overline{\langle\Sigma\rangle^{(-)}}},$$

$$H(\xi) = \frac{\langle\bar{U}\rangle}{\overline{[\![U]\!]^{(+)}} - \kappa\overline{\langle\Sigma\rangle^{(-)}}}.$$

For isotropic materials, the weight functions with a perfect interface have the following relationships (Piccolroaz and Mishuris, 2013):

$$\overline{[\![U]\!]^{(+)}} = -\frac{\mu_1 + \mu_2}{|\xi|\mu_1\mu_2}\overline{\langle\Sigma\rangle^{(-)}} = -\frac{\kappa\xi_0}{|\xi|}\overline{\langle\Sigma\rangle^{(-)}}, \quad \langle\bar{U}\rangle = -\frac{\mu_*}{2}\overline{[\![U]\!]^{(+)}}.$$

Inserting these expressions into (4.16), and noting that $[\![\bar{U}]\!] = \overline{[\![U]\!]^{(+)}}$ when a perfect interface is considered, the result shown in (4.13) is obtained.

In-plane (Modes I and II)

For the in-plane components, it was shown in Mishuris et al. (2013) that the following equation holds

$$\overline{\langle \mathbf{t} \rangle^{(+)}}(\xi) - \mathbf{F}(\xi)\frac{\xi}{i}\overline{[\![\mathbf{u}]\!]^{(-)}}(\xi) = -\mathbf{G}(\xi)\bar{\langle \mathbf{p} \rangle}(\xi) - \mathbf{H}(\xi)\bar{[\![\mathbf{p}]\!]}(\xi), \tag{4.17}$$

where only the in-plane components are considered, that is $\bar{\langle \mathbf{t} \rangle} = (\bar{t}_1, \bar{t}_2)^T$, $\bar{[\![\mathbf{u}]\!]} = (\bar{[\![u_1]\!]}, \bar{[\![u_2]\!]})^T$ and $\bar{\mathbf{p}} = (\bar{p}_1, \bar{p}_2)^T$. Explicit expressions for $\mathbf{F}, \mathbf{G}$ and $\mathbf{H}$ were found to be

$$\mathbf{F}(\xi) = \frac{1}{2}\boldsymbol{\mathcal{R}}^{-1}\left[|\xi|\boldsymbol{\mathcal{K}}^* + b\mathbf{I} - id\,\mathrm{sign}(\xi)\mathbf{E}\right]^{-T}\left[b\alpha\mathbf{I} - ib\gamma\,\mathrm{sign}(\xi)\mathbf{E}\right]^T\boldsymbol{\mathcal{R}}, \tag{4.18}$$

$$\mathbf{G}(\xi) = -i\boldsymbol{\mathcal{R}}^{-1}\left[\xi\boldsymbol{\mathcal{K}}^* b\,\mathrm{sign}(\xi)\mathbf{I} - id\mathbf{E}\right]^{-T}\boldsymbol{\mathcal{R}}, \tag{4.19}$$

$$\mathbf{H}(\xi) = \boldsymbol{\mathcal{R}}^{-1}\left[|\xi|\boldsymbol{\mathcal{K}}^* + b\mathbf{I} - id\,\mathrm{sign}(\xi)\mathbf{E}\right]^{-T}\left[b\mathbf{I} - id\,\mathrm{sign}(\xi)\mathbf{E}\right]^T\boldsymbol{\mathcal{R}}. \tag{4.20}$$

The matrices in these expressions are given by

$$\boldsymbol{\mathcal{R}} = \begin{pmatrix} -1 & 0 \\ 0 & 1 \end{pmatrix}, \quad \mathbf{I} = \begin{pmatrix} 1 & 0 \\ 0 & 1 \end{pmatrix}, \quad \mathbf{E} = \begin{pmatrix} 0 & 1 \\ -1 & 0 \end{pmatrix},$$

$$\boldsymbol{\mathcal{K}} = \begin{pmatrix} K_{11} & K_{12} \\ K_{12} & K_{22} \end{pmatrix}, \quad \boldsymbol{\mathcal{K}}^* = \boldsymbol{\mathcal{R}}\boldsymbol{\mathcal{K}}^T\boldsymbol{\mathcal{R}} = \begin{pmatrix} K_{11} & -K_{12} \\ -K_{12} & K_{22} \end{pmatrix}.$$

The scalar constants in equations (4.18), (4.19) and (4.20) depend on the materials considered and are given by

$$b = \frac{1-\nu_1}{\mu_1} + \frac{1-\nu_2}{\mu_2}, \quad d = \frac{1-2\nu_1}{2\mu_1} - \frac{1-2\nu_2}{2\mu_2},$$

$$\alpha = \frac{\mu_2(1-\nu_1) - \mu_1(1-\nu_2)}{\mu_2(1-\nu_1) + \mu_1(1-\nu_2)}, \quad \gamma = \frac{\mu_2(1-2\nu_1) + \mu_1(1-2\nu_2)}{2\mu_2(1-\nu_1) + 2\mu_1(1-\nu_2)},$$

where ν_i is the Poisson's ratio of the material.

For the in-plane case, equation (4.12) becomes

$$[\![\bar{\mathbf{U}}]\!]^T\boldsymbol{\mathcal{R}}\overline{\langle\mathbf{t}\rangle^{(+)}} - \overline{\langle\boldsymbol{\Sigma}\rangle^{(-)}}^T\boldsymbol{\mathcal{R}}[\![\bar{\mathbf{u}}]\!] = -[\![\bar{\mathbf{U}}]\!]^T\boldsymbol{\mathcal{R}}\langle\bar{\mathbf{p}}\rangle - \langle\bar{\mathbf{U}}\rangle^T\boldsymbol{\mathcal{R}}[\![\bar{\mathbf{p}}]\!], \tag{4.21}$$

where $\mathbf{U}$ and $\boldsymbol{\Sigma}$ are 2×2 matrices with each column representing the two linearly independent, in-plane weight functions that are obtainable for elastic bimaterials (Piccolroaz et al., 2009). Similar to the method described for Mode III previously, $[\![\bar{\mathbf{U}}]\!]$ and $[\![\bar{\mathbf{u}}]\!]$ are both split into the sum of their $\pm$ components. The transmission conditions $\overline{[\![\mathbf{U}]\!]^{(-)}} = 0$ and $\overline{[\![\mathbf{u}]\!]^{(+)}} = \boldsymbol{\mathcal{K}}\langle\bar{\mathbf{t}}\rangle^-$ are used to give the expression

$$(\overline{[\![\mathbf{U}]\!]^{(+)}}^T\boldsymbol{\mathcal{R}} - \overline{\langle\boldsymbol{\Sigma}\rangle^{(-)}}^T\boldsymbol{\mathcal{R}}\mathbf{K})\overline{\langle\mathbf{t}\rangle^{(+)}} - \overline{\langle\boldsymbol{\Sigma}\rangle^{(-)}}^T\boldsymbol{\mathcal{R}}\overline{[\![\mathbf{u}]\!]^{(-)}} = -[\![\bar{\mathbf{U}}]\!]^T\boldsymbol{\mathcal{R}}\langle\bar{\mathbf{p}}\rangle - \langle\bar{\mathbf{U}}\rangle^T\boldsymbol{\mathcal{R}}[\![\bar{\mathbf{p}}]\!]. \tag{4.22}$$

For isotropic bimaterials, the in-plane weight functions where a perfect interface is present have the form:

$$\overline{[\![\mathbf{U}]\!]^{(+)}}(\xi) = -\frac{1}{|\xi|}[b\mathbf{I} - id\,\mathrm{sign}(\xi)\mathbf{E}]\overline{\langle\boldsymbol{\Sigma}\rangle^{(-)}}, \tag{4.23}$$

$$\langle\bar{\mathbf{U}}\rangle(\xi) = -\frac{b}{2|\xi|}[\alpha\mathbf{I} - i\gamma\,\mathrm{sign}(\xi)\mathbf{E}]\overline{\langle\boldsymbol{\Sigma}\rangle^{(-)}}. \tag{4.24}$$

Inserting these into (4.22) yields the following equation

$$\left(-\frac{1}{|\xi|}[b\mathbf{I} - id\,\mathrm{sign}(\xi)\mathbf{E}]^T\boldsymbol{\mathcal{R}} - \boldsymbol{\mathcal{R}}\boldsymbol{\mathcal{K}}\right)\overline{\langle\mathbf{t}\rangle^{(+)}} - \boldsymbol{\mathcal{R}}\overline{[\![\mathbf{u}]\!]^{(-)}} = \left(\frac{1}{|\xi|}[b\mathbf{I} - id\,\mathrm{sign}(\xi)\mathbf{E}]^T\boldsymbol{\mathcal{R}}\right)\langle\bar{\mathbf{p}}\rangle + \left(\frac{1}{2|\xi|}[\alpha\mathbf{I} - i\gamma\,\mathrm{sign}(\xi)\mathbf{E}]^T\boldsymbol{\mathcal{R}}\right)[\![\bar{\mathbf{p}}]\!]. \tag{4.25}$$

Rearranging and simplifying this equation yields (4.17). Once again we have shown that using the perfect interface weight function yields the same results as imperfect interface ones obtained in Mishuris et al. (2013), therefore

emphasising the validity of the method that has been developed in this chapter. We now proceed to derive singular integral equations for an imperfect interface in an anisotropic bimaterial.

4.3 Integral identities for Mode III

4.3.1 Derivation of integral identities

We now seek boundary integral equations relating the Mode III interfacial traction and displacement jump over the crack in the anisotropic bimaterial. This will utilise the Betti identity in order to relate the physical solution with the perfect interface weight functions.

The equivalent results for isotropic materials have been reported previously in Section 4.2.2. However, equation (4.16) is derived by simple manipulation of the weight functions and is a general expression. Therefore it can also be used for anisotropic materials:

$$\overline{\langle t\rangle^{(+)}} - \left(\frac{\overline{\langle\Sigma\rangle^{(-)}}}{\overline{[\![U]\!]^{(+)}} - \kappa\overline{\langle\Sigma\rangle^{(-)}}}\right)\overline{[\![u]\!]^{(-)}} = -\left(\frac{\overline{[\![\bar{U}]\!]}}{\overline{[\![U]\!]^{(+)}} - \kappa\overline{\langle\Sigma\rangle^{(-)}}}\right)\bar{\langle p\rangle} - \left(\frac{\overline{\langle\bar{U}\rangle}}{\overline{[\![U]\!]^{(+)}} - \kappa\overline{\langle\Sigma\rangle^{(-)}}}\right)\bar{[\![p]\!]}. \quad (4.26)$$

From equations (4.7) and (4.8) the following relationships hold for the Mode III components of the anisotropic weight functions:

$$[\![\bar{U}]\!] = \overline{[\![U]\!]^{(+)}}(\xi) = -\frac{H_{33}}{|\xi|}\overline{\langle\Sigma\rangle^{(-)}}(\xi); \quad \langle\bar{U}\rangle = -\frac{\delta_3 H_{33}}{2|\xi|}\overline{\langle\Sigma\rangle^{(-)}}(\xi) = \frac{\delta_3}{2}[\![\bar{U}]\!](\xi); \quad (4.27)$$

when combined with equation (4.26) the following relationship is obtained:

$$\overline{\langle t\rangle^{(+)}} - A(\xi)\overline{[\![u]\!]^{(-)}} = -(1+\kappa A(\xi))\bar{\langle p\rangle} - \frac{\delta_3}{2}(1+\kappa A(\xi))\bar{[\![p]\!]}, \quad (4.28)$$

where

$$A(\xi) = -\frac{|\xi|}{\kappa|\xi| + \kappa\mathcal{H}_{33}}, \qquad \mathcal{H}_{33} = \frac{H_{33}}{\kappa}.$$

Applying the inverse Fourier transform to equation (4.28) for the two cases, $x_1 < 0$ and $x_1 > 0$, the following relationships are obtained:

$$\mathcal{F}^{-1}_{x_1<0}\left[A(\xi)\overline{[\![u]\!]^{(-)}}\right] = \mathcal{F}^{-1}_{x_1<0}\left[(1+\kappa A(\xi))\bar{\langle p\rangle}\right] + \frac{\delta_3}{2}\mathcal{F}^{-1}_{x_1<0}\left[(1+\kappa A(\xi))\bar{[\![p]\!]}\right]; \tag{4.29}$$

$$\langle t\rangle^{(+)}(x_1) = \mathcal{F}^{-1}_{x_1>0}\left[A(\xi)\overline{[\![u]\!]^{(-)}}\right] - \mathcal{F}^{-1}_{x_1>0}\left[(1+\kappa A(\xi))\bar{\langle p\rangle}\right] - \frac{\delta_3}{2}\mathcal{F}^{-1}_{x_1>0}\left[(1+\kappa A(\xi))\bar{[\![p]\!]}\right]. \tag{4.30}$$

To calculate these inversions the following relationships are used:

$$\mathcal{F}^{-1}\left[A(\xi)\bar{f}(\xi)\right] = \frac{1}{\pi\kappa}\left(S_{\mathcal{H}_{33}} * f'\right)(x_1); \tag{4.31}$$

$$\mathcal{F}^{-1}\left[(1+\kappa A(\xi))\bar{f}(\xi)\right] = -\frac{\mathcal{H}_{33}}{\pi}\left(T_{\mathcal{H}_{33}} * f\right)(x_1), \tag{4.32}$$

where

$$S_{\mathcal{H}_{33}}(x_1) = \mathrm{sign}(x_1)\mathrm{si}(\mathcal{H}_{33}|x_1|)\cos(\mathcal{H}_{33}|x_1|) - \mathrm{sign}(x_1)\mathrm{ci}(\mathcal{H}_{33}|x_1|)\sin(\mathcal{H}_{33}|x_1|), \tag{4.33}$$

$$T_{\mathcal{H}_{33}}(x_1) = \mathrm{si}(\mathcal{H}_{33}|x_1|)\sin(\mathcal{H}_{33}|x_1|) - \mathrm{ci}(\mathcal{H}_{33}|x_1|)\cos(\mathcal{H}_{33}|x_1|), \tag{4.34}$$

and si and ci are the sine and cosine integral functions respectively, given by

$$\mathrm{si}(x_1) = -\int_{x_1}^{\infty}\frac{\sin t}{t}\mathrm{d}t, \quad \mathrm{ci}(x_1) = -\int_{x_1}^{\infty}\frac{\cos t}{t}\mathrm{d}t. \tag{4.35}$$

These functions have the same properties as their counterparts from the isotropic case considered by Mishuris et al. (2013), but with different constants. In particular, the function $S_{\mathcal{H}_{33}}(x_1)$ behaves as

$$S_{\mathcal{H}_{33}}(x_1) = -\frac{\pi}{2}\mathrm{sign}(x_1) + O(|x_1|),\ x_1 \to 0, \tag{4.36}$$

$$S_{\mathcal{H}_{33}}(x_1) = -\frac{\operatorname{sign}(x_1)}{\mathcal{H}_{33}|x_1|} + O\left(\frac{1}{|x_1|^3}\right),\ x_1 \to \pm\infty, \tag{4.37}$$

while $T_{\mathcal{H}_{33}}(x_1)$ has behaviour of the form

$$T_{\mathcal{H}_{33}}(x_1) = \ln(\mathcal{H}_{33}|x_1|) + O(1),\ x_1 \to 0, \tag{4.38}$$

$$T_{\mathcal{H}_{33}}(x_1) = -\frac{1}{\mathcal{H}_{33}^2|x_1|^2} + O\left(\frac{1}{|x_1|^3}\right),\ x_1 \to \pm\infty. \tag{4.39}$$

We introduce convolution operators $\mathcal{S}_{\mathcal{H}_{33}}$ and $\mathcal{T}_{\mathcal{H}_{33}}$, as well as projection operators $\mathcal{P}_{\pm}$:

$$\mathcal{S}_{\mathcal{H}_{33}}\varphi(x_1) = (S_{\mathcal{H}_{33}} * \varphi)(x_1), \qquad \mathcal{T}_{\mathcal{H}_{33}}\varphi(x_1) = (T_{\mathcal{H}_{33}} * \varphi)(x_1), \tag{4.40}$$

$$\mathcal{P}_{\pm}\varphi(x_1) = \begin{cases} \varphi(x_1) & \pm x_1 \geq 0, \\ 0 & \text{otherwise}, \end{cases} \tag{4.41}$$

in order to rewrite the identities (4.29) and (4.30) as

$$\frac{1}{\pi\kappa}\mathcal{S}^{(s)}_{\mathcal{H}_{33}}\frac{\partial[\![u]\!]^{(-)}}{\partial x_1} - \frac{1}{\pi\kappa}[\![u]\!]^{(-)}(0^-)S_{\mathcal{H}_{33}}(x_1) = \\ - \frac{\mathcal{H}_{33}}{\pi}\mathcal{T}^{(s)}_{\mathcal{H}_{33}}\langle p\rangle(x_1) - \frac{\delta_3\mathcal{H}_{33}}{2\pi}\mathcal{T}^{(s)}_{\mathcal{H}_{33}}[\![p]\!](x_1), \quad x_1 < 0, \tag{4.42}$$

$$\langle t\rangle^{(+)}(x_1) = \frac{1}{\pi\kappa}\mathcal{S}^{(c)}_{\mathcal{H}_{33}}\frac{\partial[\![u]\!]^{(-)}}{\partial x_1} - \frac{1}{\pi\kappa}[\![u]\!]^{(-)}(0^-)S_{\mathcal{H}_{33}}(x_1) \\ + \frac{\mathcal{H}_{33}}{\pi}\mathcal{T}^{(c)}_{\mathcal{H}_{33}}\langle p\rangle(x_1) + \frac{\delta_3\mathcal{H}_{33}}{2\pi}\mathcal{T}^{(c)}_{\mathcal{H}_{33}}[\![p]\!](x_1), \quad x_1 > 0, \tag{4.43}$$

where

$$\mathcal{S}^{(s)}_{\mathcal{H}_{33}} = \mathcal{P}_-\mathcal{S}_{\mathcal{H}_{33}}\mathcal{P}_-, \qquad \mathcal{T}^{(s)}_{\mathcal{H}_{33}} = \mathcal{P}_-\mathcal{T}_{\mathcal{H}_{33}}\mathcal{P}_-, \tag{4.44}$$

are singular operators and

$$\mathcal{S}^{(c)}_{\mathcal{H}_{33}} = \mathcal{P}_+ \mathcal{S}_{\mathcal{H}_{33}} \mathcal{P}_-, \qquad \mathcal{T}^{(c)}_{\mathcal{H}_{33}} = \mathcal{P}_+ \mathcal{T}_{\mathcal{H}_{33}} \mathcal{P}_-, \tag{4.45}$$

are compact. The second term on the left hand side of (4.42) and right hand side of (4.43) appear as a result of the discontinuity of the derivative of $[\![u]\!]^{(-)}$ at $x_1 = 0$.

4.3.2 Alternative integral identities

The integral identities (4.42) and (4.43) can be formulated in alternative ways, which depending upon the specific problem parameters and loadings, can aid the ease with which computations may be performed. Combining equations (4.31), (4.32) and (4.40) yields the auxiliary relationship

$$-\frac{\mathcal{H}_{33}}{\pi} \mathcal{T}_{\mathcal{H}_{33}} \varphi = \mathcal{I}\varphi + \frac{1}{\pi} \mathcal{S}_{\mathcal{H}_{33}} \varphi'. \tag{4.46}$$

Using this relationship, equations (4.42) and (4.43) can be rewritten as follows:

$$\begin{aligned} -\frac{\mathcal{H}_{33}}{\pi\kappa} \mathcal{T}^{(s)}_{\mathcal{H}_{33}} [\![u]\!]^{(-)} - \frac{1}{\kappa} [\![u]\!]^{(-)} &= \frac{1}{\pi} \mathcal{S}^{(s)}_{\mathcal{H}_{33}} \frac{\partial \langle p \rangle}{\partial x_1} - \frac{1}{\pi} \langle p \rangle (0^-) S_{\mathcal{H}_{33}} + \langle p \rangle \\ &\quad + \frac{\delta_3}{2\pi} \mathcal{S}^{(s)}_{\mathcal{H}_{33}} \frac{\partial [\![p]\!]}{\partial x_1} - \frac{\delta_3}{2\pi} [\![p]\!](0^-) S_{\mathcal{H}_{33}} + \frac{\delta_3}{2} [\![p]\!], \quad x_1 < 0; \end{aligned} \tag{4.47}$$

$$\begin{aligned} \langle t \rangle^{(+)} = -\frac{\mathcal{H}_{33}}{\pi\kappa} \mathcal{T}^{(c)}_{\mathcal{H}_{33}} [\![u]\!]^{(-)} - \frac{1}{\pi} \mathcal{S}^{(c)}_{\mathcal{H}_{33}} \frac{\partial \langle p \rangle}{\partial x_1} + \frac{1}{\pi} \langle p \rangle (0^-) S_{\mathcal{H}_{33}} + \langle p \rangle \\ - \frac{\delta_3}{2\pi} \mathcal{S}^{(c)}_{\mathcal{H}_{33}} \frac{\partial [\![p]\!]}{\partial x_1} + \frac{\delta_3}{2\pi} [\![p]\!](0^-) S_{\mathcal{H}_{33}}, \quad x_1 > 0. \end{aligned} \tag{4.48}$$

It is also possible to write these equations using only the operator $\mathcal{T}_{\mathcal{H}_{33}}$:

$$-\frac{\mathcal{H}_{33}}{\pi\kappa}\mathcal{T}^{(s)}_{\mathcal{H}_{33}}[\![u]\!]^{(-)}-\frac{1}{\kappa}[\![u]\!]^{(-)}=-\frac{\mathcal{H}_{33}}{\pi}\mathcal{T}^{(s)}_{\mathcal{H}_{33}}\langle p\rangle-\frac{\delta_3\mathcal{H}_{33}}{2\pi}\mathcal{T}^{(s)}_{\mathcal{H}_{33}}[\![p]\!],\quad x_1<0;\tag{4.49}$$

$$\langle t\rangle^{(+)}=-\frac{\mathcal{H}_{33}}{\pi\kappa}\mathcal{T}^{(c)}_{\mathcal{H}_{33}}[\![u]\!]^{(-)}+\frac{\mathcal{H}_{33}}{\pi}\mathcal{T}^{(c)}_{\mathcal{H}_{33}}\langle p\rangle+\frac{\delta_3\mathcal{H}_{33}}{2\pi}\mathcal{T}^{(c)}_{\mathcal{H}_{33}}[\![p]\!],\quad x_1>0,\tag{4.50}$$

or solely the operator $\mathcal{S}_{\mathcal{H}_{33}}$:

$$\begin{aligned}\frac{1}{\pi\kappa}\mathcal{S}^{(s)}_{\mathcal{H}_{33}}\frac{\partial[\![u]\!]^{(-)}}{\partial x_1}-\frac{1}{\pi\kappa}[\![u]\!]^{(-)}(0^-)S_{\mathcal{H}_{33}}&=\frac{1}{\pi}\mathcal{S}^{(s)}_{\mathcal{H}_{33}}\frac{\partial\langle p\rangle}{\partial x_1}\\&-\frac{1}{\pi}\langle p\rangle(0^-)S_{\mathcal{H}_{33}}+\langle p\rangle+\frac{\delta_3}{2\pi}\mathcal{S}^{(s)}_{\mathcal{H}_{33}}\frac{\partial[\![p]\!]}{\partial x_1}-\frac{\delta_3}{2\pi}[\![p]\!](0^-)S_{\mathcal{H}_{33}}+\frac{\delta_3}{2}[\![p]\!],\quad x_1<0;\end{aligned}\tag{4.51}$$

$$\begin{aligned}\langle t\rangle^{(+)}=\frac{1}{\pi\kappa}\mathcal{S}^{(c)}_{\mathcal{H}_{33}}\frac{\partial[\![u]\!]^{(-)}}{\partial x_1}-\frac{1}{\pi\kappa}[\![u]\!]^{(-)}(0^-)S_{\mathcal{H}_{33}}-\frac{1}{\pi}\mathcal{S}^{(c)}_{\mathcal{H}_{33}}\frac{\partial\langle p\rangle}{\partial x_1}\\+\frac{1}{\pi}\langle p\rangle(0^-)S_{\mathcal{H}_{33}}+\langle p\rangle-\frac{\delta_3}{2\pi}\mathcal{S}^{(c)}_{\mathcal{H}_{33}}\frac{\partial[\![p]\!]}{\partial x_1}+\frac{\delta_3}{2\pi}[\![p]\!](0^-)S_{\mathcal{H}_{33}},\quad x_1>0.\end{aligned}\tag{4.52}$$

Each of the four formulations have advantages for numerical computations depending on the mechanical parameters of the problem and which quantities are known or unknown. The merits of alternative formulations for the analogous isotropic case have been discussed in detail in Mishuris et al. (2013).

4.3.3 Numerical results

Results from singular integral equations

In this section, the integral identities found previously will be used to calculate the jump in displacement over the crack and imperfect interface between

two orthotropic materials. Results for finite element simulations using COMSOL will also be presented and compared to the results using the integral identity approach derived previously.

We will present results for the displacement jump $[\![u]\!]$. Note for the Mode III case that for $x_1 > 0$, the interfacial tractions and displacement jump $[\![u]\!]$ are straightforwardly related via the imperfect interface transmission conditions (4.2). In particular for the Mode III displacement jump, the relationship is as follows:

$$[\![u]\!](x_1) = \kappa\langle t\rangle(x_1), \qquad x_1 > 0. \tag{4.53}$$

Here, we only consider tractions along the crack/interface line; discussions of full radial asymptotics (for stress and displacement) and their relationship to the displacement jump can be found in Lenci (2001); Mishuris (2001); Antipov et al. (2001); Vellender et al. (2013), among others.

For orthotropic materials, the material parameters H_{33} and δ_3 are given in terms of the components of the material compliance tensor, $\mathbf{S}$, in Appendix 1. It is possible to express S_{44} and S_{55} in terms of the shear moduli, μ_{ij} of the material:

$$S_{44} = \frac{1}{\mu_{23}}, \qquad S_{55} = \frac{1}{\mu_{13}}. \tag{4.54}$$

In our computations, the same orthotropic material will be used as material I and II. However, the axes corresponding to each axis of symmetry of the material in the lower half-plane is altered. The parameters used for the computations presented are shown in Table 4.1. The values of μ_{12} are given in Table 4.1 to illustrate that the materials considered are the same but differently oriented. Henceforth, the material above the crack (I) will be material A from Table 4.1.

Orientation	μ_{23}	μ_{13}	μ_{12}
A	1	2/3	1/2
B	1	1/2	2/3
C	1/2	2/3	1

Table 4.1: Material properties

We first consider a symmetric distribution of loadings given by

$$[\![p]\!](x_1) = 0, \qquad \langle p \rangle(x_1) = -\frac{F}{l} e^{\frac{x_1}{l}}. \tag{4.55}$$

Figure 4.2 plots the normalised displacement jump along the x_1-axis induced by the above loading for the three possible orientations for material II for two different degrees of interface imperfection which have been computed by numerically solving the integral equations (4.49) and (4.50) using an iterative scheme in Mathematica. The normalised displacement jump is denoted $[\![u^*]\!]$ and defined by

$$[\![u^*]\!] = \frac{1}{F\left[\sqrt{S_{44}S_{55}}\right]_I}[\![u]\!]. \tag{4.56}$$

A normalised traction, t^*, is also used in the calculations and is related to the normalised displacement jump by the relationship $[\![u^*]\!] = \kappa^* t^*$, where

$$t^* = \frac{l}{F}t, \qquad \kappa^* = \frac{1}{l\left[\sqrt{S_{44}S_{55}}\right]_I}\kappa. \tag{4.57}$$

Figure 4.2 shows that a higher value of κ gives a higher jump in displacement across the crack and interface for all orientations of the material II; this result is expected as a larger κ refers to a less stiff interface. It is also seen that for the same value of κ, the orientation of the anisotropy has a

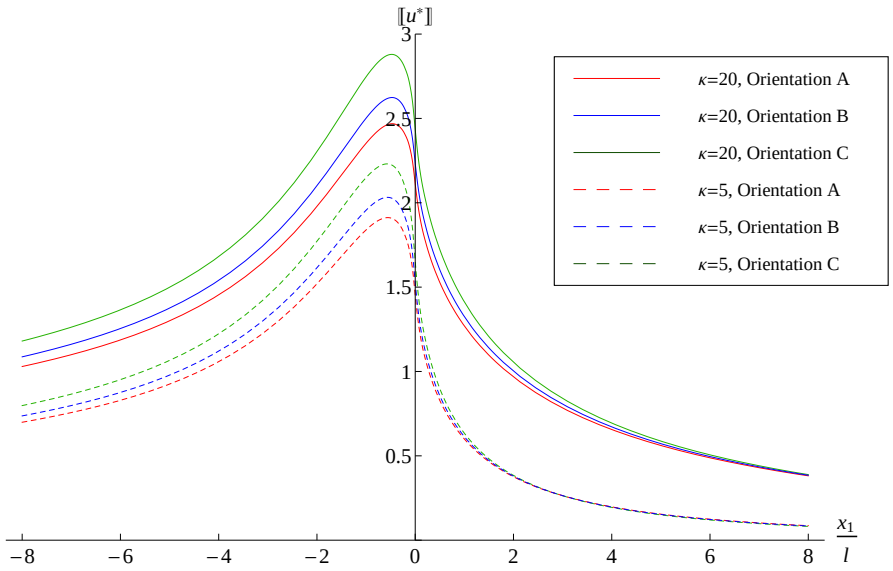

Figure 4.2: Graph of normalised displacement jump over the crack and interface induced by loading (4.55).

diminishing effect along the interface ($x_1 > 0$) as the distance from the crack tip is increased.

The difference in orientation of material II has a clear effect on the jumps in displacement shown in Figure 4.2, with the same behaviour observed for both values of κ studied here. The highest jump in both cases is seen for orientation C in the lower half-plane. This is due to the lower shear moduli contributing to the Mode III fields in this case. Orientation A leads to the smallest displacement jump; this is due to the higher shear moduli in the out-of-plane direction.

In order to demonstrate that the method is applicable for asymmetric as well as symmetric loadings, we present in Figure 4.3 a similar plot, but instead using asymmetric loadings of the form

$$p^+(x_1) = -\frac{F}{l}e^{x_1/l}, \qquad p^-(x_1) = \frac{F}{l^2}x_1 e^{x_1/l}. \tag{4.58}$$

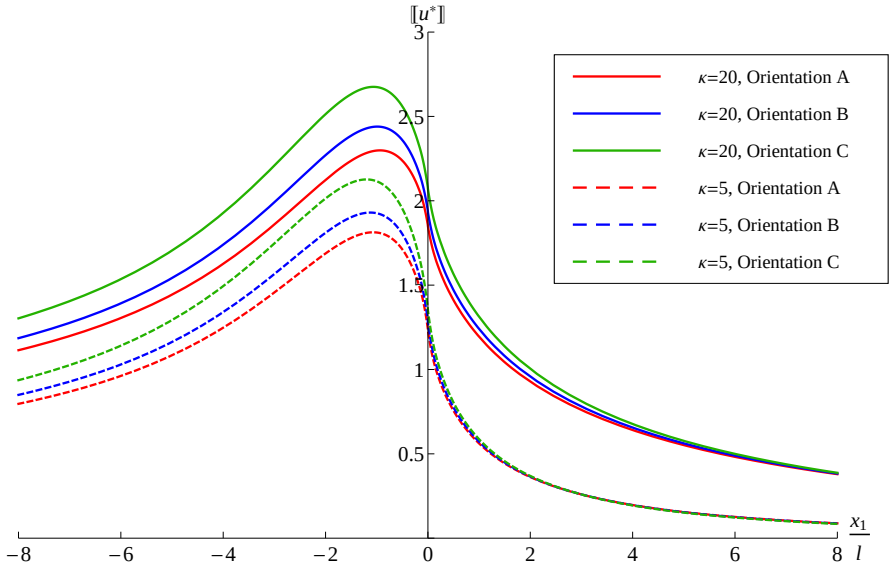

Figure 4.3: Displacement jump for asymmetric loading.

The results once again show that higher values of κ lead to a higher displacement jump. Asymmetry also varies the point of highest displacement jump for different orientations whereas this was seen to be at the same point for symmetric loading regardless of the extent of interface imperfection and material orientation.

Finite element results

We now compare results from finite element simulations performed in COMSOL for a crack along an imperfect interface with computations from the integral equations. When using COMSOL it is not possible to directly implement the transmission conditions (4.1) and (4.2) across the interface. Instead, a very thin layer of a softer material is used for the interface and the properties of that material are varied to obtain the desired value for κ (see for instance Antipov et al. (2001)). Also, it is not possible to realise

an infinite geometry in COMSOL and therefore a very large, finite geometry is used as an approximation. These issues with the finite element model demonstrate the advantage of the boundary integral formulation, since the issues of the very fine meshing required in the interface layer and the large geometries of the main material bodies are respectively replaced by imperfect interface transmission conditions and the lower dimensional nature of the boundary problem. We present results comparing the two approaches in a case where the soft interface layer is not *too* thin in order to demonstrate the comparability of the two approaches.

An example colour map of the Mode III displacement from COMSOL is shown in Figure 4.4, using material orientation A for both main material bodies and an interface layer corresponding to $\kappa = 20$.

Using COMSOL, values for the displacement jump over the crack and interface have been extracted for a number of points near the crack tip for two of the examples shown in Figure 4.2. The results of these comparisons are shown in Figure 4.5 and Table 4.2. Figure 4.5 shows good agreement

Material	-5	-4	-3	-2	-1	0	1	2	3	4	5
A, $\kappa = 5$	2.30	1.81	1.07	0.61	0.20	0.06	0.18	0.70	3.41	2.77	4.66
C, $\kappa = 20$	0.53	0.62	0.84	0.87	1.13	0.55	1.80	2.75	3.81	5.19	6.70

Table 4.2: Percentage difference between Mathematica and COMSOL.

between the results from the singular integral equations and those obtained from finite element methods. The difference in results is smallest at the crack tip but more error can be seen at a further distance along both the crack and interface, which is emphasised by the larger percentage errors shown in Table

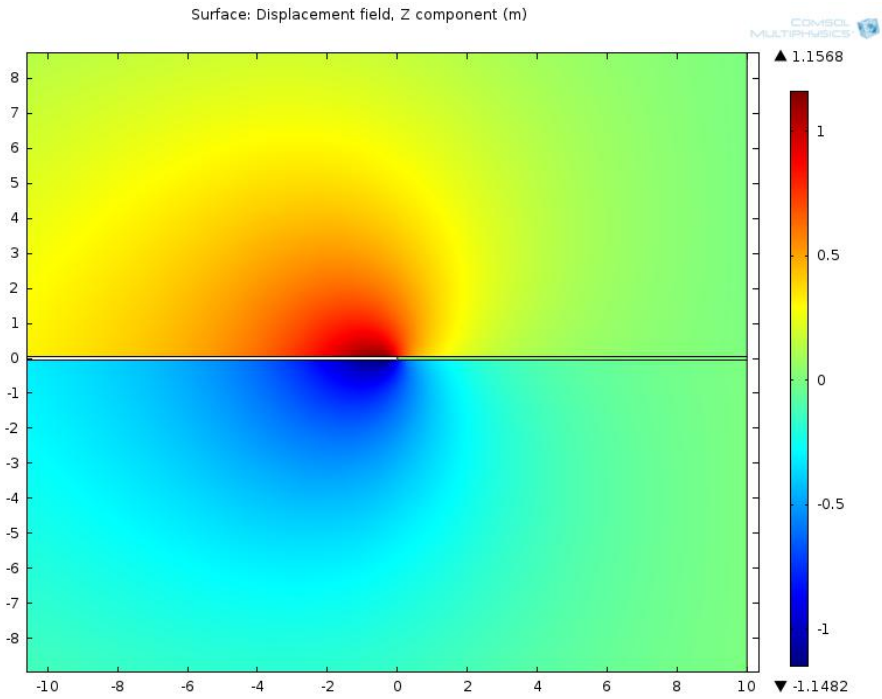

Figure 4.4: Finite element computations of displacement jump, using a thin densely-meshed soft layer in place of the imperfect interface.

4.2. This is likely caused by the finite geometry that was used in COMSOL which leads to an influence caused by the outer boundaries.

4.4 Integral identities for Mode I and II

4.4.1 Derivation of integral identities

Heretofore, we have derived integral identities for the Mode III regime only. This section seeks to find boundary integral equations relating the Mode I and II interfacial traction and displacement jump over the crack in an imperfectly bound anisotropic bimaterial. For the Mode I and II components we remind

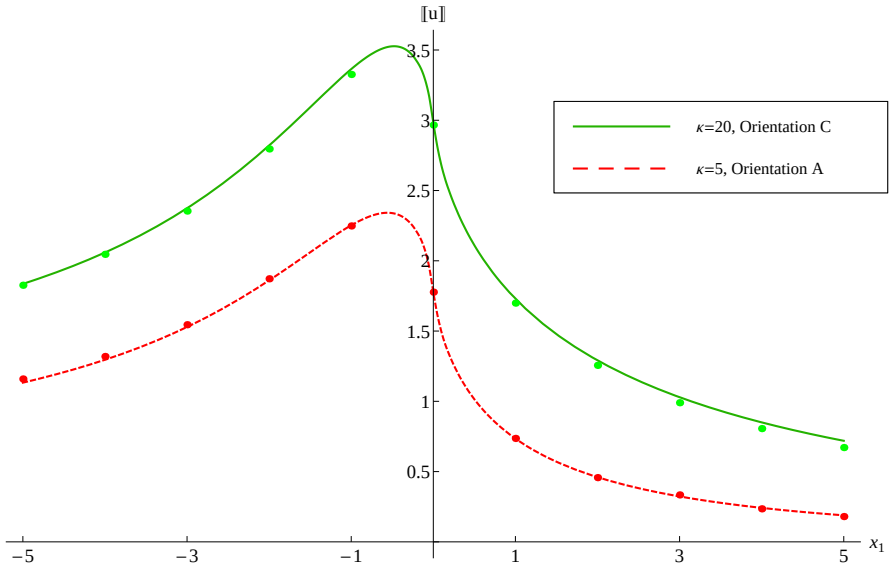

Figure 4.5: Graph of the comparison between displacement jumps from Mathematica and COMSOL. The lines show the results of computations from the integral equations while finite element computations are represented by dots.

ourselves of equation (4.12):

$$[\![\bar{\mathbf{U}}]\!]^T \boldsymbol{\mathcal{R}} \overline{\langle \mathbf{t} \rangle^{(+)}} - \overline{\langle \boldsymbol{\Sigma} \rangle^{(-)}}^T \boldsymbol{\mathcal{R}} [\![\bar{\mathbf{u}}]\!] = -[\![\bar{\mathbf{U}}]\!]^T \boldsymbol{\mathcal{R}} \langle \bar{\mathbf{p}} \rangle - \langle \bar{\mathbf{U}} \rangle^T \boldsymbol{\mathcal{R}} [\![\bar{\mathbf{p}}]\!]. \tag{4.59}$$

The matrices and vectors shown here contain only the Mode I and II components from (4.12). $\bar{\mathbf{U}}$ and $\bar{\boldsymbol{\Sigma}}$ are once again 2×2 matrices consisting of two linearly independent weight functions (Piccolroaz et al., 2009).

Splitting $[\![\bar{\mathbf{U}}]\!]$ into the sum of $\overline{[\![\mathbf{U}]\!]^{(\pm)}}$ and $[\![\bar{\mathbf{u}}]\!]$ into $\overline{[\![\mathbf{u}]\!]^{(\pm)}}$, where (as previously) superscripts $^{(\pm)}$ denote the restriction of the preceding function to the respective semi-x_1-axis, gives

$$\begin{aligned} \overline{[\![\mathbf{U}]\!]^{(+)}}^T \boldsymbol{\mathcal{R}} \overline{\langle \mathbf{t} \rangle^{(+)}} + \overline{[\![\mathbf{U}]\!]^{(-)}}^T \boldsymbol{\mathcal{R}} \overline{\langle \mathbf{t} \rangle^{(+)}} - \overline{\langle \boldsymbol{\Sigma} \rangle^{(-)}}^T \boldsymbol{\mathcal{R}} \overline{[\![\mathbf{u}]\!]^{(+)}} - \overline{\langle \boldsymbol{\Sigma} \rangle^{(-)}}^T \boldsymbol{\mathcal{R}} \overline{[\![\mathbf{u}]\!]^{(-)}} \\ = -[\![\bar{\mathbf{U}}]\!]^T \boldsymbol{\mathcal{R}} \langle \bar{\mathbf{p}} \rangle - \langle \bar{\mathbf{U}} \rangle^T \boldsymbol{\mathcal{R}} [\![\bar{\mathbf{p}}]\!]. \end{aligned} \tag{4.60}$$

Applying the transmission conditions, $\overline{[\![\mathbf{U}]\!]^{(-)}} = 0$ and $\overline{[\![\mathbf{u}]\!]^{(+)}} = \boldsymbol{\mathcal{K}} \overline{\langle \mathbf{t} \rangle^{(+)}}$,

along with equations (4.7) and (4.8) gives the following expression:

$$\overline{\langle \mathbf{t} \rangle^{(+)}} - \mathbf{B}(\xi) \frac{\xi}{i} \overline{[\![\mathbf{u}]\!]^{(-)}} = -\mathbf{C}(\xi) \langle \bar{\mathbf{p}} \rangle - \mathbf{A}(\xi) [\![\bar{\mathbf{p}}]\!], \tag{4.61}$$

where

$$\mathbf{A}(\xi) = \frac{1}{2} \boldsymbol{\mathcal{R}}^{-1} (|\xi| \boldsymbol{\mathcal{K}}^* + \mathbf{R_H} - i \text{sign}(\xi) \mathbf{I_H})^{-T} (\mathbf{R_W} - i \text{sign}(\xi) \mathbf{I_W})^T \boldsymbol{\mathcal{R}},$$

$$\mathbf{B}(\xi) = -i \boldsymbol{\mathcal{R}}^{-1} (\xi \boldsymbol{\mathcal{K}}^* + \text{sign}(\xi) \mathbf{R_H} - i \mathbf{I_H})^{-T} \boldsymbol{\mathcal{R}},$$

$$\mathbf{C}(\xi) = \boldsymbol{\mathcal{R}}^{-1} (|\xi| \boldsymbol{\mathcal{K}}^* + \mathbf{R_H} - i \text{sign}(\xi) \mathbf{I_H})^{-T} (\mathbf{R_H} - i \text{sign}(\xi) \mathbf{I_H})^T \boldsymbol{\mathcal{R}}.$$

Here, $\mathbf{R_H} = \text{Re}(\mathbf{H})$, $\mathbf{R_W} = \text{Re}(\mathbf{W})$, $\mathbf{I_H} = \text{Im}(\mathbf{H})$, $\mathbf{I_W} = \text{Im}(\mathbf{W})$ and $\boldsymbol{\mathcal{K}}^* = \boldsymbol{\mathcal{R}} \boldsymbol{\mathcal{K}} \boldsymbol{\mathcal{R}}$.

Matrices $\mathbf{A}(\xi)$, $\mathbf{B}(\xi)$ and $\mathbf{C}(\xi)$ have the following form

$$\mathbf{A}(\xi) = \frac{1}{2D} \begin{pmatrix} A_{11} & A_{12} \\ A_{21} & A_{22} \end{pmatrix}, \quad \mathbf{B}(\xi) = \frac{1}{D} \begin{pmatrix} B_{11} & B_{12} \\ B_{21} & B_{22} \end{pmatrix}, \quad \mathbf{C}(\xi) = \frac{1}{D} \begin{pmatrix} C_{11} & C_{12} \\ C_{21} & C_{22} \end{pmatrix} \tag{4.62}$$

where the denominator D is defined as

$$D = d_0 + d_1 |\xi| + d_2 |\xi|^2, \tag{4.63}$$

$$d_0 = H_{11} H_{22} (1 - \beta^2), \quad d_1 = K_{11} H_{22} + K_{22} H_{11}, \quad d_2 = K_{11} K_{22} - K_{12}^2,$$

and the elements A_{ij}, B_{ij}, C_{ij} are given by

$$A_{11} = H_{11} H_{22} (\delta_1 + \beta\gamma) + |\xi| (\delta_1 H_{11} K_{22} - i\gamma K_{12} \sqrt{H_{11} H_{22}} \text{ sign}(\xi)),$$

$$A_{12} = -i \text{ sign}(\xi) H_{22} \sqrt{H_{11} H_{22}} (\gamma + \beta\delta_2) - |\xi| (i\gamma K_{22} \sqrt{H_{11} H_{22}} \text{ sign}(\xi) + \delta_2 H_{22} K_{12}),$$

$$A_{21} = i \text{ sign}(\xi) H_{11} \sqrt{H_{11} H_{22}} (\delta_1 \beta + \gamma) - |\xi| (\delta_1 H_{11} K_{12} - i\gamma K_{11} \sqrt{H_{11} H_{22}} \text{ sign}(\xi)),$$

$$A_{22} = H_{11} H_{22} (\beta\gamma + \delta_2) + |\xi| (\delta_2 H_{22} K_{11} + i\gamma K_{12} \sqrt{H_{11} H_{22}} \text{ sign}(\xi)),$$

$$B_{11} = -i(\xi K_{22} + H_{22}\ \mathrm{sign}(\xi)), \quad B_{12} = i\xi K_{12} - \beta\sqrt{H_{11}H_{22}},$$

$$B_{21} = i\xi K_{12} + \beta\sqrt{H_{11}H_{22}}, \quad B_{22} = -i(\xi K_{11} + H_{11}\ \mathrm{sign}(\xi)),$$

$$C_{11} = H_{11}H_{22}(1-\beta^2) + |\xi|(H_{11}K_{22} + i\beta K_{12}\sqrt{H_{11}H_{22}}\ \mathrm{sign}(\xi)),$$

$$C_{12} = -|\xi|(H_{22}K_{12} - i\beta\ \mathrm{sign}(\xi)K_{22}\sqrt{H_{11}H_{22}}),$$

$$C_{21} = -|\xi|(H_{11}K_{12} + i\beta\ \mathrm{sign}(\xi)K_{11}\sqrt{H_{11}H_{22}}),$$

$$C_{22} = H_{11}H_{22}(1-\beta^2) + |\xi|(H_{22}K_{11} - i\beta K_{12}\sqrt{H_{11}H_{22}}\ \mathrm{sign}(\xi)).$$

Applying the inverse Fourier transform to equation (4.61) for the two cases, $x_1 < 0$ and $x_1 > 0$, the following relationships are obtained:

$$\mathcal{F}^{-1}_{x_1<0}\left[\mathbf{B}(\xi)\frac{\xi}{i}\overline{[\![\mathbf{u}]\!]^{(-)}}\right] = \mathcal{F}^{-1}_{x_1<0}\left[\mathbf{C}(\xi)\bar{\langle\mathbf{p}\rangle}\right] + \mathcal{F}^{-1}_{x_1<0}\left[\mathbf{A}(\xi)\bar{[\![\mathbf{p}]\!]}\right]; \tag{4.64}$$

$$\langle\mathbf{t}\rangle(x_1) = \mathcal{F}^{-1}_{x_1>0}\left[\mathbf{B}(\xi)\frac{\xi}{i}\overline{[\![\mathbf{u}]\!]^{(-)}}\right] - \mathcal{F}^{-1}_{x_1>0}\left[\mathbf{C}(\xi)\bar{\langle\mathbf{p}\rangle}\right] - \mathcal{F}^{-1}_{x_1>0}\left[\mathbf{A}(\xi)\bar{[\![\mathbf{p}]\!]}\right]. \tag{4.65}$$

The inverse Fourier transforms of the matrices $\mathbf{A}(\xi)$, $\mathbf{B}(\xi)$ and $\mathbf{C}(\xi)$ are derived in Appendix 2. The singular integral equations obtained for the in-plane fields are thus

$$\boldsymbol{\mathcal{B}}^{(s)}\frac{\partial[\![\mathbf{u}]\!]^{(-)}}{\partial x_1} + \frac{1}{\pi d_2(\xi_2-\xi_1)}\sum_{j=1}^{2}\mathbf{B}_R^{(j)}T_{\xi_j}(x_1)[\![\mathbf{u}]\!]^{(-)}(0^-)$$
$$+ \frac{1}{\pi d_2(\xi_2-\xi_1)}\sum_{j=1}^{2}\mathbf{B}_I^{(j)}S_{\xi_j}(x_1)[\![\mathbf{u}]\!]^{(-)}(0^-) = \boldsymbol{\mathcal{C}}^{(s)}\langle\mathbf{p}\rangle(x_1) + \boldsymbol{\mathcal{A}}^{(s)}[\![\mathbf{p}]\!](x_1), \tag{4.66}$$

for $x_1 < 0$, and

$$\langle \mathbf{t} \rangle(x_1) = \boldsymbol{\mathcal{B}}^{(c)} \frac{\partial [\![\mathbf{u}]\!]^{(-)}}{\partial x_1} + \frac{1}{\pi d_2 (\xi_2 - \xi_1)} \sum_{j=1}^{2} \mathbf{B}_R^{(j)} T_{\xi_j}(x_1) [\![\mathbf{u}]\!]^{(-)}(0^-)$$
$$+ \frac{1}{\pi d_2 (\xi_2 - \xi_1)} \sum_{j=1}^{2} \mathbf{B}_I^{(j)} S_{\xi_j}(x_1) [\![\mathbf{u}]\!]^{(-)}(0^-) - \boldsymbol{\mathcal{C}}^{(c)} \langle \mathbf{p} \rangle(x_1) - \boldsymbol{\mathcal{A}}^{(c)} [\![\mathbf{p}]\!](x_1), \tag{4.67}$$

for $x_1 > 0$. The operators used in equations (4.66) and (4.67) are given by

$$\boldsymbol{\mathcal{A}}^{(s,c)} = -\frac{1}{2\pi d_2 (\xi_2 - \xi_1)} \left\{ \sum_{j=1}^{2} \mathbf{A}_R^{(j)} \mathcal{T}_{\xi_j}^{(s,c)}(x_1) + \sum_{j=1}^{2} \mathbf{A}_I^{(j)} \mathcal{S}_{\xi_j}^{(s,c)}(x_1) \right\}, \tag{4.68}$$

$$\boldsymbol{\mathcal{B}}^{(s,c)} = -\frac{1}{\pi d_2 (\xi_2 - \xi_1)} \left\{ \sum_{j=1}^{2} \mathbf{B}_R^{(j)} \mathcal{T}_{\xi_j}^{(s,c)}(x_1) + \sum_{j=1}^{2} \mathbf{B}_I^{(j)} \mathcal{S}_{\xi_j}^{(s,c)}(x_1) \right\}, \tag{4.69}$$

$$\boldsymbol{\mathcal{C}}^{(s,c)} = -\frac{1}{\pi d_2 (\xi_2 - \xi_1)} \left\{ \sum_{j=1}^{2} \mathbf{C}_R^{(j)} \mathcal{T}_{\xi_j}^{(s,c)}(x_1) + \sum_{j=1}^{2} \mathbf{C}_I^{(j)} \mathcal{S}_{\xi_j}^{(s,c)}(x_1) \right\}. \tag{4.70}$$

Further details on these operators, including their derivation, can be found in Appendix 2.

4.4.2 Numerical examples

In this section we present an illustrative example of applying the derived integral equations (4.66) and (4.67) to find the in-plane tractions and displacement jump when an asymmetrical, Mode I loading is applied to the crack faces. For the purpose of these calculations, incompressible orthotropic materials will be used. It was shown by Itskov and Aksel (2002) that for such materials only four parameters are required to express the components of $\mathbf{S}$, which are related to the matrices $\mathbf{H}$ and $\mathbf{W}$ (as seen in Appendix 1). The

components are

$$S_{11} = \frac{1}{E_1}, \quad S_{22} = \frac{1}{E_2}, \quad S_{66} = \frac{1}{\mu_{12}},$$
$$S_{12} = \frac{1}{2}\left(\frac{1}{E_3} - \frac{1}{E_1} - \frac{1}{E_2}\right), \tag{4.71}$$

where E_i are the Young's moduli of the material in question. The materials considered here will have the properties shown in Table 4.3.

Material	E_1	E_2	E_3	μ_{12}
I	20	10	10	5
II	20	10	15	5

Table 4.3: Material parameters.

We present computations resulting from an applied asymmetric crack face loading of the form

$$\mathbf{p}^+(x_1) = \begin{pmatrix} 0 \\ -\frac{F}{l}e^{x_1/l} \end{pmatrix}, \quad \mathbf{p}^-(x_1) = \begin{pmatrix} 0 \\ \frac{F}{l^2}x_1 e^{x_1/l} \end{pmatrix}, \tag{4.72}$$

with $F = 1$ and $l = 1$; the interfacial imperfection parameters are $K_{11} = 10$, $K_{12} = 2$, $K_{22} = 3$. The interfacial tractions are shown in Figure 4.6, along with the displacement jump in the x_1 and x_2 directions. Note that since the crack face loadings were applied in the x_2-direction, the displacement jump across the crack and interface, as well as the interfacial traction, is dominant in that direction. Note in particular that the presence of the imperfect interface causes components of stress to remain bounded at the crack tip along the interface/crack line, in contrast to the analogous perfect interface problem.

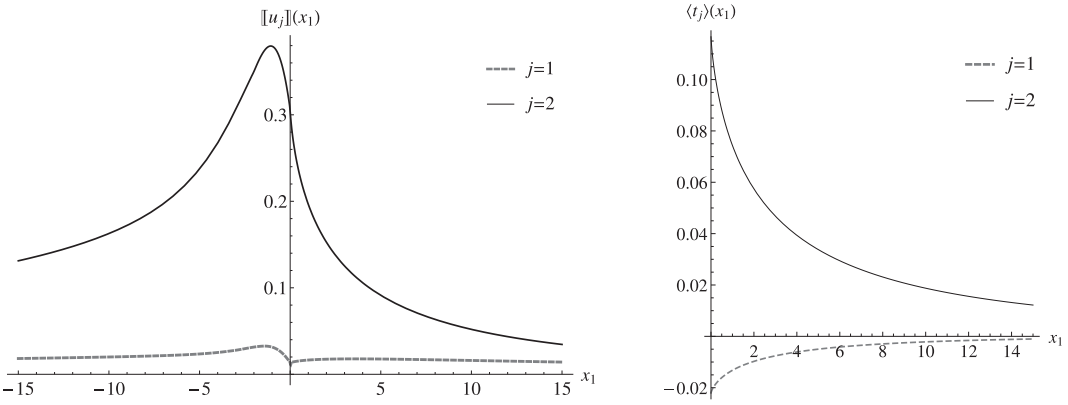

Figure 4.6: In-plane displacement jump across the crack and interface line (left), and interfacial stresses for $x_1 > 0$ (right).

4.5 Conclusions

Singular integral equations have been derived which relate the loading on crack faces to the consequent crack opening displacement and interfacial tractions for a semi-infinite crack situated along a soft anisotropic imperfect interface for an anisotropic bimaterial. The derivation made efficient use of perfect interface weight functions applied to an imperfect interface physical problem; this did not require derivation of new weight functions. As in the previously studied analogous isotropic problem, the imperfect interface's presence causes a logarithmic singularity in the kernel of the integral operator. Alternative formulations have been presented for the Mode III case and used to perform computations for orthotropic materials, which display a good degree of accuracy when compared against finite element simulations. Examples were given for both symmetric and asymmetric loadings to illustrate the benefits of the equations here as a number of previous results in the literature have restricted the loading to be symmetric which is not always

possible. For the in-plane problem equations have been solved numerically for an asymmetric loading configuration and the results obtained exhibit the known properties of displacements and tractions when an imperfect interface is present.

Chapter 5

Weight functions and singular integral equations for a piezoelectric bimaterial containing a perfect interface

This final chapter of original work sees the incorporation of piezoelectric materials into the bimaterial structure. A static semi-infinite crack along a perfect interface in a piezoelectric bimaterial is considered. When analysing such a problem the fields for Modes I, II and III are considered along with the electrical effects (often referred to as Mode IV). The purpose of the work seen here is to extend the weight function of Willis and Movchan (1995) to the piezoelectric setting. Once this has been done we then proceed to formulate singular integral equations relating physical and electrostatic loadings applied on the crack faces to the interfacial fields.

The problem of a static semi-infinite interfacial crack between dissimilar anisotropic piezoelectric materials under symmetric loading conditions has been studied in Suo et al. (1992) using an approach based on the Stroh formalism (Stroh, 1962) and Riemann-Hilbert formulation. As an alternative to this method, singular integral formulations for two-dimensional interfacial crack problems in piezoelectric bimaterials have been derived by means of approaches based on Green's function method (Gao and Wang, 2001). Although Green's functions for several crack problems in piezoelectric bimaterials have been derived (Pan, 2003; Pan and Yuan, 2000), their utilisation in evaluating physical displacements and stress fields on the crack faces requires challenging numerical estimation of integrals for which convergence should be asserted carefully. Moreover, both the complex variable formulation proposed by Suo et al. (1992) and the approaches based on Green's function method work when the tractions applied on the discontinuity surface are symmetric, but not in the case of asymmetric loading acting on the crack faces. The aim of the work seen in this chapter is to enable the incorporation of asymmetric loading to the problem whilst also introducing singular integral equations which avoid the use of Green's functions and the resulting challenging computations.

The remainder of the chapter is structured as follows: in Chapter 5.1 we introduce the mathematical model used for the remainder of the chapter and also recall the Riemann-Hilbert problem and the resulting eigenvalue problem which will be used extensively when deriving the weight functions for piezoelectric bimaterials. We then proceed to introduce the general form of the Willis and Movchan (1995) weight function for piezoelectric bimaterials

and the extension of the Betti identity to the piezoelectric setting in Chapter 5.2. Chapter 5.3 sees the beginning of the new content and from this stage onwards two specific examples of transversely isotropic piezoelectric bimaterials will be used to see the effect of poling direction on the bimaterial. Only the fields affected by the piezoelectric effect will be analysed in detail as the non-affected fields will behave identically to how they would in an anisotropic bimaterial. Chapter 5.3 sees the derivation of explicit expressions for the symmetric and skew-symmetric parts of the weight function before we proceed to formulate our singular integral equations in Chapter 5.4. Finally, in Chapter 5.5 we show some examples of how the derived equations can be used for a number of mechanical and electrical loading configurations on the crack faces. We also show a comparison with results for the analogous problem in COMSOL.

5.1 Problem formulation

In this section we introduce the mathematical model used for the remainder of the chapter. We consider a semi-infinite crack lying along a perfect interface between two dissimilar piezoelectric half-planes, referred to as materials I and II. The crack occupies the region $\{x_1 < 0, x_2 = 0\}$, as illustrated in Figure 5.1. The perfect interface conditions in a piezoelectric bimaterial are continuity of displacement, traction, electric potential and the electric displacement. The loading along the crack faces, for $x_1 < 0$, is known and given by the functions

$$p_j^{\pm}(x_1) = \sigma_{2j}(x_1, 0^{\pm}), \quad \text{for } j = 1, 2, 3, \quad p_4^{\pm}(x_1) = D_2(x_1, 0^{\pm}), \tag{5.1}$$

where σ_{ij} and D_i represent tractions and electrical displacements respectively.

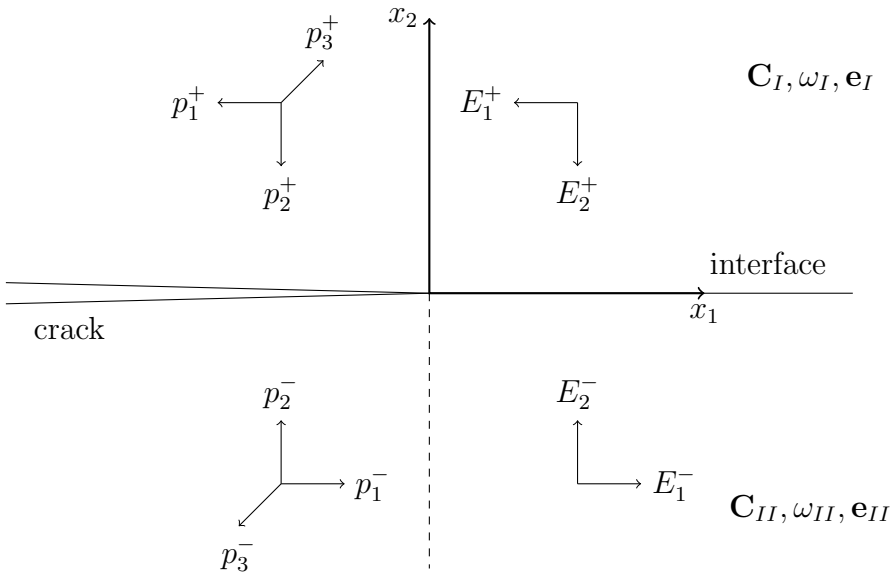

Figure 5.1: A semi-infinite crack along an interface between two dissimilar piezoelectric materials subject to the state of generalised plane strain and short circuit ($\varepsilon_3^{\pm} = E_3^{\pm} = 0$)

As reported in Chapter 2 the eigenvalue which is used in the derivation of extended traction and displacement fields in piezoelectric materials takes the form (Suo et al., 1992):

$$[\mathbf{Q} + \mu(\mathbf{R} + \mathbf{R}^T) + \mu^2\mathbf{T}]\mathbf{A} = 0, \tag{5.2}$$

where the material matrices take the form:

$$\mathbf{Q} = \begin{pmatrix} C_{11} & C_{16} & C_{15} & e_{11} \\ C_{16} & C_{66} & C_{56} & e_{16} \\ C_{15} & C_{56} & C_{55} & e_{15} \\ e_{11} & e_{16} & e_{15} & -\omega_{11} \end{pmatrix}, \quad \mathbf{R} = \begin{pmatrix} C_{16} & C_{12} & C_{14} & e_{16} \\ C_{66} & C_{26} & C_{46} & e_{12} \\ C_{56} & C_{25} & C_{45} & e_{14} \\ e_{21} & e_{26} & e_{25} & -\omega_{12} \end{pmatrix},$$

$$\mathbf{T} = \begin{pmatrix} C_{66} & C_{26} & C_{46} & e_{26} \\ C_{26} & C_{22} & C_{24} & e_{22} \\ C_{46} & C_{24} & C_{44} & e_{24} \\ e_{26} & e_{22} & e_{24} & -\omega_{22} \end{pmatrix}.$$

where C, ω and e are components of the stiffness, permittivity and piezoelectric tensors respectively.

Solving the eigenvalue problem (5.2) enables the evaluation of the material matrix $\mathbf{B}$, introduced in Chapter 2. We also remind ourselves of the bimaterial matrices $\mathbf{H}$ and $\mathbf{W}$ which are used throughout the remainder of the chapter:

$$\mathbf{H} = \mathbf{B}_I + \mathbf{B}_{II}^{\star}, \qquad \mathbf{W} = \mathbf{B}_I - \mathbf{B}_{II}^{\star}. \tag{5.3}$$

It was found in Suo et al. (1992) that the solution to the bimaterial interfacial crack problem is governed by the following Riemann-Hilbert problem along the negative x_1- axis:

$$\mathbf{h}^{+}(x_1) + (\mathbf{H}^{\star})^{-1}\mathbf{H}\mathbf{h}^{-}(x_1) = 0, \quad -\infty < x_1 < 0. \tag{5.4}$$

A solution was found in the form $\mathbf{h}(z) = \mathbf{w}z^{-\frac{1}{2}+i\epsilon}$ with the branch cut situated along the negative real axis. Inserting this solution into equation (5.4) yielded the eigenvalue problem

$$\mathbf{H}^{\star}\mathbf{w} = e^{2\pi\epsilon}\mathbf{H}\mathbf{w}. \tag{5.5}$$

The four sets of eigenvectors and eigenvalues are:

$$(\epsilon, \mathbf{w}),\ (-\epsilon, \mathbf{w}^{\star}),\ (-i\kappa, \mathbf{w}_3),\ (i\kappa, \mathbf{w}_4). \tag{5.6}$$

From here Suo et al. (1992) then proceeded to find expressions for the extended interfacial traction, $\mathbf{t} = (\sigma_{2i}, D_2)^T$, and displacement jump, $[\![\mathbf{u}]\!] =$

$([\![u_i]\!], [\![\phi]\!])^T$ along with an expression for the energy release rate at the crack tip. Further details on this have previously been reported in Chapter 2.2.2.

5.2 Weight functions and Betti's reciprocal identity for piezoelectric bimaterials

In this section we show the extension of some of the results used previously in the thesis to the piezoelectric setting. We begin by showing how the weight function of Willis and Movchan (1995) is extended to a piezoelectric bimaterial. We then show the work of Hadjesfandiari (2013) which extended the Betti identity to incorporate the extended tractions and displacements introduced by Suo et al. (1992).

5.2.1 Weight functions

The weight function for piezoelectric materials is given by the extended singular displacement field, $\mathbf{U}$ incorporating both displacement and electric potential, corresponding to a homogeneous, traction-free problem similar to Fig. 5.1 with the crack occupying the region $x_1 > 0$ and the perfect interface lying along the region $x_1 < 0$. The symmetric and skew-symmetric parts of the weight function across the plane $x_2 = 0$ are given by

$$[\![\mathbf{U}]\!](x_1) = \mathbf{U}(x_1, 0^+) - \mathbf{U}(x_1, 0^-), \tag{5.7}$$

$$\langle \mathbf{U} \rangle(x_1) = \frac{1}{2}\left[\mathbf{U}(x_1, 0^+) + \mathbf{U}(x_1, 0^-)\right]. \tag{5.8}$$

To satisfy the perfect interface conditions it is clear that $[\![\mathbf{U}]\!] = 0$ for $x_1 < 0$.

The extended traction field corresponding to the extended displacement $\mathbf{U}$, is denoted $\mathbf{\Sigma}$. The following Riemann-Hilbert problem is found along the positive portion of the x_1-axis

$$\mathbf{h}^+(x_1) + (\mathbf{H}^\star)^{-1}\mathbf{H}\mathbf{h}^-(x) = 0, \quad 0 < x_1 < \infty. \tag{5.9}$$

A solution for $\mathbf{h}(z)$ is now sought in the form $\mathbf{h} = \mathbf{v}z^{-\frac{3}{2}+i\epsilon}$. The branch cut of $\mathbf{h}$ is situated along the positive part of the x_1-axis. Inserting this solution into (5.9) yields the following eigenvalue problem

$$\mathbf{H}^\star\mathbf{v} = e^{-2\pi\epsilon}\mathbf{H}\mathbf{v}. \tag{5.10}$$

It is immediately clear by considering the solutions of equation (5.5) (given in (5.6)) that $\mathbf{v} = \mathbf{w}^\star$, $\mathbf{v}_3 = \mathbf{w}_4$ and $\mathbf{v}_4 = \mathbf{w}_3$.

Along the negative part of the real axis $\mathbf{\Sigma}$ is given by

$$\mathbf{h}^+(x_1) + (\mathbf{H}^\star)^{-1}\mathbf{H}\mathbf{h}^-(x) = \mathbf{\Sigma}(x_1), \quad -\infty < x_1 < 0. \tag{5.11}$$

Therefore the extended traction vector corresponding to the weight function $\mathbf{U}$ is given by

$$\mathbf{\Sigma}(x_1) = \frac{(-x_1)^{-3/2}}{2\sqrt{2\pi}}\left[C(-x_1)^{i\epsilon}\mathbf{w}^\star + C^\star(-x_1)^{-i\epsilon}\mathbf{w} + C_3(-x_1)^{-\kappa}\mathbf{w}_3 + C_4(-x_1)^{\kappa}\mathbf{w}_4\right], \tag{5.12}$$

where $C = C_1 + iC_2$, C_3 and C_4 are constants defined in the same manner as the stress and electric intensity factors for the physical problem.

For anisotropic materials it was shown in Morini et al. (2013b) that the Fourier transforms of the symmetric and skew-symmetric parts of the weight functions are related to $\bar{\mathbf{\Sigma}}$ in the following manner

$$[\![\bar{\mathbf{U}}]\!]^+(\xi) = \frac{1}{|\xi|}(i\text{sign}(\xi)\text{Im}(\mathbf{H}) - \text{Re}(\mathbf{H}))\bar{\mathbf{\Sigma}}^-(\xi), \tag{5.13}$$

$$\langle \bar{\mathbf{U}} \rangle(\xi) = \frac{1}{2|\xi|}(i\text{sign}(\xi)\text{Im}(\mathbf{W}) - \text{Re}(\mathbf{W}))\bar{\mathbf{\Sigma}}^{-}(\xi), \tag{5.14}$$

As the method used in Morini et al. (2013b) was for general matrices $\mathbf{H}$ and $\mathbf{W}$, it can be deduced that these results also hold for the extended weight functions in piezoelectric bimaterials by following the same procedure.

5.2.2 The generalised Betti formula

We now consider the Betti identity in the context of a semi-infinite crack in a piezoelectric bimaterial. The Betti formula is used to form a relationship between the physical fields and the weight function introduced in the previous part of the paper. Originally used to relate the displacement and traction fields (Willis and Movchan, 1995; Piccolroaz et al., 2007) the approach was extended to the piezoelectric setting (with electric potential and electric displacement) by Hadjesfandiari (2013) and is reported here.

Two sets of stresses, strains, electric fields and electrical displacements acting on the same physical space are assumed and denoted by the superscripts $^{(1)}$ and $^{(2)}$, respectively. The energy based equations relating these fields are (Hadjesfandiari, 2013):

$$\sigma_{ij}^{(1)}\varepsilon_{ij}^{(2)} - D_j^{(1)}E_j^{(2)} = \sigma_{ij}^{(2)}\varepsilon_{ij}^{(1)} - D_j^{(2)}E_j^{(1)}. \tag{5.15}$$

Taking the integral of (5.15) over a volume, V, yields:

$$\int_V \left[(\sigma_{ij}^{(1)}u_i^{(2)})_{,j} + (D_j^{(1)}\phi^{(2)})_{,j}\right] \mathrm{d}V = \int_V \left[(\sigma_{ij}^{(2)}u_i^{(1)})_{,j} + (D_j^{(2)}\phi^{(1)})_{,j}\right] \mathrm{d}V, \tag{5.16}$$

where the following definitions of strain and electric fields have been used:

$$\varepsilon_{ij} = \frac{1}{2}(u_{i,j} + u_{j,i}), \quad E_i = -\phi_{,i}. \tag{5.17}$$

Making use of the Divergence Theorem and then rearranging gives

$$\int_S \left[\sigma_{ji}^{(1)} n_j u_i^{(2)} + D_j^{(1)} n_j \phi^{(2)} - \sigma_{ji}^{(2)} n_j u_i^{(1)} - D_j^{(2)} n_j \phi^{(1)}\right] \mathrm{d}S = 0, \tag{5.18}$$

where S is the boundary of the volume V.

Taking V to be a hemisphere in the upper half-plane, with flat edge along the x_2-plane, in equation (5.18), leads to the following equation:

$$\int_{x_2=0^+} \left[\sigma_{2i}^{(1)} u_i^{(2)} + D_2^{(1)} \phi^{(2)} - \sigma_{2i}^{(2)} u_i^{(1)} - D_2^{(2)} \phi^{(1)}\right] \mathrm{d}x_1 = 0, \tag{5.19}$$

which can written in terms of the extended displacement and traction vectors used for piezoelectric materials

$$\int_{x_2=0^+} \left[\mathbf{t}^{(1)} \cdot \mathbf{u}^{(2)} - \mathbf{t}^{(2)} \cdot \mathbf{u}^{(1)}\right] \mathrm{d}x_1. \tag{5.20}$$

Taking (5.21) $\mathbf{u}^{(1)}$ and $\mathbf{t}^{(1)}$ as the physical fields, $\mathbf{u}^{(2)} = \boldsymbol{\mathcal{R}}\mathbf{U}$ and $\mathbf{t}^{(2)} = \boldsymbol{\mathcal{R}}\boldsymbol{\Sigma}$ gives:

$$\int_{x_2=0^+} \left[\boldsymbol{\mathcal{R}}\mathbf{U}(x_1' - x_1, 0^+) \cdot \mathbf{t}(x_1, 0^+) - \boldsymbol{\mathcal{R}}\boldsymbol{\Sigma}(x_1' - x_1, 0^+) \cdot \mathbf{u}(x_1, 0^+)\right] \mathrm{d}x_1 = 0, \tag{5.21}$$

where $\boldsymbol{\mathcal{R}}$ is given by

$$\boldsymbol{\mathcal{R}} = \begin{pmatrix} -1 & 0 & 0 & 0 \\ 0 & 1 & 0 & 0 \\ 0 & 0 & -1 & 0 \\ 0 & 0 & 0 & -1 \end{pmatrix}.$$

The equivalent equation for a semi-circular domain in the lower half-plane gives

$$\int_{x_2=0^-} \left[\boldsymbol{\mathcal{R}}\mathbf{U}(x_1' - x_1, 0^-) \cdot \mathbf{t}(x_1, 0^-) - \boldsymbol{\mathcal{R}}\boldsymbol{\Sigma}(x_1' - x_1, 0^-) \cdot \mathbf{u}(x_1, 0^-)\right] \mathrm{d}x_1 = 0. \tag{5.22}$$

Subtracting equation (5.22) from (5.21) yields the following relationship

$$\boldsymbol{\mathcal{R}}[\![\mathbf{U}]\!] * \mathbf{t}^{(+)} - \boldsymbol{\mathcal{R}}\boldsymbol{\Sigma}^{(-)} * [\![\mathbf{u}]\!] = -\boldsymbol{\mathcal{R}}[\![\mathbf{U}]\!] * \langle \mathbf{p} \rangle - \boldsymbol{\mathcal{R}}\langle \mathbf{U} \rangle * [\![\mathbf{p}]\!], \tag{5.23}$$

where $*$ represents the convolution with respect to x_1 and $^{(\pm)}$ is used to represent the restriction of a function to the positive or negative portion of the x_1-axis respectively. It can be easily deduced that in equation (5.23) the contribution to the generalised traction vector defined on the negative semi-axis $x_1 < 0$ is given by the loading functions $\mathbf{t}^{(-)} = (\sigma_{21}^{(-)}, \sigma_{22}^{(-)}, \sigma_{23}^{(-)}, D_2^{(-)})^T = (p_1, p_2, p_3, p_4)^T = \mathbf{p}$, and the symmetrical and skew-symmetrical part of the load, respectively $\langle \mathbf{p} \rangle$ and $[\![\mathbf{p}]\!]$, are defined in the usual manner.

Applying the Fourier transform to (5.23) gives the following relationship

$$[\![\bar{\mathbf{U}}]\!]^T \boldsymbol{\mathcal{R}} \bar{\mathbf{t}}^+ - (\bar{\boldsymbol{\Sigma}}^-)^T \boldsymbol{\mathcal{R}} [\![\bar{\mathbf{u}}]\!] = -[\![\bar{\mathbf{U}}]\!]^T \boldsymbol{\mathcal{R}} \langle \bar{\mathbf{p}} \rangle - \langle \bar{\mathbf{U}} \rangle^T \boldsymbol{\mathcal{R}} [\![\bar{\mathbf{p}}]\!], \tag{5.24}$$

which will be used in Section 5.4 when our singular integral equations are derived.

In the next sections, explicit expressions for the weight function matrices (5.13) and (5.14) are derived and used together with the the generalised Betti identity (5.24) for formulating the considered interface crack problem in terms of singular integral equations. Since the bimaterial matrices $\mathbf{H}$ and $\mathbf{W}$ involved in the weight functions (5.13) and (5.14) depend on the surface admittance tensors of both piezoelectric half-planes , in order to derive explicit expressions for these matrices the solution of the Stroh's eigenvalue problem (5.2) is needed. In the general fully anisotropic case, this eigenvalue problem must be solved numerically. Nevertheless, exact algebraic expressions of Stroh's eigenvalues and eigenvectors have been obtained for the class of transversely isotropic piezoelectric materials in Suo et al. (1992) and Hwu

(2008), with the latter making use of the extended Lekhnitskii formalism given in Chapter 2.2.3. This class of materials has practical significance, because many poled ceramics that are actually in use fall into this category.

5.3 Weight functions

For the remainder of the chapter piezoelectric materials occupying both lower and upper half-planes in Figure 5.1 are assumed to be transversely isotropic. In this section, using eigenvalue matrices and surface admittance tensors, explicit weight functions are derived for the cases where poling directions of both materials are parallel to the x_2 and x_3 axes respectively.

5.3.1 Poling direction parallel to the x_2-axis

Poling direction directed along the x_2-axis is assumed for both upper and lower piezoelectric half-planes. Considering the geometry of the model shown in Figure 5.1, it is easy to observe that in this case the poling direction is perpendicular to the crack plane.

When considering transverse isotropic materials with poling direction parallel to the x_2-axis the stiffness tensor, $\mathbf{C}$, simplifies to

$$\mathbf{C} = \begin{pmatrix} C_{11} & C_{12} & C_{13} & 0 & 0 & 0 \\ C_{12} & C_{22} & C_{12} & 0 & 0 & 0 \\ C_{13} & C_{12} & C_{11} & 0 & 0 & 0 \\ 0 & 0 & 0 & C_{44} & 0 & 0 \\ 0 & 0 & 0 & 0 & (C_{11} - C_{13})/2 & 0 \\ 0 & 0 & 0 & 0 & 0 & C_{44} \end{pmatrix},$$

and the permittivity and piezoelectric tensors simplify to

$$\omega = \begin{pmatrix} \omega_{11} & 0 & 0 \\ 0 & \omega_{22} & 0 \\ 0 & 0 & \omega_{11} \end{pmatrix}, \qquad \mathbf{e} = \begin{pmatrix} 0 & 0 & 0 & 0 & 0 & e_{16} \\ e_{21} & e_{22} & e_{21} & 0 & 0 & 0 \\ 0 & 0 & 0 & e_{16} & 0 & 0 \end{pmatrix}.$$

This is the same system as used in Hwu (2008). Using these conditions the matrices from equation (5.2) reduce to

$$\mathbf{Q} = \begin{pmatrix} C_{11} & 0 & 0 & 0 \\ 0 & C_{44} & 0 & e_{16} \\ 0 & 0 & (C_{11} - C_{13})/2 & 0 \\ 0 & e_{16} & 0 & -\omega_{11} \end{pmatrix}, \quad \mathbf{R} = \begin{pmatrix} 0 & C_{12} & 0 & e_{21} \\ C_{44} & 0 & 0 & 0 \\ 0 & 0 & 0 & 0 \\ e_{16} & 0 & 0 & 0 \end{pmatrix},$$

$$\mathbf{T} = \begin{pmatrix} C_{44} & 0 & 0 & 0 \\ 0 & C_{22} & 0 & e_{22} \\ 0 & 0 & C_{44} & 0 \\ 0 & e_{22} & 0 & -\omega_{22} \end{pmatrix}.$$

Under these conditions the Mode III component of the solution decouple from Modes I and II and the piezoelectric effect (Ou and Wu, 2003; Hwu, 2008). This means that the antiplane tractions and displacement have no dependency on the electric field and therefore behave in the same way as they would in an elastic material with no piezoelectric effect.

The focus of this chapter is to study the piezoelectric effect in the bimaterial so from this stage forwards only the in-plane and electric fields will be considered when a poling direction parallel to the x_2-axis is used. The sought solutions are therefore $\mathbf{u} = (u_1, u_2, \phi)^T$ and $\mathbf{t} = (\sigma_{21}, \sigma_{22}, D_2)^T$. The

decoupled part of the eigenvalue problem (5.2) now has matrices

$$\mathbf{Q} = \begin{pmatrix} C_{11} & 0 & 0 \\ 0 & C_{44} & e_{16} \\ 0 & e_{16} & -\omega_{11} \end{pmatrix}, \quad \mathbf{R} = \begin{pmatrix} 0 & C_{12} & e_{16} \\ C_{44} & 0 & 0 \\ e_{21} & 0 & 0 \end{pmatrix},$$

$$\mathbf{T} = \begin{pmatrix} C_{44} & 0 & 0 \\ 0 & C_{11} & e_{22} \\ 0 & e_{22} & -\omega_{22} \end{pmatrix}. \tag{5.25}$$

The surface admittance tensor $\mathbf{B}$ then takes the form:

$$\mathbf{B} = \begin{pmatrix} B_{11} & iB_{12} & iB_{14} \\ -iB_{12} & B_{22} & B_{24} \\ -iB_{14} & B_{24} & B_{44} \end{pmatrix}. \tag{5.26}$$

The expressions for the components of the matrix $\mathbf{B}$, found by Hwu (2008) for the two-dimensional state of generalised plane strain and open circuit, are quoted in Appendix 3.

With an expression for $\mathbf{B}$ it is now possible to construct the bimaterial matrices required. The bimaterial matrices $\mathbf{H}$ and $\mathbf{W}$ can be written as

$$\mathbf{H} = \begin{pmatrix} H_{11} & iH_{12} & iH_{14} \\ -iH_{12} & H_{22} & H_{24} \\ -iH_{14} & H_{24} & H_{44} \end{pmatrix}, \quad \mathbf{W} = \begin{pmatrix} W_{11} & iW_{12} & iW_{14} \\ -iW_{12} & W_{22} & W_{24} \\ -iW_{14} & W_{24} & W_{44} \end{pmatrix}, \tag{5.27}$$

where

$$H_{\alpha\alpha} = [B_{\alpha\alpha}]_I + [B_{\alpha\alpha}]_{II}, \quad W_{\alpha\alpha} = [B_{\alpha\alpha}]_I - [B_{\alpha\alpha}]_{II}, \quad \text{for } \alpha = 1, 2, 4,$$

$$H_{1\beta} = [B_{1\beta}]_I - [B_{1\beta}]_{II}, \quad , W_{1\beta} = [B_{1\beta}]_I + [B_{1\beta}]_{II}, \quad \text{for } \beta = 2, 4,$$

$$H_{24} = [B_{24}]_I + [B_{24}]_{II}, \quad W_{24} = [B_{24}]_I - [B_{24}]_{II}.$$

Having found the bimaterial matrix $\mathbf{H}$ it is now possible to find expressions for the traction field, $\mathbf{\Sigma}$ using the eigenvalue problem (5.5). From $(5.27)_{(1)}$ it is only necessary to find three sets of eigenvalues and eigenvectors. They have the form

$$(\epsilon, \mathbf{w}),\ (-\epsilon, \mathbf{w}^\star),\ (i\kappa, \mathbf{w}_4).$$

As the Mode III components of the solutions have decoupled and behave purely elastically it is expected that $\kappa = 0$. Therefore it is expected that the eigenvalues are given by two non-zero real valued numbers, with the same magnitude but differing in sign, and 0. With these particular eigenvalues and eigenvectors the expression for Σ is given by

$$\mathbf{\Sigma}(x_1) = \frac{(-x_1)^{-3/2}}{2\sqrt{2\pi}} \left[C(-x_1)^{i\epsilon}\mathbf{w}^\star + C^\star(-x_1)^{-i\epsilon}\mathbf{w} + C_4\mathbf{w}_4 \right]. \tag{5.28}$$

To find the eigenvalues from (5.5) the following equation must be solved

$$||\mathbf{H}^\star - e^{2\pi\epsilon}\mathbf{H}|| = 0, \tag{5.29}$$

where $||.||$ is used to denote the determinant of a matrix. Substituting $(5.27)_{(1)}$ in (5.29) the following equation is derived

$$\begin{aligned}(1 - e^{2\pi\epsilon})[(1 - e^{2\pi\epsilon})^2 H_{11}(H_{22}H_{44} - H_{24}^2) \\ -(1 + e^{2\pi\epsilon})^2(H_{12}^2 H_{44} + H_{14}^2 H_{24} - 2H_{12}H_{14}H_{24})] = 0.\end{aligned} \tag{5.30}$$

As expected solving the equation $1 - e^{2\pi\epsilon} = 0$ yields the eigenvalue 0. The other eigenvalues are given by

$$\pm\epsilon = \pm\frac{1}{2\pi}\ln\left(\frac{1-\beta}{1+\beta}\right), \tag{5.31}$$

where

$$\beta^2 = \frac{B}{A}, \quad A = H_{11}(H_{22}H_{44} - H_{24}^2), \quad B = 2(H_{12}^2 H_{44} + H_{14}^2 H_{24} - 2H_{12}H_{14}H_{24}).$$

Using these eigenvalues it is possible to find expressions for the eigenvectors $\mathbf{w}$ and $\mathbf{w_4}$. The expressions chosen here are made for notational convenience. The expression for $\mathbf{w_4}$ is

$$\mathbf{w_4} = \frac{1}{2}\begin{pmatrix} 0 \\ H_{14} \\ -H_{12} \end{pmatrix}. \tag{5.32}$$

There are three possible expressions for the eigenvector $\mathbf{w}$. They are

$$\mathbf{w} = \frac{1}{2}\begin{pmatrix} -i\beta(H_{24}^2 - H_{22}H_{44}) \\ H_{44}H_{12} - H_{14}H_{24} \\ H_{14}H_{22} - H_{24}H_{12} \end{pmatrix}, \text{ or } \frac{1}{2}\begin{pmatrix} -i\beta(H_{14}H_{22} - H_{12}H_{24}) \\ \beta^2 H_{11}H_{24} - H_{12}H_{14} \\ H_{12}^2 - \beta^2 H_{11}H_{22} \end{pmatrix},$$

$$\text{or } \frac{1}{2}\begin{pmatrix} -i\beta(H_{14}H_{24} - H_{12}H_{44}) \\ \beta^2 H_{11}H_{44} - H_{14}^2 \\ H_{12}H_{14} - \beta^2 H_{11}H_{24} \end{pmatrix}. \tag{5.33}$$

For the purpose of the remaining results derived in this section the first representation of $\mathbf{w}$ from equation (5.33) shall be used.

Using (5.28) it is possible, using the method described in Piccolroaz et al. (2009), to construct three independent traction vectors using the following three cases:

1. $C_1 = 1, C_2 = C_4 = 0,$
2. $C_2 = 1, C_1 = C_4 = 0,$
3. $C_4 = 1, C_1 = C_2 = 0.$

Using (5.33) the three traction vectors obtained are

$$\mathbf{\Sigma}^1(x_1) = \frac{(-x_1)^{-3/2}}{2\sqrt{2\pi}} \begin{pmatrix} i\beta(H_{24}^2 - H_{22}H_{44})[(-x_1)^{i\epsilon} - (-x_1)^{-i\epsilon}] \\ (H_{44}H_{12} - H_{14}H_{24})[(-x_1)^{i\epsilon} + (-x_1)^{-i\epsilon}] \\ (H_{14}H_{22} - H_{24}H_{12})[(-x_1)^{i\epsilon} + (-x_1)^{-i\epsilon}] \end{pmatrix}, \quad (5.34)$$

$$\mathbf{\Sigma}^2(x_1) = \frac{(-x_1)^{-3/2}}{2\sqrt{2\pi}} \begin{pmatrix} -\beta(H_{24}^2 - H_{22}H_{44})[(-x_1)^{i\epsilon} + (-x_1)^{-i\epsilon}] \\ i(H_{44}H_{12} - H_{14}H_{24})[(-x_1)^{i\epsilon} - (-x_1)^{-i\epsilon}] \\ i(H_{14}H_{22} - H_{24}H_{12})[(-x_1)^{i\epsilon} - (-x_1)^{-i\epsilon}] \end{pmatrix}, \quad (5.35)$$

$$\mathbf{\Sigma}^4(x_1) = \frac{(-x_1)^{-3/2}}{2\sqrt{2\pi}} \begin{pmatrix} 0 \\ H_{14} \\ -H_{12} \end{pmatrix}. \quad (5.36)$$

Here, a superscript 4 has been used instead of 3 in equation (5.36) so as not to confuse this with the Mode III components which have already been decoupled.

In order to calculate explicit expressions for $[\![\bar{\mathbf{U}}]\!]^+$ and $\langle\bar{\mathbf{U}}\rangle$ it is necessary to find the Fourier transforms of (5.34), (5.35) and (5.36)

$$\bar{\mathbf{\Sigma}}^1(\xi) = \frac{\sqrt{2}(i\xi)^{1/2}}{(1+4\epsilon^2)\sqrt{\pi}} \begin{pmatrix} i\beta(H_{24}^2 - H_{22}H_{44})G^- \\ (H_{44}H_{12} - H_{14}H_{24})G^+ \\ (H_{14}H_{22} - H_{24}H_{12})G^+ \end{pmatrix}, \quad (5.37)$$

$$\bar{\mathbf{\Sigma}}^2(\xi) = \frac{\sqrt{2}(i\xi)^{1/2}}{(1+4\epsilon^2)\sqrt{\pi}} \begin{pmatrix} -\beta(H_{24}^2 - H_{22}H_{44})G^+ \\ i(H_{44}H_{12} - H_{14}H_{24})G^- \\ i(H_{14}H_{22} - H_{24}H_{12})G^- \end{pmatrix}, \quad (5.38)$$

$$\bar{\mathbf{\Sigma}}^4(\xi) = \frac{(i\xi)^{1/2}}{\sqrt{2}} \begin{pmatrix} 0 \\ -H_{14} \\ H_{12} \end{pmatrix}, \quad (5.39)$$

where

$$G^{\pm} = \left(-\frac{1}{2} - i\epsilon\right)\Gamma\left(\frac{1}{2} + i\epsilon\right)(i\xi)^{-i\epsilon} \pm \left(-\frac{1}{2} + i\epsilon\right)\Gamma\left(\frac{1}{2} - i\epsilon\right)(i\xi)^{i\epsilon}.$$

With these expressions it is now possible to use a 3×3 matrix, whose columns are the three linearly independent traction vectors found, along with equations (5.13) and (5.14) to find expressions for $[\![\mathbf{U}]\!]$ and $\langle\mathbf{U}\rangle$ (Piccolroaz et al., 2009).

5.3.2 Poling direction parallel to the x_3-axis

Observing Figure 5.1, it can be noted that in the case where both the upper and lower piezoelectric half-planes are assumed to be poled along the x_3-axis, the poling axis coincides with the crack front. For a transversely isotropic with said poling direction the stiffness tensor, C, simplifies to

$$C = \begin{pmatrix} C_{11} & C_{12} & C_{13} & 0 & 0 & 0 \\ C_{12} & C_{11} & C_{13} & 0 & 0 & 0 \\ C_{13} & C_{13} & C_{33} & 0 & 0 & 0 \\ 0 & 0 & 0 & C_{44} & 0 & 0 \\ 0 & 0 & 0 & 0 & C_{44} & 0 \\ 0 & 0 & 0 & 0 & 0 & (C_{11} - C_{12})/2 \end{pmatrix},$$

and the permittivity and piezoelectric tensors are

$$\omega = \begin{pmatrix} \omega_{11} & 0 & 0 \\ 0 & \omega_{11} & 0 \\ 0 & 0 & \omega_{33} \end{pmatrix}, \qquad e = \begin{pmatrix} 0 & 0 & 0 & 0 & e_{15} & 0 \\ 0 & 0 & 0 & e_{15} & 0 & 0 \\ e_{31} & e_{31} & e_{33} & 0 & 0 & 0 \end{pmatrix}.$$

Using these conditions the matrices from equation (5.2) reduce to

$$\mathbf{Q} = \begin{pmatrix} C_{11} & 0 & 0 & 0 \\ 0 & (C_{11}-C_{12})/2 & 0 & 0 \\ 0 & 0 & C_{44} & e_{15} \\ 0 & 0 & e_{15} & -\omega_{11} \end{pmatrix}, \quad \mathbf{R} = \begin{pmatrix} 0 & C_{12} & 0 & 0 \\ (C_{11}-C_{12})/2 & 0 & 0 & 0 \\ 0 & 0 & 0 & 0 \\ 0 & 0 & 0 & 0 \end{pmatrix},$$

$$\mathbf{T} = \begin{pmatrix} (C_{11}-C_{12})/2 & 0 & 0 & 0 \\ 0 & C_{11} & 0 & 0 \\ 0 & 0 & C_{44} & e_{15} \\ 0 & 0 & e_{15} & -\omega_{11} \end{pmatrix}.$$

For this example the Mode I and Mode II components of the displacement and stress fields decouple from the Mode III fields and piezoelectric effects on the material (Ou and Wu, 2003; Hwu, 2008). This means that the in-plane fields will behave similarly to those for purely elastic materials with no piezoelectric behaviour. Noting once again that the focus of the work in this chapter is to explore the piezoelectric behaviour of a material and therefore only the out-of-plane and piezoelectric components are considered, that is: $\mathbf{u} = (u_3, \phi)^T$ and $\mathbf{t} = (\sigma_{23}, D_2)^T$.

In this case $\mathbf{Q}$ and $\mathbf{T}$ are reduced to 2×2 matrices and $\mathbf{R}$ vanishes:

$$\mathbf{Q} = \mathbf{T} = \begin{pmatrix} C_{44} & e_{15} \\ e_{15} & -\omega_{11} \end{pmatrix}, \qquad \mathbf{R} = \mathbf{0}. \tag{5.40}$$

The surface admittance tensor, $\mathbf{B}$, then becomes

$$\mathbf{B} = \begin{pmatrix} B_{33} & B_{34} \\ B_{34} & B_{44} \end{pmatrix}. \tag{5.41}$$

Explicit expressions for the components of this matrix are given by (Hwu, 2008):

$$B_{33} = \frac{\omega_{11}}{e_{15}^2 + \omega_{11} C_{44}}, \quad B_{44} = \frac{-C_{44}}{e_{15}^2 + \omega_{11} C_{44}},$$
$$B_{34} = \frac{e_{15}}{e_{15}^2 + \omega_{11} C_{44}}.$$

Consequently, the bimaterial matrices $\mathbf{H}$ and $\mathbf{W}$ can be computed and have the form

$$\mathbf{H} = \begin{pmatrix} H_{33} & H_{34} \\ H_{34} & H_{44} \end{pmatrix}, \qquad \mathbf{W} = \begin{pmatrix} \delta_3 H_{33} & \gamma H_{34} \\ \gamma H_{34} & \delta_4 H_{44} \end{pmatrix}, \tag{5.42}$$

where:

$$H_{\alpha\beta} = [B_{\alpha\beta}]_I + [B_{\alpha\beta}]_{II}, \quad \text{for } \alpha, \beta = 3, 4,$$
$$\delta_\alpha = \frac{[B_{\alpha\alpha}]_I - [B_{\alpha\alpha}]_{II}}{[B_{\alpha\alpha}]_I + [B_{\alpha\alpha}]_{II}}, \quad \text{for } \alpha = 3, 4,$$
$$\gamma = \frac{[B_{34}]_I - [B_{34}]_{II}}{H_{34}}.$$

In order to obtain the weight functions for the materials considered here the Riemann-Hilbert problem (5.4) must again be considered. For this case the bimaterial matrix $\mathbf{H}$ has no imaginary part, and then substituting expression $(5.42)_{(1)}$ into equation (5.4) we get

$$\mathbf{h}^+(x_1) + \mathbf{h}^-(x) = 0, \quad -\infty < x_1 < 0. \tag{5.43}$$

For this special case it was shown in Suo et al. (1992) that the extended traction along the interface and displacement jump across the crack are given by

$$\mathbf{t}(x_1) = (2\pi x_1)^{-\frac{1}{2}} \begin{pmatrix} K_3 \\ K_4 \end{pmatrix}, \qquad \text{for } x_1 > 0, \tag{5.44}$$

$$[\![\mathbf{u}]\!](x_1) = \left(\frac{2(-x_1)}{\pi}\right)^{\frac{1}{2}} \mathbf{H} \begin{pmatrix} K_3 \\ K_4 \end{pmatrix} \qquad \text{for } x_1 < 0. \tag{5.45}$$

Knowing the traction fields makes it possible to evaluate the weight function traction $\mathbf{\Sigma}$ for these particular materials. The expression for $\mathbf{\Sigma}$ is

$$\mathbf{\Sigma}(x_1) = \frac{(-x_1)^{-\frac{3}{2}}}{\sqrt{2\pi}} \begin{pmatrix} C_3 \\ C_4 \end{pmatrix}, \quad \text{for } x_1 < 0. \tag{5.46}$$

The Fourier transforms of the symmetric and skew-symmetric parts of the weight function, $[\![\bar{\mathbf{U}}]\!]$ and $\langle \bar{\mathbf{U}} \rangle$, are once again given by equations (5.13) and (5.14). However, due to $\mathbf{H}$, and therefore $\mathbf{W}$ being purely real the expressions simplify to

$$[\![\bar{\mathbf{U}}]\!]^+(\xi) = -\frac{1}{|\xi|}\mathbf{H}\bar{\mathbf{\Sigma}}^-(\xi), \tag{5.47}$$

$$\langle \bar{\mathbf{U}} \rangle(\xi) = -\frac{1}{2|\xi|}\mathbf{W}\bar{\mathbf{\Sigma}}^-(\xi), \tag{5.48}$$

where $\bar{\mathbf{\Sigma}}$ is the 2×2 matrix consisting of two independent tractions. The linearly independent tractions are given by the case $C_3 = 1, C_4 = 0$ and $C_3 = 0, C_4 = 1$ in equation (5.46). The results obtained are;

$$\mathbf{\Sigma}^3(x_1) = \frac{(-x_1)^{-\frac{3}{2}}}{\sqrt{2\pi}} \begin{pmatrix} 1 \\ 0 \end{pmatrix}, \quad \mathbf{\Sigma}^4(x_1) = \frac{(-x_1)^{-\frac{3}{2}}}{\sqrt{2\pi}} \begin{pmatrix} 0 \\ 1 \end{pmatrix}. \tag{5.49}$$

The Fourier transforms of these vectors are given by

$$\bar{\mathbf{\Sigma}}^3(\xi) = (i\xi)^{\frac{1}{2}} \begin{pmatrix} -\sqrt{2} \\ 0 \end{pmatrix}, \quad \bar{\mathbf{\Sigma}}^4(\xi) = (i\xi)^{\frac{1}{2}} \begin{pmatrix} 0 \\ -\sqrt{2} \end{pmatrix}. \tag{5.50}$$

It is now possible to use these vectors, along with equations (5.47) and (5.48), to construct the matricial expressions for the symmetric and skew-symmetric parts of the weight function.

5.4 Integral identities

In this section the weight function matrices are used together with the Betti identity, (5.24), to formulate the considered crack problem in terms of singular integral equations. Integral identities relating the applied loading to the resulting crack opening and traction ahead of the tip are derived for transversely isotropic piezoelectric materials in both the cases where poling direction is parallel to the x_2 and x_3 axes.

5.4.1 Poling direction parallel to the x_2-axis

Considering the case where both upper and lower transversely isotropic piezoelectric half-spaces possess poling direction parallel to the x_2-axis (perpendicular to the crack plane), the in-plane fields and piezoelectric effect decouple from the antiplane displacement and traction. Consequently, the Betti formula still has the form

$$[\![\bar{\mathbf{U}}]\!]^T \boldsymbol{\mathcal{R}} \bar{\mathbf{t}}^+ - \bar{\boldsymbol{\Sigma}}^T \boldsymbol{\mathcal{R}} [\![\bar{\mathbf{u}}]\!]^- = -[\![\bar{\mathbf{U}}]\!]^T \boldsymbol{\mathcal{R}} \langle \bar{\mathbf{p}} \rangle - \langle \bar{\mathbf{U}} \rangle^T \boldsymbol{\mathcal{R}} [\![\bar{\mathbf{p}}]\!], \tag{5.51}$$

where $[\![\bar{\mathbf{U}}]\!]$ and $\langle \bar{\mathbf{U}} \rangle$ are given by expressions (5.13) and (5.14) together with matrices (5.27), and the rotational matrix $\boldsymbol{\mathcal{R}}$ becomes

$$\boldsymbol{\mathcal{R}} = \begin{pmatrix} -1 & 0 & 0 \\ 0 & 1 & 0 \\ 0 & 0 & -1 \end{pmatrix}.$$

Multiplying both sides of (5.51) by $\boldsymbol{\mathcal{R}}^{-1} [\![\bar{\mathbf{U}}]\!]^{-T}$ yields the following equation

$$\bar{\mathbf{t}}^+ - \mathbf{N} [\![\bar{\mathbf{u}}]\!]^- = -\langle \bar{\mathbf{p}} \rangle - \mathbf{M} [\![\bar{\mathbf{p}}]\!], \tag{5.52}$$

where $\mathbf{M}$ and $\mathbf{N}$ are given by

$$\mathbf{M} = \boldsymbol{\mathcal{R}}^{-1}[\![\bar{\mathbf{U}}]\!]^{-T}\langle\bar{\mathbf{U}}\rangle^{T}\boldsymbol{\mathcal{R}}, \qquad \mathbf{N} = \boldsymbol{\mathcal{R}}^{-1}[\![\bar{\mathbf{U}}]\!]^{-T}\bar{\boldsymbol{\Sigma}}^{T}\boldsymbol{\mathcal{R}}. \tag{5.53}$$

Using (5.13) and (5.14) full expressions for $\mathbf{M}$ and $\mathbf{N}$ can be found:

$$\mathbf{M} = \frac{1}{2D}\left(\mathbf{M}' + i\text{sign}(\xi)\mathbf{M}''\right), \tag{5.54}$$

$$\mathbf{N} = \frac{|\xi|}{D}\left(\mathbf{N}' + i\text{sign}(\xi)\mathbf{N}''\right), \tag{5.55}$$

where explicit expressions for $D, \mathbf{M}', \mathbf{M}'', \mathbf{N}'$ and $\mathbf{N}''$ can be found in Appendix 4.

Taking the inverse Fourier transform of equation (5.52), the following equations are found for $x_1 < 0$ and $x_1 > 0$ respectively:

$$\mathcal{F}^{-1}_{x_1<0}[\mathbf{N}[\![\bar{\mathbf{u}}]\!]^{-}] = \langle\mathbf{p}\rangle(x_1) + \mathcal{F}^{-1}_{x_1<0}[\mathbf{M}[\![\bar{\mathbf{p}}]\!]], \quad x_1 < 0, \tag{5.56}$$

$$\mathbf{t}^{(+)}(x_1) + \mathcal{F}^{-1}_{x_1>0}[\mathbf{M}[\![\bar{\mathbf{p}}]\!]] = \mathcal{F}^{-1}_{x_1>0}[\mathbf{N}[\![\bar{\mathbf{u}}]\!]^{-}], \quad x_1 > 0. \tag{5.57}$$

The term involving $\bar{\mathbf{t}}$ cancels for $x_1 < 0$ as it is only defined along the interface and $\langle\bar{\mathbf{p}}\rangle$ does not appear for $x_1 > 0$ as it is only defined along the crack.

In order to derive explicit expressions for equations (5.56) and (5.57), we need to compute the inverse Fourier transform of terms of the form $i\text{sign}(\xi)\bar{f}(\xi)$, $|\xi|\bar{f}(\xi)$ and $i\xi\bar{f}(\xi)$. Using the Fourier convolution theorem and the knowledge that the inverse Fourier transform of $\text{sign}(\xi)$ is given by $-i/(\pi x_1)$ gives:

$$\begin{aligned}\mathcal{F}^{-1}[i\text{sign}(\xi)\bar{f}(\xi)] &= i\mathcal{F}^{-1}[\text{sign}(\xi)] * \mathcal{F}^{-1}[\bar{f}(\xi)], \\ &= i\Big(\frac{-i}{\pi x_1}\Big) * f(x_1), \\ &= \frac{1}{\pi}\int_{-\infty}^{\infty}\frac{f(\eta)}{x_1-\eta}\mathrm{d}\eta.\end{aligned} \tag{5.58}$$

The inverse Fourier transform of $|\xi|\bar{f}(\xi)$ is found:

$$\begin{aligned}\mathcal{F}^{-1}[|\xi|\bar{f}(\xi)] &= \mathcal{F}^{-1}[\text{sign}(\xi)] * \mathcal{F}^{-1}[\xi\bar{f}(\xi)], \\ &= \Big(-\frac{i}{\pi x_1}\Big) * i\frac{\partial f}{\partial x_1}, \\ &= \Big(\frac{1}{\pi x_1}\Big) * \frac{\partial f}{\partial x_1}. \end{aligned} \tag{5.59}$$

Finally, the inverse Fourier transform of $i\text{sign}(\xi)|\xi|\bar{f}(\xi)$ is given by

$$\begin{aligned}\mathcal{F}^{-1}[i\text{sign}(\xi)|\xi|\bar{f}(\xi)] &= \mathcal{F}^{-1}[i\xi\bar{f}(\xi)], \\ &= -\frac{\partial f}{\partial x_1}. \end{aligned} \tag{5.60}$$

We now introduce the singular operator $\mathcal{S}$ and reintroduce the orthogonal projectors $\mathcal{P}_\pm$ seen in Chapter 4:

$$\mathcal{S}\psi = \frac{1}{\pi x_1} * \psi(x_1), \tag{5.61}$$

$$\mathcal{P}_\pm\psi = \begin{cases} \psi(x_1), & \pm x_1 > 0, \\ 0, & \text{otherwise.} \end{cases} \tag{5.62}$$

Introducing the singular integral operator $\mathcal{S}^{(s)} = \mathcal{P}_-\mathcal{S}\mathcal{P}_-$ and the compact operator $\mathcal{S}^{(c)} = \mathcal{P}_+\mathcal{S}\mathcal{P}_-$, equations (5.56) and (5.57) become

$$\mathcal{N}^{(s)}\frac{\partial[\![\mathbf{u}]\!]^{(-)}}{\partial x_1} = \langle\mathbf{p}\rangle(x_1) + \mathcal{M}^{(s)}[\![\mathbf{p}]\!], \quad x_1 < 0, \tag{5.63}$$

$$\mathbf{t}^{(+)}(x_1) + \mathcal{M}^{(c)}[\![\mathbf{p}]\!] = \mathcal{N}^{(c)}\frac{\partial[\![\mathbf{u}]\!]^{(-)}}{\partial x_1}, \quad x_1 > 0. \tag{5.64}$$

The matrix operators $\mathcal{M}^{(s)}, \mathcal{M}^{(c)}, \mathcal{N}^{(s)}$ and $\mathcal{N}^{(c)}$ are given by

$$\mathcal{M}^{(s)} = \frac{1}{2D}\left(\mathbf{M}' + \mathbf{M}''\mathcal{S}^{(s)}\right), \quad \mathcal{N}^{(s)} = \frac{1}{D}\left(\mathbf{N}'\mathcal{S}^{(s)} - \mathbf{N}''\right), \tag{5.65}$$

$$\mathcal{M}^{(c)} = \frac{1}{2D}\mathbf{M}''\mathcal{S}^{(c)}, \quad \mathcal{N}^{(c)} = \frac{1}{D}\mathbf{N}'\mathcal{S}^{(c)}. \tag{5.66}$$

An example of the use of these integral equations when a known load is applied to the crack faces is given in Chapter 5.5.

5.4.2 Poling direction parallel to the x_3-axis

For the case where both upper and lower transversely isotropic piezoelectric half-spaces possess poling direction parallel to the x_3 axis, the weight functions consist of the 2×2 matrices (5.47) and (5.48). The Betti identity (5.24) then becomes a 2×2 matricial integral equation, where the rotational matrix $\boldsymbol{\mathcal{R}}$ is given by

$$\boldsymbol{\mathcal{R}} = \begin{pmatrix} -1 & 0 \\ 0 & -1 \end{pmatrix}.$$

Therefore, equation (5.24) can be simplified further to give

$$[\![\bar{\mathbf{U}}]\!]^T\bar{\mathbf{t}}^+ - \bar{\boldsymbol{\Sigma}}^T[\![\bar{\mathbf{u}}]\!]^- = -[\![\bar{\mathbf{U}}]\!]^T\langle\bar{\mathbf{p}}\rangle - \langle\bar{\mathbf{U}}\rangle^T[\![\bar{\mathbf{p}}]\!]. \tag{5.67}$$

Multiplying both sides of equation (5.67) by $[\![\bar{\mathbf{U}}]\!]^{-T}$ gives

$$\bar{\mathbf{t}}^+ - [\![\bar{\mathbf{U}}]\!]^{-T}\bar{\boldsymbol{\Sigma}}^T[\![\bar{\mathbf{u}}]\!]^- = -\langle\bar{\mathbf{p}}\rangle - [\![\bar{\mathbf{U}}]\!]^{-T}\langle\bar{\mathbf{U}}\rangle^T[\![\bar{\mathbf{p}}]\!]^-. \tag{5.68}$$

Using (5.47) and (5.48) gives

$$\bar{\mathbf{t}}^+ - \mathbf{Z}(\xi)[\![\bar{\mathbf{u}}]\!]^- = -\langle\bar{\mathbf{p}}\rangle - \mathbf{Y}[\![\bar{\mathbf{p}}]\!]^-, \tag{5.69}$$

where

$$\mathbf{Y} = \frac{1}{2}\mathbf{H}^{-1}\mathbf{W} = \frac{1}{2(H_{33}H_{44}-H_{34}^2)}\begin{pmatrix} \delta_3H_{33}H_{44}-\gamma H_{34}^2 & H_{44}H_{34}(\gamma-\delta_4) \\ H_{33}H_{34}(\gamma-\delta_3) & \delta_4H_{33}H_{44}-\gamma H_{34}^2 \end{pmatrix}, \tag{5.70}$$

$$\mathbf{Z}(\xi) = -|\xi|\mathbf{H}^{-1} = -\frac{|\xi|}{H_{33}H_{44}-H_{34}^2}\begin{pmatrix} H_{44} & -H_{34} \\ -H_{34} & H_{33} \end{pmatrix}. \tag{5.71}$$

Taking inverse Fourier transforms and methods seen in Piccolroaz and Mishuris (2013) and Morini et al. (2013a) gives the following singular integral equations

$$\mathcal{Q}^{(s)}\frac{\partial[\![\mathbf{u}]\!]^{(-)}}{\partial x_1} = -\langle\mathbf{p}\rangle(x_1) - \mathbf{Y}[\![\mathbf{p}]\!](x_1), \quad \text{for } x_1<0, \tag{5.72}$$

$$\mathbf{t}(x_1) = -\mathcal{Q}^{(c)} \frac{\partial [\![\mathbf{u}]\!]^{(-)}}{\partial x_1}, \quad \text{for } x_1 > 0, \tag{5.73}$$

where $\mathcal{Q}^{(s)} = \mathbf{H}^{-1}\mathcal{S}^{(s)}$ and $\mathcal{Q}^{(c)} = \mathbf{H}^{-1}\mathcal{S}^{(c)}$.

The integral identities (5.63), (5.64), (5.72) and (5.73) relate the mechanical and electrostatic loading applied on the crack faces to the corresponding crack opening and tractions ahead of the tip. The crack opening associated with an arbitrary non-symmetrical mechanical or electrostatic loading can be derived by the inversion of the matricial operators $\mathcal{N}^{(s)}$ and $\mathcal{Q}^{(s)}$ in equations (5.63) and (5.72). Using the obtained crack opening functions in (5.64) and (5.73), explicit expressions for the tractions ahead of the crack tip are yielded. Some simple illustrative examples of this procedure are reported in next section.

5.5 Illustrative Examples

In this section we consider some examples of loadings for both poling directions and find solutions using the singular integral equations derived in the previous section. Both mechanical and electrical configurations will be considered. Explicit expressions for crack opening and tractions ahead of the tip corresponding to both symmetrical and skew-symmetrical mechanical and electrostatic loading configurations are derived. The proposed illustrative cases show that the obtained integral identities represent a very useful tool for studying interfacial crack problems in piezoelectric bimaterials.

To begin with we consider a symmetric distribution of point loadings when the poling direction is parallel to the x_2-axis before considering both symmetric and asymmetric loading configurations for the piezoelectric bima-

terial poled in the direction of the x_3-axis. For the decoupled Mode III and IV example with symmetric loading we also present a comparison between the results from our singular integral equations and those obtained using finite element methods in COMSOL Multiphysics.

5.5.1 Poling direction parallel to the x_2-axis under symmetric mechanical loading

We consider a symmetric system of two perpendicular point loads of varying magnitude on each crack faces acting in the opposite direction to their corresponding load on the opposite crack face at a distance a behind the crack. Mathematically these forces are represented as

$$\langle \mathbf{p} \rangle (x_1) = \begin{pmatrix} -F_1 \delta(x_1 + a) \\ -F_2 \delta(x_1 + a) \\ 0 \end{pmatrix}, \qquad [\![\mathbf{p}]\!] = \mathbf{0}. \tag{5.74}$$

where δ represents the Dirac delta distribution. Under such a loading the singular integral equations used to find $[\![\mathbf{u}]\!]$ and $\mathbf{t}$ reduce to

$$\mathcal{N}^{(s)} \frac{\partial [\![\mathbf{u}]\!]^{(-)}}{\partial x_1} = \langle \mathbf{p} \rangle (x_1), \quad \text{for } x_1 < 0, \tag{5.75}$$

$$\mathbf{t}^{(+)}(x_1) = \mathcal{N}^{(c)} \frac{\partial [\![\mathbf{u}]\!]^{(-)}}{\partial x_1}, \quad \text{for } x_1 > 0. \tag{5.76}$$

To simplify the problem we consider the set of bimaterials for which the matrix $\mathbf{H}$ from equation $(5.27)_{(1)}$ has no imaginary part, that is $H_{12} = H_{14} = 0$. An example of when this may occur is when the upper and lower materials are the same. Under these conditions the matrix $\mathbf{N}'' = \mathbf{0}$ and therefore the

integral equation for $x_1 < 0$ becomes

$$\frac{1}{D}\begin{pmatrix} N_{11} & 0 & 0 \\ 0 & N_{22} & N_{24} \\ 0 & N_{24} & N_{44} \end{pmatrix} \mathcal{S}^{(s)} \frac{\partial [\![\mathbf{u}]\!]^{(-)}}{\partial x_1} = \begin{pmatrix} -F_1 \delta(x_1 + a) \\ -F_2 \delta(x_1 + a) \\ 0 \end{pmatrix}. \tag{5.77}$$

From the system (5.77) it is possible to obtain the following three equations for the derivatives of the displacements and electric potential

$$N_{11} \mathcal{S}^{(s)} \frac{\partial [\![u_1]\!]^{(-)}}{\partial x_1} = -F_1 D \delta(x_1 + a), \tag{5.78}$$

$$\mathcal{S}^{(s)} \left[N_{22} \frac{\partial [\![u_2]\!]^{(-)}}{\partial x_1} + N_{24} \frac{\partial [\![\phi]\!]}{\partial x_1} \right] = -F_2 D \delta(x_1 + a), \tag{5.79}$$

$$\mathcal{S}^{(s)} \left[N_{24} \frac{\partial [\![u_2]\!]^{(-)}}{\partial x_1} + N_{44} \frac{\partial [\![\phi]\!]}{\partial x_1} \right] = 0. \tag{5.80}$$

It is clear from these equations that the x_1 directed part of the solution for the example considered decouples from the component of the solution in the x_2 direction and the electrical effects. As a result of this we first proceed with solving for u_1 before proceeding to find expressions for u_2 and ϕ.

We begin by inverting the integral operator $\mathcal{S}^{(s)}$ in equation (5.78) using the methods seen in Piccolroaz and Mishuris (2013) and Morini et al. (2013a), which were based on the work of Muskhelishvili (1963) seen in Chapter 2:

$$\frac{\partial [\![u_1]\!]^{(-)}}{\partial x_1} = \frac{F_1 D}{N_{11} \pi} \int_{-\infty}^{0} \sqrt{\frac{\eta}{x_1}} \frac{\delta(\eta + a)}{x_1 - \eta} \mathrm{d}\eta = \frac{F_1 D}{N_{11} \pi} \sqrt{\frac{-a}{x_1}} \frac{1}{x_1 + a}. \tag{5.81}$$

Using the expressions for D and N_{11} reported in Appendix 4, this expression simplifies to

$$\frac{\partial [\![u_1]\!]^{(-)}}{\partial x_1} = -\frac{F_1 H_{11}}{\pi} \sqrt{-\frac{a}{x_1}} \frac{1}{x_1 + a}, \tag{5.82}$$

which agrees with those results found in Piccolroaz and Mishuris (2013) and Morini et al. (2013a) when a component of a displacement field decouples

from all other components. Note here that the results differ from those in Piccolroaz and Mishuris (2013) due to the anisotropy of the material and they differ from that in Morini et al. (2013a) due to u_1 being decoupled here whereas in their work it was u_2 that separated from the rest of the solution. It is also important to note that, despite the similarity of the appearance of these results with these papers, the piezoelectric nature of the bimaterial still has an effect here contained in the material parameter H_{11}.

Integrating (5.82) gives the following expressions for the displacement jump along the crack

$$[\![u_1]\!](x_1) = \frac{2F_1H_{11}}{\pi}\operatorname{arctanh}\sqrt{-\frac{x_1}{a}}, \quad \text{for } -a < x_1 < 0, \tag{5.83}$$

$$[\![u_1]\!](x_1) = \frac{2F_1H_{11}}{\pi}\operatorname{arctanh}\sqrt{-\frac{a}{x_1}}, \quad \text{for } x_1 < -a. \tag{5.84}$$

We now proceed to invert the operator in equations (5.79) and (5.80) in the same manner. The resulting equations are therefore

$$N_{22}\frac{\partial[\![u_2]\!]^{(-)}}{\partial x_1} + N_{24}\frac{\partial[\![\phi]\!]^{(-)}}{\partial x_1} = \frac{F_2D}{\pi}\sqrt{-\frac{a}{x_1}}\frac{1}{x_1+a}, \tag{5.85}$$

$$N_{24}\frac{\partial[\![u_2]\!]^{(-)}}{\partial x_1} + N_{44}\frac{\partial[\![\phi]\!]^{(-)}}{\partial x_1} = 0. \tag{5.86}$$

Solving these equations and simplifying gives the following expressions

$$\frac{\partial[\![u_2]\!]^{(-)}}{\partial x_1} = -\frac{F_2H_{22}}{\pi}\sqrt{-\frac{a}{x_1}}\frac{1}{x_1+a}, \tag{5.87}$$

$$\frac{\partial[\![\phi]\!]^{(-)}}{\partial x_1} = \frac{F_2H_{24}}{\pi}\sqrt{-\frac{a}{x_1}}\frac{1}{x_1+a}. \tag{5.88}$$

Integrating these expressions gives the following expressions for the jump in displacement and potential over the crack

$$\begin{pmatrix}[\![u_2]\!]^{(-)}\\ [\![\phi]\!]^{(-)}\end{pmatrix} = \frac{2F_2}{\pi}\operatorname{arctanh}\sqrt{-\frac{x_1}{a}}\begin{pmatrix}H_{22}\\ -H_{24}\end{pmatrix}, \quad \text{for } -a < x_1 < 0, \tag{5.89}$$

$$\begin{pmatrix} [\![u_2]\!]^{(-)} \\ [\![\phi]\!]^{(-)} \end{pmatrix} = \frac{2F_2}{\pi} \operatorname{arctanh} \sqrt{-\frac{a}{x_1}} \begin{pmatrix} H_{22} \\ -H_{24} \end{pmatrix}, \quad \text{for } x_1 < -a. \tag{5.90}$$

Using equation (5.76) the following expressions, for use in finding expressions for the interfacial traction and electric displacement, are obtained

$$\begin{pmatrix} \sigma_{21} \\ \sigma_{22} \\ D_2 \end{pmatrix} = \frac{1}{D} \begin{pmatrix} N_{11} & 0 & 0 \\ 0 & N_{22} & N_{24} \\ 0 & N_{24} & N_{44} \end{pmatrix} \mathcal{S}^{(c)} \frac{\partial [\![\mathbf{u}]\!]^{(-)}}{\partial x_1}. \tag{5.91}$$

The decoupled traction component can now be found:

$$\sigma_{21}^{(+)}(x_1) = \frac{N_{11}}{D\pi} \int_{-\infty}^{0} \frac{1}{x_1 - \eta} \frac{\partial [\![u_1]\!]^{(-)}}{\partial \eta} \mathrm{d}\eta = \frac{F_1}{\pi} \sqrt{\frac{a}{x_1}} \frac{1}{x_1 + a}. \tag{5.92}$$

Once again the obtained result is identical to that obtained for a decoupled field in anisotropic bimaterials (Morini et al., 2013a), with the only difference here arising from the difference in direction of the decoupled field. Using the same method, the expressions for the coupled portion of the traction and electric displacement field are given as

$$\sigma_{22}(x_1)^{(+)} = \frac{F_2}{\pi} \sqrt{\frac{a}{x_1}} \frac{1}{x_1 + a}, \qquad D_2^{(+)}(x_1) = 0. \tag{5.93}$$

It is seen that the mechanical part of the solution behaves identically to that in an anisotropic bimaterial and there is no electrical displacement component along the interface for any bimaterial with the given conditions.

5.5.2 Poling direction parallel to the x_3-axis

Symmetric mechanical loading

The loading considered here consists of a point load acting in opposite directions on each of the crack faces at a distance a from the crack tip. Mathematically this system of forces is represented using the Dirac delta distribution.

The expressions for the symmetric and skew-symmetric parts of the extended loading are given by:

$$\langle \mathbf{p} \rangle(x_1) = \begin{pmatrix} -F\delta(x_1 + a) \\ 0 \end{pmatrix}, \quad [\![\mathbf{p}]\!](x_1) = 0. \tag{5.94}$$

Inserting these expressions into equation (5.72) gives the singular integral equation

$$\mathcal{S}^{(s)} \frac{\partial [\![\mathbf{u}]\!]^{(-)}}{\partial x_1} = F \begin{pmatrix} H_{33} \\ H_{34} \end{pmatrix} \delta(x_1 + a). \tag{5.95}$$

Inverting the operator $\mathcal{S}^{(s)}$ in a similar way to that seen previously gives:

$$\begin{aligned} \frac{\partial [\![\mathbf{u}]\!]^{(-)}}{\partial x_1} &= -\frac{F}{\pi} \begin{pmatrix} H_{33} \\ H_{34} \end{pmatrix} \int_{-\infty}^{0} \sqrt{\frac{\eta}{x_1}} \frac{\delta(\eta + a)}{x_1 - \eta} \mathrm{d}\eta \\ &= -\frac{F}{\pi} \sqrt{-\frac{a}{x_1}} \frac{1}{x_1 + a} \begin{pmatrix} H_{33} \\ H_{34} \end{pmatrix}. \end{aligned} \tag{5.96}$$

Integrating this equation gives the result

$$\begin{pmatrix} [\![u_3]\!] \\ [\![\phi]\!] \end{pmatrix} = \frac{2F}{\pi} \operatorname{arctanh} \sqrt{-\frac{x_1}{a}} \begin{pmatrix} H_{33} \\ H_{34} \end{pmatrix}, \quad \text{for } -a < x_1 < 0, \tag{5.97}$$

$$\begin{pmatrix} [\![u_3]\!] \\ [\![\phi]\!] \end{pmatrix} = \frac{2F}{\pi} \operatorname{arctanh} \sqrt{-\frac{a}{x_1}} \begin{pmatrix} H_{33} \\ H_{34} \end{pmatrix}, \quad \text{for } x_1 < -a. \tag{5.98}$$

Making use of equation (5.73) it is possible to obtain the expression for

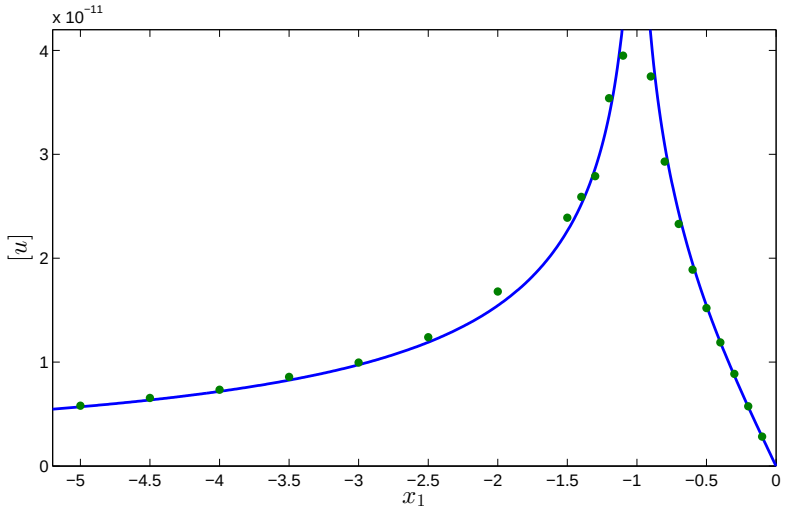

Figure 5.2: Displacement jump for symmetric mechanical loading. The green dots represent values obtained from COMSOL Multiphysics.

the extended traction vector, $\mathbf{t}$, along the interface:

$$\begin{aligned}\mathbf{t}^{(+)}(x_1) &= -\frac{\mathbf{H}^{-1}}{\pi}\int_{-\infty}^{0}\frac{1}{x_1-\eta}\frac{\partial[\![\mathbf{u}]\!]}{\partial\eta}\mathrm{d}\eta,\\ &= \frac{F}{\pi}\sqrt{\frac{a}{x_1}}\frac{1}{x_1+a}\mathbf{H}^{-1}\begin{pmatrix}H_{33}\\H_{34}\end{pmatrix},\\ &= \frac{F}{\pi}\sqrt{\frac{a}{x_1}}\frac{1}{x_1+a}\begin{pmatrix}1\\0\end{pmatrix}.\end{aligned} \tag{5.99}$$

It is now possible to use (5.99) to obtain expressions for the stress intensity factor, K_3, and the electric intensity factor, K_4:

$$\begin{pmatrix}K_3\\K_4\end{pmatrix} = \lim_{x_1\to 0}\sqrt{2\pi x_1}\begin{pmatrix}t_3(x_1)\\D_2(x_1)\end{pmatrix} = F\sqrt{\frac{2}{\pi a}}\begin{pmatrix}1\\0\end{pmatrix}. \tag{5.100}$$

Figures 5.2 and 5.3 show a comparison between the derived results and the equivalent results using finite element computations in COMSOL Multiphysics. The materials used above and below the crack were Barium Titanate

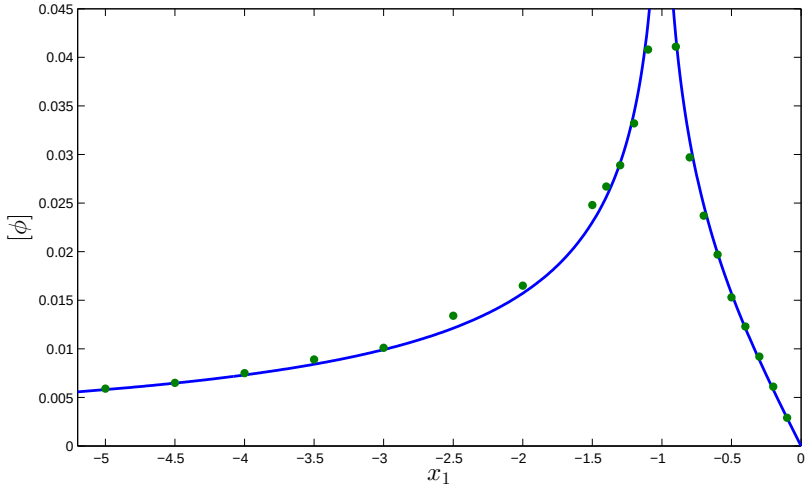

Figure 5.3: Electric potential jump for symmetric mechanical loading. The green dots represent values obtained from COMSOL Multiphysics.

and PZT respectively. The material parameters are quoted in Table 5.1, with those for Barium titanate obtained from Geis et al. (2004) and those for PZT taken from Liu and Hsia (2003).

Material	C_{44}(GPa)	e_{15}(CM^2)	ω_{11}(C^2/Nm^2)
Barium Titanate	44	11.4	9.87 x 10^{-9}
PZT	24.5	14.0	1.51 x 10^{-8}

Table 5.1: Material properties

Asymmetric mechanical loading

The second example considered has point loadings at a distance a acting on the upper and lower crack faces. However, for this asymmetric example it is said that they both act in the same direction. Mathematically this is

presented as:

$$\langle \mathbf{p} \rangle (x_1) = 0, \quad [\![\mathbf{p}]\!](x_1) = \begin{pmatrix} -2F\delta(x_1 + a) \\ 0 \end{pmatrix}. \tag{5.101}$$

The resultant singular integral equation is given by

$$\mathcal{S}^{(s)} \frac{\partial [\![\mathbf{u}]\!]^{(-)}}{\partial x_1} = -\frac{1}{2} \mathbf{W} [\![\mathbf{p}]\!]. \tag{5.102}$$

Using the same method as was used for the symmetric loading previously considered it is shown that

$$\begin{pmatrix} [\![u_3]\!] \\ [\![\phi]\!] \end{pmatrix} = \frac{2F}{\pi} \operatorname{arctanh} \sqrt{-\frac{x_1}{a}} \begin{pmatrix} \delta_3 H_{33} \\ \gamma H_{34} \end{pmatrix}, \quad \text{for } -a < x_1 < 0, \tag{5.103}$$

$$\begin{pmatrix} [\![u_3]\!] \\ [\![\phi]\!] \end{pmatrix} = \frac{2F}{\pi} \operatorname{arctanh} \sqrt{-\frac{a}{x_1}} \begin{pmatrix} \delta_3 H_{33} \\ \gamma H_{34} \end{pmatrix}, \quad \text{for } x_1 < -a. \tag{5.104}$$

Making use of equation (5.73) it is possible to obtain the expression for the extended traction vector, $\mathbf{t}$, along the interface:

$$\begin{aligned} \mathbf{t}^{(+)}(x_1) &= -\frac{\mathbf{H}^{-1}}{\pi} \int_{-\infty}^{0} \frac{1}{x_1 - \eta} \frac{\partial [\![\mathbf{u}]\!]}{\partial \eta} \mathrm{d}\eta, \\ &= \frac{F}{\pi} \sqrt{\frac{a}{x_1}} \frac{1}{x_1 + a} \mathbf{H}^{-1} \begin{pmatrix} \delta_3 H_{33} \\ \gamma H_{34} \end{pmatrix}, \\ &= \frac{F}{\pi} \sqrt{\frac{a}{x_1}} \frac{1}{x_1 + a} \frac{1}{H_{33} H_{44} - H_{34}^2} \begin{pmatrix} \delta_3 H_{33} H_{44} - \gamma H_{34}^2 \\ (\gamma - \delta_3) H_{33} H_{34} \end{pmatrix}. \end{aligned} \tag{5.105}$$

It is now possible to use (5.105) to obtain expressions for the stress intensity factor, K_3, and the electric intensity factor, K_4:

$$\begin{pmatrix} K_3 \\ K_4 \end{pmatrix} = \lim_{x_1 \to 0} \sqrt{2\pi x_1} \begin{pmatrix} t_3(x_1) \\ D_2(x_1) \end{pmatrix} = F \sqrt{\frac{2}{\pi a}} \frac{1}{H_{33} H_{44} - H_{34}^2} \begin{pmatrix} \delta_3 H_{33} H_{44} - \gamma H_{34}^2 \\ (\gamma - \delta_3) H_{33} H_{34} \end{pmatrix}. \tag{5.106}$$

Symmetric electrical loading

We consider a symmetric system of electrical point loads on the crack faces at a distance a behind the crack tip. Mathematically the Dirac delta distribution is once again used in order to represent the charges on the crack faces:

$$\langle \mathbf{p} \rangle (x_1) = \begin{pmatrix} 0 \\ -G\delta(x_1 + a) \end{pmatrix}, \quad [\![\mathbf{p}]\!] = \mathbf{0}. \tag{5.107}$$

Making use of equation (5.72) and the method previously used for mechanical loading gives

$$\frac{\partial [\![\mathbf{u}]\!]^{(-)}}{\partial x_1} = -\frac{G}{\pi} \sqrt{-\frac{a}{x_1}} \frac{1}{x_1 + a} \begin{pmatrix} H_{34} \\ H_{44} \end{pmatrix}. \tag{5.108}$$

When integrated, this gives

$$\begin{pmatrix} [\![u_3]\!] \\ [\![\phi]\!] \end{pmatrix} = \frac{2G}{\pi} \operatorname{arctanh} \sqrt{-\frac{x_1}{a}} \begin{pmatrix} H_{34} \\ H_{44} \end{pmatrix}, \quad \text{for } -a < x_1 < 0, \tag{5.109}$$

$$\begin{pmatrix} [\![u_3]\!] \\ [\![\phi]\!] \end{pmatrix} = \frac{2G}{\pi} \operatorname{arctanh} \sqrt{-\frac{a}{x_1}} \begin{pmatrix} H_{34} \\ H_{44} \end{pmatrix}, \quad \text{for } x_1 < -a. \tag{5.110}$$

The resulting expressions for the extended traction vector is therefore

$$\mathbf{t}^{(+)}(x_1) = -\frac{\mathbf{H}^{-1}}{\pi} \int_{-\infty}^{0} \frac{1}{x_1 - \eta} \frac{\partial [\![\mathbf{u}]\!]^{(-)}}{\partial \eta} \mathrm{d}\eta = \frac{G}{\pi} \sqrt{\frac{a}{x_1}} \frac{1}{x_1 + a} \begin{pmatrix} 0 \\ 1 \end{pmatrix}. \tag{5.111}$$

The stress intensity factors are then given by

$$\begin{pmatrix} K_3 \\ K_4 \end{pmatrix} = \lim_{x_1 \to 0} \sqrt{2\pi x_1}\, \mathbf{t}^{(+)}(x_1) = G\sqrt{\frac{2}{\pi a}} \begin{pmatrix} 0 \\ 1 \end{pmatrix}. \tag{5.112}$$

Asymmetric electrical loading

Here we consider electrical loading acting in the same direction on the top and bottom crack faces at a distance a behind the crack tip. This loading can be written as

$$\langle \mathbf{p} \rangle(x_1) - \mathbf{0}, \quad [\![\mathbf{p}]\!](x_1) = \begin{pmatrix} 0 \\ -2G\delta(x_1 + a) \end{pmatrix}. \tag{5.113}$$

The resulting fields obtained using equations (5.72) and (5.73) are:

$$\frac{\partial [\![\mathbf{u}]\!]^{(-)}}{\partial x_1} = -\frac{G}{\pi}\sqrt{-\frac{a}{x_1}}\frac{1}{x_1 + a}\begin{pmatrix} \gamma H_{34} \\ \delta_4 H_{44} \end{pmatrix}, \tag{5.114}$$

$$\begin{pmatrix} [\![u_3]\!] \\ [\![\phi]\!] \end{pmatrix} = \frac{2G}{\pi}\operatorname{arctanh}\sqrt{-\frac{x_1}{a}}\begin{pmatrix} \gamma H_{34} \\ \delta_4 H_{44} \end{pmatrix}, \quad \text{for } -a < x_1 < 0, \tag{5.115}$$

$$\begin{pmatrix} [\![u_3]\!] \\ [\![\phi]\!] \end{pmatrix} = \frac{2G}{\pi}\operatorname{arctanh}\sqrt{-\frac{a}{x_1}}\begin{pmatrix} \gamma H_{34} \\ \delta_4 H_{44} \end{pmatrix}, \quad \text{for } x_1 < -a. \tag{5.116}$$

$$\mathbf{t}^{(+)}(x_1) = \frac{G}{\pi}\sqrt{\frac{a}{x_1}}\frac{1}{(x_1 + a)(H_{33}H_{44} - H_{34}^2)}\begin{pmatrix} (\gamma - \delta_4)H_{34}H_{44} \\ \delta_4 H_{33}H_{44} - \gamma H_{34}^2 \end{pmatrix}. \tag{5.117}$$

The stress intensity factor and electric intensity factor obtained are therefore

$$\begin{pmatrix} K_3 \\ K_4 \end{pmatrix} = \lim_{x_1 \to 0}\sqrt{2\pi x_1}\mathbf{t}^{(+)}(x_1) = G\sqrt{\frac{2}{\pi a}}\frac{1}{H_{33}H_{44} - H_{34}^2}\begin{pmatrix} (\gamma - \delta_4)H_{34}H_{44} \\ \delta_4 H_{33}H_{44} - \gamma H_{34}^2 \end{pmatrix}. \tag{5.118}$$

Now that solutions have been found for the individual examples of symmetric and asymmetric loading for both mechanical and electrical loading it is possible to use these results if a combination of the loads was used. This ability to combine the solutions is caused by the linearity of the problem being considered.

5.6 Conclusions

A general approach for the derivation of the symmetric and skew-symmetric weight functions for plane interfacial cracks in anisotropic piezoelectric bimaterials has been developed. Further to this, explicit weight function matrices are obtained for an interfacial crack between two transversely isotropic piezoelectric materials, considering both the case where the poling direction of the two materials is perpendicular and coincident to the crack front. Since many poled ceramics that are commonly used in industrial applications possess transversely isotropic symmetry, this class of piezoelectric materials has a practical significance, and the derived weight functions can be used for computing the stress intensity factors corresponding to any arbitrary non-symmetric mechanical and electrostatic load acting on the crack faces.

Using symmetric and skew-symmetric weight functions we have derived integral equations relating the applied load on the crack faces to the resulting interfacial tractions and crack opening. The proposed method avoids the need of the use of Green's functions and therefore the consequent numerical procedures associated with such methods are not required (Gao and Wang, 2001). The integral identities have been derived under the plane strain and short circuit conditions for the cases when the material poling direction is either perpendicular or coincident to the crack front. Examples of the application of the integral equations when point forces and charges are applied to the crack faces have been given with expressions for both the extended interfacial tractions, crack opening and jump in potential over the crack faces given. For one of the examples given a comparison has been made between the analytic results obtained from the integral equations and similar com-

putations using finite element simulations in COMSOL Multiphysics. The results for both the crack opening displacement and difference in potential over the crack faces show good agreement between the analytical expressions we have derived and the finite element results.

Chapter 6

Conclusions

This thesis has considered a number of problems involving semi-infinite cracks along an interface in both anisotropic and piezoelectric bimaterials. The variety of conditions include material properties, crack propagation speed and the extent of imperfection of the bonded portion of the interface.

The first original problem seen involved a dynamic crack along a perfect interface in an anisotropic bimaterial. Making use of a steady-state formulation along with weight functions and the Betti identity we derived general integral expressions for the asymptotic coefficients of the in-plane traction and displacements at the crack tip. The method developed can be applied to a general asymmetric loading system applied to the crack faces. The examples considered show that the most energetically beneficial system is that with a symmetric load with an increase in the extent of load asymmetry and crack speed both leading to a rise in ERR. A sub-Rayleigh velocity at which one component of the stress intensity factor changes sign was also found for certain bimaterials. This velocity, which would result in a change in propagation behaviour, corresponds to the disappearance of the oscillatory effects

at the crack tip and therefore is not present for every bimaterial.

We then analysed a static crack with a thin layer of soft adhesive now bonding the two materials. This bonding agent was replaced by suitable imperfect interface transmission conditions: continuity of tractions but discontinuity of displacements. Singular integral equations relating the applied loading to the crack faces with the unknown interfacial tractions and crack displacement jump for both the in-plane and out-of-plane problems were found. These were solved numerically for both cases and the results obtained agree with the expected results from the literature, in particular the now bounded traction at the crack tip. For the out-of-plane example the results were also computed using finite element simulations in COMSOL and good agreement was seen. However, in order to compute the same results in COMSOL an unrealistically thick layer of adhesive was used in the model as the small mesh in a typical layer was computationally inefficient. Therefore the singular integral equations derived are both a viable and efficient way of computing the desired results.

The final problem considered was a perfect interface in a piezoelectric bimaterial. Making use of the extended Stroh formalism we found explicit expressions for the general weight functions for piezoelectric materials. Explicit expressions for weight functions for transversely isotropic bimaterials were also found. We also made use of these weight functions, along with the reciprocal identity, to derive singular integral equations relating both physical and electrical loadings to the mechanical and electrical fields. All of the results were derived for two different poling directions of the bimaterials. It was seen that the poling direction has a great impact on the results, in par-

ticular whether the electrical effects couple with the in-plane or out-of-plane fields. For the example where the electric fields are coupled with the out-of-plane displacements and tractions we once again performed simulations in COMSOL for the same problem which had good agreement with the results obtained from our integral formulations.

Future work

Although a number of problems have been seen in the thesis there are still a number of ways in which the field of research can be furthered. The simplest way to progress would be to consider different subclasses of anisotropic materials to those seen here. An example of this would be monoclinic materials which result in more complicated Stroh matrices as they only have one plane of symmetry.

It is also possible to extend the work on piezoelectric materials to involve an imperfect interface. Once this has been done it would be possible to use the transmission conditions of a thin metal layer along the interface to model piezoelectric actuators. It would then be possible to use the near-tip fields to see how the ends of electrodes are damaged as an actuator is used which could be used to predict and prevent failure.

Another field of wide interest involving fracture is hydrofracturing. In recent years hydrofracturing has become a more common technique of extracting natural oils and gases. The mathematical models involved in such problems are highly non-linear and usually require the use of complicated numerical algorithms to get efficient results.

Bibliography

Antipov, Y. A., Avila-Pozos, O., Kolaczkowski, S. T., Movchan, A. B., 2001. Mathematical model of delamination cracks on imperfect interfaces. Int. J. Solids Struct. 38(36-37), 6665–6697.

Atkinson, C., 1977. On stress singularities and interfaces in linear elastic fracture mechanics. Int. J. Fracture 13, 807–820.

Bassani, J. L., Qu, J., 1989. Finite crack on bimaterial and bicrystal interfaces. J. Mech. Phys. Solids 37, 435–453.

Benveniste, Y., 2006. A general interface model for a three-dimensional curved thin anisotropic interphase between two anisotropic media. J. Mech. Phys. Solids 54(4), 708–734.

Benveniste, Y., Miloh, T., 2001. Imperfect soft and stiff interfaces in two-dimensional elasticity. Mech. Materials 33, 309–323.

Bercial-Velez, J. P., Antipov, Y. A., Movchan, A. B., 2005. High-order asymptotics and perturbation problems for 3d interfacial cracks. J. Mech. Phys. Solids 53, 1128–1162.

Bower, A. F., 2009. Applied mechanics of solids, 1st Edition. CRC Press, Boca Raton, Florida.

Bueckner, H. F., 1970. A novel principle for the computation of stress intensity factors. Zeit. Angew. Math. Mech. 50, 529–546.

Bueckner, H. F., 1985. Weight functions and fundamental fields for the penny-shaped and the half plane crack in three-space. Int. J. Solids Struct. 23, 57–93.

Cherepanov, G. P., 1967. The propagation of cracks in continuous medium. Journal of Applied Mathematics and Mechanics 31(3), 503–512.

Cottrell, A. H., 1962. Theoretical aspects of radiation damage and brittle fracture in steel pressure vessels. Iron Steel Institute Special Report 69, 281–296.

Duduchava, R., 1979. Integral equations with fixed singularities. Teubner, Leipzig.

Eshelby, J. D., Read, W. T., Shockley, W., 1953. Anisotropic elasticity with applications to dislocation theory. Acta Metallurgica 1(3), 251–259.

Fett, T., Diegele, E., Munz, D., Rizzi, G., 1996. Weight functions for edge cracks in thin surface layers. Int. J. Fract. 81 (3), 205–215.

Fett, T., Munz, D., 1997. Stress intensity factors and weight functions. Computational Mechanics Publications, Southampton.

Gao, C.-F., Wang, M.-Z., 2001. Green's functions for an interfacial crack

between two dissimilar piezoelectric media. Int. J. Solids Struct. 38, 5323–5334.

Geis, W., Mishuris, G., Sandig, A., 2004. Asymptotic models for piezoelectric stack actuators with thin metal inclusions. Preprint 2004/001, Univeristy of Stuttgart, http://preprints.ians.uni-stuttgart.de.

Glinka, G., Shen, G., 1991. Universal features of weight functions for cracks in mode I. Eng. Frac. Mech. 40, 1135–1146.

Gohberg, I. C., Krein, M. G., 1960. Systems of integral equations on a half line with kernels depending on the difference of arguments (english translation). Amer. Math. Soc. Transl. 14, 217–287.

Griffith, A. A., 1920. The phenomenon of rupture and flow in solids. Philosophical Transactions of the Royal Society (London) 221, 163–198.

Hadjesfandiari, A. R., 2013. Size-dependent piezoelectricity. Int. J. Solids. Struct. 50, 2781–2791.

Hoenig, A., 1982. Near-tip behavior of a crack in a plane of anisotropic elastic body. Eng. Frac. Mech. 16(3), 393–403.

Hwu, C., 1993. Explicit solutions for collinear interface crack problems. Int. J. Solid Structures 30, 301–312.

Hwu, C., 2008. Some explicit expressions of extended stroh formalism for two-dimensional piezoelectric anisotropic elasticity. Int. J. Solids Struct. 45, 4460–4473.

Inglis, C. E., 1913. Stresses in a plate due to the presence of cracks and sharp corners. Transactions of the institute of naval architects 55, 219–241.

Irwin, G. R., 1957. Analysis of stresses and strains near the end of a crack traversing a plate. J. Appl. Mech 24, 361–364.

Itskov, M., Aksel, N., 2002. Elastic constants and their admissable values for incompressible and slightly compressible anisotropic materials. Acta Mechanica 157, 81–96.

Kanninen, M. F., Rybicki, E. F., Stonesifer, R. B., Broek, D., Rosenfiels, A. R., Marschall, C. W., Hahn, G. T., 1979. Elastic-plastic fracture mechanics for two dimensional stable crack growth and instability problems. Elastic-Plastic Fracture ASTM STP 668, 121–150.

Kassir, M. K., Sih, G. C., 1973. Application of papkovich-neuber potentials to a crack problem. Int. J. Solids Struct. 9, 643–654.

Kuo, C. M., Barnett, D. M., 1991. Stress singularities of interfacial cracks in bonded piezoelectric half-spaces. Modern Theory of Anisotropic Elasticity and Applications ed J J Wu et al. 33-50. Philadelphia: SIAM.

Lekhnitskii, S. G., 1963. Theory of Elasticity of an Anisotropic Body. MIR, Moscow.

Lenci, S., 2001. Analysis of a crack at a weak interface. Int. J. Fract. 108, 275–290.

Liu, M., Hsia, K. J., 2003. Interfacial cracks between piezoelectric and elastic materials under in-plane electric loading. J. Mech. Phys. Solids 51, 921–944.

Mishuris, G., 2001. Interface crack and nonideal interface concept (mode iii). Int. J. Fract. 107(3), 279–296.

Mishuris, G., Kuhn, G., 2001. Asymptotic behaviour of the elastic solution near the tip of a crack situated at a nonideal interface. Zeitschrift fur Angewandte Mathematik und Mechanik 81(12), 811–826.

Mishuris, G., Piccolroaz, A., Vellender, A., 2013. Boundary integral formulation for cracks at imperfect interfaces. Q. J. Mech. Appl. Math. 67 (3), 363–387.

Mishuris, G. S., 1997a. 2-d boundary value problems of thermoelasticity in a multi-wedge – multi-layered region. part 1. sweep method. Arch. Mech. 49(6), 1103–1134.

Mishuris, G. S., 1997b. 2-d boundary value problems of thermoelasticity in a multi-wedge – multi-layered region. part 2. systems of integral equations. Arch. Mech. 49(6), 1135–1165.

Morini, L., Piccolroaz, A., Mishuris, G., Radi, E., 2013a. Integral identities for a semi-infinite interfacial crack in anisotropic elastic bimaterials. Int. J. Solids Struct. 50, 1437–1448.

Morini, L., Radi, E., Movchan, A. B., Movchan, N. V., 2013b. Stroh formalism in analysis of skew-symmetric and symmetric weight functions for interfacial cracks. Math. Mech. Solids 18, 135–152.

Mott, N. F., 1948. Brittle fracture in mild steel plates. Engineering 165, 16–18.

Muskhelishvili, N. I., 1963. Some Basic Problems of the Mathematical Theory of Elasticity. Groningen: P.Noordhoff, Netherlands.

Obrezanova, O., Willis, J. R., Movchan, A. B., 2002a. Dynamic stability of a propagating crack. J. Mech. Phys. Solids 50, 2637–2668.

Obrezanova, O., Willis, J. R., Movchan, A. B., 2002b. Stability of an advancing crack to small perturbation of its path. J. Mech. Phys. Solids 50, 57–80.

Ou, Z. C., Wu, X., 2003. On the crack-tip stress singularity of interfacial cracks in transversely isotropic materials. Int. J. Solids Struct. 40, 7499–7511.

Pak, Y. E., 1990. Crack extension force in a piezoelectric material. J. Appl. Mech. 57, 647–653.

Pan, E., 2003. Some new three-dimensional greens functions in anisotropic piezoelectric bimaterials. Electron. J. Bound. Elem. 1, 236–269.

Pan, E., Yuan, F. G., 2000. Three-dimensional greens functions in anisotropic piezoelectric bimaterials. Int. J. Eng. Sci. 38, 1939–1960.

Parton, V. Z., 1976. Fracture mechanics of piezoelectric materials. Acta Astronautica 3, 671–683.

Piccolroaz, A., Mishuris, G., 2013. Integral identities for a semi-infinite interfacial crack in 2d and 3d elasticity. J. Elasticity 110, 117–140.

Piccolroaz, A., Mishuris, G., Movchan, A. B., 2007. Evaluation of the lazarus-

leblond constants in the asymptotic model for the interfacial wavy crack. J. Mech. Phys. Solids 55, 1575–1600.

Piccolroaz, A., Mishuris, G., Movchan, A. B., 2009. Symmetric and skew-symmetric weight functions in 2d perturbation models for semi-infinite interfacial cracks. J. Mech. Phys. Solids 57, 1657–1682.

Pryce, L., Morini, L., Mishuris, G., 2013. Weight function approach to study a crack propagating along a bimaterial interface under arbitrary loading in anisotropic solids. JoMMS 8, 479–500.

Pryce, L., Morini, L., Zagnetko, A., 2015. Interfacial fracture in piezoelectric bimaterials: Weight functions and singular integral formulation. http://arxiv.org/abs/1501.02114.

Pryce, L., Vellender, A., Zagnetko, A., 2014. Integral identities for an interfacial crack in an anisotropic bimaterial with an imperfect interface. http://arxiv.org/abs/1406.4431v3.

Qu, J., Bassani, J. L., 1989. Cracks on bimaterial interfaces. J. Mech. Phys. Solids 37, 417–433.

Rice, J. R., 1968. A path independent integral and the approximate analysis of strain concentrations by notches and cracks. Journal of Applied Mechanics 35, 379–386.

Rice, J. R., Sorenson, E. P., 1978. Continuing crack tip deformation and fracture for plane strain crack growth in elastic-plastic solids. J. Mech. Phys. Solids 26, 163–186.

Shih, C. F., de Lorenzi, H. G., Andrews, W. R., 1979. Studies on crack initiation and stable crack growth. Elastic-Plastic Fracture ASTM STP 668, 65–120.

Stroh, A. N., 1958. Dislocations and cracks in anisotropic elasticity. Phil. Mag. 7, 625–646.

Stroh, A. N., 1962. Steady state problems in anisotropic elasticity. Math. Phys 41, 77–103.

Suo, Z., 1990. Singularities, interfaces and cracks in dissimilar anisotropic media. Proc. R. Soc. Lond 427, 331–358.

Suo, Z., Kuo, C. M., Barnett, D. M., Willis, J. R., 1992. Fracture mechanics for piezoelectric ceramics. J. Mech. Phys. Solids 40, 739–765.

Ting, T. C. T., 1996. Anisotropic elasticity: theory and applications. Oxford University Press.

Vellender, A., Mishuris, G. S., 2012. Eigenfrequency correction of bloch-floquet waves in a thin periodic bi-material strip with cracks lying on perfect and imperfect interfaces. Wave Motion 49(2), 258–270.

Vellender, A., Mishuris, G. S., Movchan, A. B., 2011. Weight function in a bimaterial strip containing an interfacial crack and an imperfect interface. application to a bloch-floquet analysis in a thin inhomogeneous structure with cracks. Multiscale Model. Simul. 9(4), 1327–1349.

Vellender, A., Mishuris, G. S., Piccolroaz, A., 2013. Perturbation analysis for an imperfect interface crack problem using weight function techniques. Int. J. Solids Struct. 50(24), 4098–4107.

Wells, A. A., 1961. Unstable crack propagation in metals: Cleavage and fracture. Proceedings of the crack propagation symposium, Cranfield, 210–230.

Williams, M. L., 1959. The stresses around a fault or crack in dissimilar media. Bul. Seismol. Soc. Am. 49, 199–204.

Willis, J. R., 1971. Fracture mechanics of interfacial cracks. J. Mech. Phys. Solids 19, 353–368.

Willis, J. R., Movchan, A. B., 1995. Dynamic weight function for a moving crack. I. Mode I loading. J. Mech. Phys. Solids, 319–341.

Wu, X. R., Carlsson, A. J., 1991. Weight functions and stress intensity factor solutions. Pergamon Press, Oxford.

Yang, W., Suo, Z., Shih, C. F., 1991. Mechanics of dynamic debonding. Proc. Mathematical and Physical Sciences 433, 679–697.

Yu, H. H., Suo, Z., 2000. Intersonic crack growth on an interface. Proc. R. Soc. Lond 456, 223–246.

Zheng, X. J., Glinka, G., Dubey, R. N., 1996. Stress intensity factors and weight functions for a corner crack in a finite thickness plate. Eng. Frac. Mech. 54(1), 49–61.

Appendices

A1: Stroh matrices for orthotropic materials

In this appendix explicit expressions are given for the material matrices obtained through use of the Stroh formalism for orthotropic materials. For the static case (used in Chapter 4) expressions are given for both the in-plane and out-of-plane components as both are required. The expressions given for the dynamic material consider only the in-plane expressions as this is the case studied in Chapter 3.

Static

The results reported here are found in Morini et al. (2013b). The matrices **H** and **W** have the form

$$\mathbf{H} = \begin{pmatrix} H_{11} & -i\beta\sqrt{H_{11}H_{22}} & 0 \\ i\beta\sqrt{H_{11}H_{22}} & H_{22} & 0 \\ 0 & 0 & H_{33} \end{pmatrix}, \tag{6.1}$$

$$\mathbf{W} = \begin{pmatrix} \delta_1 H_{11} & i\gamma\sqrt{H_{11}H_{22}} & 0 \\ -i\gamma\sqrt{H_{11}H_{22}} & \delta_2 H_{22} & 0 \\ 0 & 0 & \delta_3 H_{33} \end{pmatrix}. \tag{6.2}$$

For orthotropic materials it is possible to obtain explicit expressions for the these matrices in terms of the components of the material compliance tensors.

The out-of-plane components are given by

$$H_{33} = \left[\sqrt{S_{44}S_{55}}\right]_I + \left[\sqrt{S_{44}S_{55}}\right]_{II}, \quad \delta_3 = \frac{\left[\sqrt{S_{44}S_{55}}\right]_I - \left[\sqrt{S_{44}S_{55}}\right]_{II}}{H_{33}}. \tag{6.3}$$

The in-plane components of $\mathbf{H}$ can be found in Morini et al. (2013b) and are given as

$$H_{11} = \left[2n\lambda^{1/4}\sqrt{S_{11}S_{22}}\right]_I + \left[2n\lambda^{1/4}\sqrt{S_{11}S_{22}}\right]_{II}, \tag{6.4}$$

$$H_{22} = \left[2n\lambda^{-1/4}\sqrt{S_{11}S_{22}}\right]_I + \left[2n\lambda^{-1/4}\sqrt{S_{11}S_{22}}\right]_{II}, \tag{6.5}$$

$$\beta = \frac{\left[S_{12} + \sqrt{S_{11}S_{22}}\right]_{II} - \left[S_{12} + \sqrt{S_{11}S_{22}}\right]_I}{\sqrt{H_{11}H_{22}}}, \tag{6.6}$$

where

$$\lambda = \frac{S_{11}}{S_{22}}, \quad n = \sqrt{(1+\rho)/2}, \quad \rho = \frac{2S_{12} + S_{66}}{2\sqrt{S_{11}S_{22}}}.$$

The in-plane components of $\mathbf{W}$ were also given in Morini et al. (2013b):

$$\delta_1 = \frac{\left[2n\lambda^{1/4}\sqrt{S_{11}S_{22}}\right]_I - \left[2n\lambda^{1/4}\sqrt{S_{11}S_{22}}\right]_{II}}{H_{11}}, \tag{6.7}$$

$$\delta_2 = \frac{\left[2n\lambda^{-1/4}\sqrt{S_{11}S_{22}}\right]_I - \left[2n\lambda^{-1/4}\sqrt{S_{11}S_{22}}\right]_{II}}{H_{22}}, \tag{6.8}$$

$$\gamma = \frac{\left[S_{12} + \sqrt{S_{11}S_{22}}\right]_I + \left[S_{12} + \sqrt{S_{11}S_{22}}\right]_{II}}{\sqrt{H_{11}H_{22}}}. \tag{6.9}$$

Dynamic

For orthotropic materials the matrices $\mathbf{Q}, \mathbf{R}$ and $\mathbf{T}$ are given by

$$\mathbf{Q} = \begin{pmatrix} C_{11} - \rho v^2 & 0 \\ 0 & C_{66} - \rho v^2 \end{pmatrix}, \mathbf{R} = \begin{pmatrix} 0 & C_{12} \\ C_{66} & 0 \end{pmatrix}, \mathbf{T} = \begin{pmatrix} C_{66} & 0 \\ 0 & C_{22} \end{pmatrix}. \tag{6.10}$$

Previously, expressions were found for the Stroh matrices for an orthotropic bimaterial with a crack propagating at a constant speed, v, in Yang et al. (1991), where the following parameters were defined

$$\kappa_{\gamma\beta} = \frac{C_{\gamma\beta}}{C_{66}}, \qquad \alpha_1 = \sqrt{1 - \frac{\rho v^2}{C_{11}}}, \qquad \alpha_2 = \sqrt{1 - \frac{\rho v^2}{C_{66}}},$$

$$\xi = \alpha_1\alpha_2\sqrt{\frac{\kappa_{11}}{\kappa_{22}}}, \text{ and } s = \frac{\alpha_2^2 + \kappa_{11}\kappa_{22}\alpha_1^2 - (1+\kappa_{12})^2}{2\alpha_1\alpha_2\sqrt{\kappa_{11}\kappa_{22}}}.$$

It is seen that the eigenvalues, with positive imaginary part, of equation (3.6) are given by

$$\mu_{1,2} = \begin{cases} i\sqrt{\xi}\left(\sqrt{\frac{s+1}{2}} \pm \sqrt{\frac{s-1}{2}}\right), & \text{for } s \geq 1 \\ \sqrt{\xi}\left(\pm\sqrt{\frac{1-s}{2}} + i\sqrt{\frac{1+s}{2}}\right), & \text{for } -1 < s < 1. \end{cases} \tag{6.11}$$

Using the same normalisation as used in Yang et al. (1991) the matrices $\mathbf{A}$ and $\mathbf{L}$ are given by

$$\mathbf{A} = \begin{pmatrix} 1 & -\lambda_2^{-1} \\ -\lambda_1 & 1 \end{pmatrix}, \tag{6.12}$$

$$\mathbf{L} = C_{66}\begin{pmatrix} \mu_1 - \lambda_1 & 1 - \mu_2\lambda_2^{-1} \\ \kappa_{12} - \kappa_{22}\mu_1\lambda_1 & \kappa_{22}\mu_2 - \kappa_{12}\lambda_2^{-1} \end{pmatrix}, \tag{6.13}$$

where

$$\lambda_i = \frac{\kappa_{11}\alpha_1^2 + \mu_i^2}{(1+\kappa_{12})\mu_i}.$$

Yang et al. (1991) then found an expression for the Hermitian matrix $\mathbf{B}$

$$\mathbf{B} = i\mathbf{A}\mathbf{L}^{-1} = \frac{1}{C_{66}R}\begin{pmatrix} \kappa_{22}\alpha_2^2\sqrt{2(1+s)/\xi} & i(\kappa_{22} - \kappa_{12}\alpha_2^2/\xi) \\ -i(\kappa_{22} - \kappa_{12}\alpha_2^2/\xi) & \kappa_{22}\sqrt{2\xi(1+s)} \end{pmatrix}, \tag{6.14}$$

where R is the generalized Rayleigh wave function given by

$$R = \kappa_{22}(\kappa_{22}\xi - 1 + \alpha_2^2) - \kappa_{12}^2\alpha_2^2/\xi.$$

The Rayleigh wave speed of a material can be found by solving the equation, $R = 0$.

The bimaterial matrix $\mathbf{H}$ has the form

$$\mathbf{H} = \begin{pmatrix} H_{11} & -i\beta\sqrt{H_{11}H_{22}} \\ i\beta\sqrt{H_{11}H_{22}} & H_{22} \end{pmatrix}. \tag{6.15}$$

From (6.14) it is seen that

$$H_{11} = \left[\frac{\kappa_{22}\alpha_2^2\sqrt{2(1+s)/\xi}}{C_{66}R}\right]_I + \left[\frac{\kappa_{22}\alpha_2^2\sqrt{2(1+s)/\xi}}{C_{66}R}\right]_{II},$$

$$H_{22} = \left[\frac{\kappa_{22}\sqrt{2\xi(1+s)}}{C_{66}R}\right]_I + \left[\frac{\kappa_{22}\sqrt{2\xi(1+s)}}{C_{66}R}\right]_{II},$$

$$\beta\sqrt{H_{11}H_{22}} = \left[\frac{\kappa_{22} - \kappa_{12}\alpha_2^2/\xi}{C_{66}R}\right]_{II} - \left[\frac{\kappa_{22} - \kappa_{12}\alpha_2^2/\xi}{C_{66}R}\right]_I.$$

In order to compute the weight functions the eigenvalues and eigenvectors of (3.8) are required. Using the representation (6.15) it is found that

$$\mathbf{w} = \begin{pmatrix} -\frac{i}{2} \\ \frac{1}{2}\sqrt{\frac{H_{11}}{H_{22}}} \end{pmatrix}, \qquad \epsilon = \frac{1}{2\pi}\ln\left(\frac{1-\beta}{1+\beta}\right). \tag{6.16}$$

Another key component for calculating the weight functions is the bimaterial matrix $\mathbf{W}$; using (6.14) it is seen that

$$\mathbf{W} = \sqrt{H_{11}H_{22}}\begin{pmatrix} \delta_1\sqrt{\frac{H_{11}}{H_{22}}} & i\gamma \\ -i\gamma & \delta_2\sqrt{\frac{H_{22}}{H_{11}}} \end{pmatrix}, \tag{6.17}$$

where

$$\gamma = \frac{\left[\frac{\kappa_{22}-\kappa_{12}\alpha_2^2/\xi}{C_{66}R}\right]_I + \left[\frac{\kappa_{22}-\kappa_{12}\alpha_2^2/\xi}{C_{66}R}\right]_{II}}{\sqrt{H_{11}H_{22}}},$$

$$\delta_1 = \frac{\left[\frac{\kappa_{22}\alpha_2^2\sqrt{2(1+s)/\xi}}{C_{66}R}\right]_I - \left[\frac{\kappa_{22}\alpha_2^2\sqrt{2(1+s)/\xi}}{C_{66}R}\right]_{II}}{H_{11}},$$

$$\delta_2 = \frac{\left[\frac{\kappa_{22}\sqrt{2\xi(1+s)}}{C_{66}R}\right]_I - \left[\frac{\kappa_{22}\sqrt{2\xi(1+s)}}{C_{66}R}\right]_{II}}{H_{22}}.$$

A2: Fourier transforms of matrices $\mathbf{A}(\xi), \mathbf{B}(\xi)$ and $\mathbf{C}(\xi)$

This appendix describes the method used to derive the inverse Fourier transforms for the in-plane problem seen in Chapter 4.

General procedure

The method outlined in Mishuris et al. (2013) is used in order to perform the Fourier inversion of the matrices $\mathbf{A}(\xi)$, $\mathbf{B}(\xi)$ and $\mathbf{C}(\xi)$ and is reported here. The denominator D defined in (4.63) is factorised in the following manner

$$D = d_2(|\xi| + \xi_1)(|\xi| + \xi_2), \tag{6.18}$$

where

$$\xi_{1,2} = \frac{d_1 \mp \sqrt{d_1^2 - 4d_2d_0}}{2d_2} > 0, \tag{6.19}$$

The typical term to invert is of the form

$$F(\xi) = \frac{F_R + F_R^\dagger|\xi|}{D} + i\frac{F_I \text{ sign}(\xi) + F_I^\dagger\xi}{D}, \tag{6.20}$$

The function F has the following property

$$F(-\xi) = \overline{F(\xi)}, \tag{6.21}$$

therefore, the Fourier inversion can be obtained as

$$\begin{aligned}\mathcal{F}^{-1}[F(\xi)] &= \frac{1}{\pi}\mathrm{Re}\int_0^\infty F(\xi)e^{-ix_1\xi}\mathrm{d}\xi \\ &= \frac{1}{\pi}\int_0^\infty \mathrm{Re}[F(\xi)]\cos(x_1\xi)\mathrm{d}\xi + \frac{1}{\pi}\int_0^\infty \mathrm{Im}[F(\xi)]\sin(x_1\xi)\mathrm{d}\xi,\end{aligned} \tag{6.22}$$

where for $\xi > 0$

$$\mathrm{Re}[F(\xi)] = \frac{F_R + F_R^\dagger \xi}{D} = \sum_{j=1}^{2} \frac{F_R^{(j)}}{d_2(\xi_2 - \xi_1)(\xi + \xi_j)}, \tag{6.23}$$

$$\mathrm{Im}[F(\xi)] = \frac{F_I + F_I^\dagger \xi}{D} = \sum_{j=1}^{2} \frac{F_I^{(j)}}{d_2(\xi_2 - \xi_1)(\xi + \xi_j)}, \tag{6.24}$$

and

$$F_{R,I}^{(1)} = F_{R,I} - F_{R,I}^\dagger \xi_1, \quad F_{R,I}^{(2)} = -F_{R,I} + F_{R,I}^\dagger \xi_2. \tag{6.25}$$

The following formulae can now be used

$$\begin{aligned}\int_0^\infty \mathrm{Re}[F(\xi)]\cos(x_1\xi)\mathrm{d}\xi &= \sum_{j=1}^{2} \frac{F_R^{(j)}}{d_2(\xi_2 - \xi_1)} \int_0^\infty \frac{\cos(x_1\xi)}{\xi + \xi_j}\mathrm{d}\xi \\ &= -\frac{1}{d_2(\xi_2 - \xi_1)} \sum_{j=1}^{2} F_R^{(j)} T_{\xi_j}(x_1),\end{aligned} \tag{6.26}$$

$$\begin{aligned}\int_0^\infty \mathrm{Im}[F(\xi)]\sin(x_1\xi)\mathrm{d}\xi &= \sum_{j=1}^{2} \frac{F_I^{(j)}}{d_2(\xi_2 - \xi_1)} \int_0^\infty \frac{\sin(x_1\xi)}{\xi + \xi_j}\mathrm{d}\xi \\ &= -\frac{1}{d_2(\xi_2 - \xi_1)} \sum_{j=1}^{2} F_I^{(j)} S_{\xi_j}(x),\end{aligned} \tag{6.27}$$

where functions $S_{\xi_j}(x)$ and $T_{\xi_j}(x)$ are defined as in (4.33) and (4.34), respectively.

Finally the Fourier inversion of the general term $F(\xi)$ as given as

$$\mathcal{F}^{-1}[F(\xi)] = -\frac{1}{\pi d_2(\xi_2 - \xi_1)} \left\{ \sum_{j=1}^{2} F_R^{(j)} T_{\xi_j}(x_1) + \sum_{j=1}^{2} F_I^{(j)} S_{\xi_j}(x_1) \right\}. \tag{6.28}$$

Fourier inversion of $\mathbf{A}(\xi)$.

For $\xi > 0$, $\mathbf{A}(\xi)$ can be written as

$$\begin{aligned}\mathbf{A}(\xi) &= \frac{1}{2D}(\mathbf{A}_R + \mathbf{A}_R^\dagger \xi) + \frac{i}{2D}(\mathbf{A}_I + \mathbf{A}_I^\dagger \xi) \\ &= \frac{1}{2d_2(\xi_2 - \xi_1)} \left\{ \sum_{j=1}^{2} \frac{1}{\xi + \xi_j} \mathbf{A}_R^{(j)} + i \sum_{j=1}^{2} \frac{1}{\xi + \xi_j} \mathbf{A}_I^{(j)} \right\}, \end{aligned} \tag{6.29}$$

where

$$\mathbf{A}_R = H_{11}H_{22} \begin{pmatrix} \delta_1 + \beta\gamma & 0 \\ 0 & \delta_2 + \beta\gamma \end{pmatrix}, \quad \mathbf{A}_R^\dagger = \begin{pmatrix} \delta_1 H_{11} K_{22} & -\delta_2 H_{22} K_{12} \\ -\delta_1 H_{11} K_{12} & \delta_2 H_{22} K_{11} \end{pmatrix},$$

$$\mathbf{A}_I = \sqrt{H_{11}H_{22}} \begin{pmatrix} 0 & -H_{22}(\delta_2\beta + \gamma) \\ H_{11}(\delta_1\beta + \gamma) & 0 \end{pmatrix},$$

$$\mathbf{A}_I^\dagger = \gamma\sqrt{H_{11}H_{22}} \begin{pmatrix} -K_{12} & -K_{22} \\ K_{11} & K_{12} \end{pmatrix},$$

$$\begin{aligned}\mathbf{A}_R^{(1)} &= \mathbf{A}_R - \mathbf{A}_R^\dagger \xi_1 \\ &= \begin{pmatrix} H_{11}(H_{22}(\delta_1 + \beta\gamma) - \delta_1 K_{22}\xi_1) & \delta_2 H_{22} K_{12} \xi_1 \\ \delta_1 H_{11} K_{12} \xi_1 & H_{22}(H_{11}(\delta_2 + \beta\gamma) - \delta_2 K_{11}\xi_1) \end{pmatrix}, \end{aligned}$$

$$\begin{aligned}\mathbf{A}_R^{(2)} &= -\mathbf{A}_R + \mathbf{A}_R^\dagger \xi_2 \\ &= \begin{pmatrix} -H_{11}(H_{22}(\delta_1 + \beta\gamma) - \delta_1 K_{22}\xi_2) & -\delta_2 H_{22} K_{12} \xi_2 \\ -\delta_1 H_{11} K_{12} \xi_2 & -H_{22}(H_{11}(\delta_2 + \beta\gamma) - \delta_2 K_{11}\xi_2) \end{pmatrix}, \end{aligned}$$

$$\begin{aligned}\mathbf{A}_I^{(1)} &= \mathbf{A}_I - \mathbf{A}_I^\dagger \xi_1 \\ &= \sqrt{H_{11}H_{22}} \begin{pmatrix} \gamma K_{12}\xi_1 & -H_{22}(\beta\delta_2 + \gamma) + \gamma K_{22}\xi_1 \\ H_{11}(\beta\delta_1 + \gamma) - \gamma K_{11}\xi_1 & -\gamma K_{12}\xi_1 \end{pmatrix}, \end{aligned}$$

$$\mathbf{A}_I^{(2)} = -\mathbf{A}_I + \mathbf{A}_I^{\dagger}\xi_2$$
$$= \sqrt{H_{11}H_{22}} \begin{pmatrix} -\gamma K_{12}\xi_2 & H_{22}(\beta\delta_2+\gamma) - \gamma K_{22}\xi_2 \\ -H_{11}(\beta\delta_1+\gamma) + \gamma K_{11}\xi_2 & \gamma K_{12}\xi_2 \end{pmatrix}.$$

The Fourier inverse of the matrix $\mathbf{A}(\xi)$ is given by

$$\mathcal{F}^{-1}[\mathbf{A}(\xi)] = -\frac{1}{2\pi d_2(\xi_2-\xi_1)} \left\{ \sum_{j=1}^{2} \mathbf{A}_R^{(j)} T_{\xi_j}(x_1) + \sum_{j=1}^{2} \mathbf{A}_I^{(j)} S_{\xi_j}(x_1) \right\}. \quad (6.30)$$

Fourier inversion of the matrix $\mathbf{B}(\xi)$.

For $\xi > 0$ $\mathbf{B}(\xi)$ can be written as

$$\mathbf{B}(\xi) = \frac{1}{D}(\mathbf{B}_R + \mathbf{B}_R^{\dagger}\xi) + \frac{i}{D}(\mathbf{B}_I + \mathbf{B}_I^{\dagger}\xi)$$
$$= \frac{1}{d_2(\xi_2-\xi_1)} \left\{ \sum_{j=1}^{2} \frac{1}{\xi+\xi_j} \mathbf{B}_R^{(j)} + i \sum_{j=1}^{2} \frac{1}{\xi+\xi_j} \mathbf{B}_I^{(j)} \right\}, \quad (6.31)$$

where

$$\mathbf{B}_R = \beta\sqrt{H_{11}H_{22}} \begin{pmatrix} 0 & -1 \\ 1 & 0 \end{pmatrix}, \quad \mathbf{B}_R^{\dagger} = \mathbf{0},$$

$$\mathbf{B}_I = \begin{pmatrix} -H_{22} & 0 \\ 0 & -H_{11} \end{pmatrix}, \quad \mathbf{B}_I^{\dagger} = \begin{pmatrix} -K_{22} & K_{12} \\ K_{12} & -K_{11} \end{pmatrix},$$

$$\mathbf{B}_R^{(1)} = \mathbf{B}_R - \mathbf{B}_R^{\dagger}\xi_1 = \beta\sqrt{H_{11}H_{22}} \begin{pmatrix} 0 & -1 \\ 1 & 0 \end{pmatrix},$$

$$\mathbf{B}_R^{(2)} = -\mathbf{B}_R + \mathbf{B}_R^{\dagger}\xi_2 = \beta\sqrt{H_{11}H_{22}} \begin{pmatrix} 0 & 1 \\ -1 & 0 \end{pmatrix},$$

$$\mathbf{B}_I^{(1)} = \mathbf{B}_I - \mathbf{B}_I^{\dagger}\xi_1 = \begin{pmatrix} -H_{22} + K_{22}\xi_1 & -K_{12}\xi_1 \\ -K_{12}\xi_1 & -H_{11} + K_{11}\xi_1 \end{pmatrix},$$

$$\mathbf{B}_I^{(2)} = -\mathbf{B}_I + \mathbf{B}_I^{\dagger}\xi_2 = \begin{pmatrix} H_{22} - K_{22}\xi_2 & K_{12}\xi_2 \\ K_{12}\xi_2 & H_{11} - K_{11}\xi_2 \end{pmatrix}.$$

The Fourier inverse of the matrix $\mathbf{B}(\xi)$ is then

$$\mathcal{F}^{-1}[\mathbf{B}(\xi)] = -\frac{1}{\pi d_2(\xi_2-\xi_1)}\left\{\sum_{j=1}^{2}\mathbf{B}_R^{(j)}T_{\xi_j}(x_1)+\sum_{j=1}^{2}\mathbf{B}_I^{(j)}S_{\xi_j}(x_1)\right\}. \quad (6.32)$$

Fourier inversion of the matrix $\mathbf{C}(\xi)$.

For $\xi > 0$ $\mathbf{C}(\xi)$ can be written as

$$\begin{aligned}\mathbf{C}(\xi) &= \frac{1}{D}(\mathbf{C}_R+\mathbf{C}_R^{\dagger}\xi)+\frac{i}{D}(\mathbf{C}_I+\mathbf{C}_I^{\dagger}\xi)\\ &= \frac{1}{d_2(\xi_2-\xi_1)}\left\{\sum_{j=1}^{2}\frac{1}{\xi+\xi_j}\mathbf{C}_R^{(j)}+i\sum_{j=1}^{2}\frac{1}{\xi+\xi_j}\mathbf{C}_I^{(j)}\right\}, \quad (6.33)\end{aligned}$$

where

$$\mathbf{C}_R = \begin{pmatrix} H_{11}H_{22}(1-\beta^2) & 0\\ 0 & H_{11}H_{22}(1-\beta^2)\end{pmatrix}, \quad \mathbf{C}_R^{\dagger} = \begin{pmatrix} H_{11}K_{22} & -H_{22}K_{12}\\ -H_{11}K_{12} & H_{22}K_{11}\end{pmatrix},$$

$$\mathbf{C}_I = \mathbf{0}, \quad \mathbf{C}_I^{\dagger} = \beta\sqrt{H_{11}H_{22}}\begin{pmatrix} K_{12} & K_{22}\\ -K_{11} & -K_{12}\end{pmatrix},$$

$$\begin{aligned}\mathbf{C}_R^{(1)} &= \mathbf{C}_R-\mathbf{C}_R^{\dagger}\xi_1\\ &= \begin{pmatrix} H_{11}(H_{22}(1-\beta^2)-K_{22}\xi_1) & H_{22}K_{12}\xi_1\\ H_{11}K_{12}\xi_1 & H_{22}(H_{11}(1-\beta^2)-K_{11}\xi_1)\end{pmatrix},\end{aligned}$$

$$\begin{aligned}\mathbf{C}_R^{(2)} &= -\mathbf{C}_R+\mathbf{C}_R^{\dagger}\xi_2\\ &= \begin{pmatrix} -H_{11}(H_{22}(1-\beta^2)-K_{22}\xi_2) & -H_{22}K_{12}\xi_2\\ -H_{11}K_{12}\xi_2 & -H_{22}(H_{11}(1-\beta^2)-K_{11}\xi_2)\end{pmatrix},\end{aligned}$$

$$\mathbf{C}_I^{(1)} = \mathbf{C}_I-\mathbf{C}_I^{\dagger}\xi_1 = \beta\sqrt{H_{11}H_{22}}\xi_1\begin{pmatrix} -K_{12} & -K_{22}\\ K_{11} & K_{12}\end{pmatrix},$$

$$\mathbf{C}_I^{(2)} = -\mathbf{C}_I + \mathbf{C}_I^{\dagger}\xi_2 = -\beta\sqrt{H_{11}H_{22}}\xi_2 \begin{pmatrix} -K_{12} & -K_{22} \\ K_{11} & K_{12} \end{pmatrix}.$$

The Fourier inverse of the matrix $\mathbf{C}(\xi)$ is then

$$\mathcal{F}^{-1}[\mathbf{C}(\xi)] = -\frac{1}{\pi d_2(\xi_2 - \xi_1)} \left\{ \sum_{j=1}^{2} \mathbf{C}_R^{(j)} T_{\xi_j}(x_1) + \sum_{j=1}^{2} \mathbf{C}_I^{(j)} S_{\xi_j}(x_1) \right\}. \quad (6.34)$$

A3: Extended Stroh matrices for poling direction parallel to the x_2-axis

Full analytic expressions are given for the matrices obtained through use of the extended Stroh matrices for a transversely isotropic material with poling direction parallel to the x_2-axis. In such a case the general form of the matrix $\mathbf{B} = i\mathbf{A}\mathbf{L}^{-1}$ is

$$\mathbf{B} = \begin{pmatrix} B_{11} & iB_{12} & iB_{14} \\ -iB_{12} & B_{22} & B_{24} \\ -iB_{14} & B_{24} & B_{44} \end{pmatrix}. \quad (6.35)$$

The expressions for these components were derived in Hwu (2008).

The following components of the compliance tensor: $\mathbf{S}$, piezoelectric

strain/voltage tensor: $\mathbf{g}$, and dielectric non-permittivity: β, are introduced:

$$\begin{aligned}
\hat{S'}_{11} &= \frac{C_{22}}{C_{11}C_{22} - C_{12}^2} - \frac{(e_{21}C_{11} - e_{22}C_{12})^2}{C^*[C_{11}C_{22} - C_{12}^2]}, \\
\hat{S'}_{12} &= -\frac{e_{21}e_{22}[C_{11}^2 - C_{12}^2]}{C^*[C_{11}C_{22} - C_{12}^2]} + \frac{\omega_{22}C_{12}}{C^*}, \\
\hat{S'}_{22} &= \frac{e_{21}^2[C_{11}^2 - C_{12}^2]}{C^*[C_{11}C_{22} - C_{12}^2]} + \frac{\omega_{22}C_{11}}{C^*}, \\
\hat{S'}_{66} &= \frac{\omega_{11}}{e_{16}^2 + \omega_{11}C_{44}}, \\
\hat{g'}_{21} &= \frac{e_{21}C_{11} - e_{22}C_{12}}{C^*}, \\
\hat{g'}_{22} &= \frac{e_{22}C_{11} - e_{21}C_{12}}{C^*}, \\
\hat{g'}_{16} &= \frac{e_{16}}{e_{16}^2 + \omega_{11}C_{44}}, \\
\hat{\beta'}_{11} &= \frac{C_{44}}{e_{16}^2 + \omega_{11}C_{44}}, \\
\hat{\beta'}_{22} &= \frac{C_{11}C_{22} - C_{12}^2}{C^*},
\end{aligned}$$

where

$$C^* = (e_{21}^2 + e_{22}^2)C_{11} - 2e_{21}e_{22}C_{12} + \omega_{22}[C_{11}C_{22} - C_{12}^2].$$

Through using the Lekhnitskii formalism, extended to piezoelectric materials, Hwu (2008) found that the eigenvalues, μ, are found through the equation

$$l_4\rho_2 - m_3^2 = 0, \tag{6.36}$$

where l_4, ρ_2 and m_3 are functions of μ and are given by

$$l_4 = \hat{S'}_{11}\mu^4 + (2\hat{S'}_{12} + \hat{S'}_{66})\mu^2 + \hat{S'}_{22}, \quad m_3 = -(\hat{g'}_{21} + \hat{g'}_{16})\mu^2 - \hat{g'}_{22},$$

$$\rho_2 = -(\hat{\beta'}_{11}\mu^2 + \hat{\beta'}_{22}). \tag{6.37}$$

This sextic equation must be solved numerically but is easily shown to have

roots of the form

$$\mu_2 = \alpha_2 + i\beta_2, \quad \mu_3 = -\alpha_2 + i\beta_2, \quad \mu_4 = i\beta_4. \tag{6.38}$$

With the eigenvalues known, Hwu (2008) proceeded to find explicit expressions for the components of **B**. It was shown that

$$\begin{aligned}
B_{11} &= 2\hat{S'}_{11}\mathrm{Im}\{\mu_2^2\eta_2^\star + (\mu_4^2\eta_2 - \mu_2^2\eta_4)\}/\lambda, \\
B_{22} &= 2\mathrm{Im}\{[\gamma_2\mu_2^\star\mu_4\eta_4 + (\gamma_2\mu_4^2 - \gamma_4\mu_2^2)\eta_2^\star]/\mu_2\mu_4\}/\lambda, \\
B_{44} &= -2\hat{\beta'}_{11}\mathrm{Im}\{\mu_2\mu_2^\star\eta_2 + \mu_2\mu_4(\eta_2 - \eta_4)\}/\lambda, \\
B_{24} &= 2\hat{\beta'}_{11}\mathrm{Im}\{\mu_2\mu_2^\star\eta_2\eta_4 + \mu_2\mu_4\eta_2^\star(\eta_2 - \eta_4)\}/\lambda, \\
B_{12} &= \hat{S'}_{12} + 2\mathrm{Re}\{[\gamma_2\mu_4\eta_2 + (\gamma_4\mu_2\eta_2 - \gamma_2\mu_4\eta_4)]/\mu_2\mu_4\}/\lambda, \\
B_{14} &= -\hat{g'}_{16} + 2\hat{\beta'}_{11}\mathrm{Re}\{\mu_2\eta_2\bar{\eta_2} - \eta_2\eta_4(\mu_2 - \mu_4)\}/\lambda,
\end{aligned}$$

where

$$\lambda = 2\mathrm{Re}\{\mu_2^\star\eta_2 + (\mu_4\eta_2 - \mu_2\eta_4)\},$$

$$\gamma_k = \hat{S'}_{22} + \hat{g'}_{22}\eta_k, \quad \eta_k = \frac{l_4(\mu_k)}{m_3(\mu_k)}, \quad \text{for k=2,4.}$$

A4: Explicit expressions for matrices M and N

In this appendix explicit expressions for the matrices **M** and **N** are quoted. They have the form

$$\mathbf{M} = \frac{1}{2D}\left(\mathbf{M'} + i\mathrm{sign}(\xi)\mathbf{M''}\right), \tag{6.39}$$

$$\mathbf{N} = \frac{|\xi|}{D}\left(\mathbf{N'} + i\mathrm{sign}(\xi)\mathbf{N''}\right), \tag{6.40}$$

where

$$D = H_{14}^2 H_{22} + H_{12}^2 H_{44} + H_{24}^2 H_{11} - H_{11}H_{22}H_{44} - 2H_{14}H_{12}H_{24}. \qquad (6.41)$$

The matrices $\mathbf{M}', \mathbf{M}'', \mathbf{N}'$ and $\mathbf{N}''$ have the form

$$\mathbf{M}' = \begin{pmatrix} M_{11} & 0 & 0 \\ 0 & M_{22} & M_{24} \\ 0 & M_{42} & M_{44} \end{pmatrix}, \qquad \mathbf{M}'' = \begin{pmatrix} 0 & M_{12} & M_{14} \\ M_{21} & 0 & 0 \\ M_{41} & 0 & 0 \end{pmatrix}, \qquad (6.42)$$

$$\mathbf{N}' = \begin{pmatrix} N_{11} & 0 & 0 \\ 0 & N_{22} & N_{24} \\ 0 & N_{24} & N_{44} \end{pmatrix}, \qquad \mathbf{N}'' = \begin{pmatrix} 0 & N_{12} & N_{14} \\ -N_{12} & 0 & 0 \\ -N_{14} & 0 & 0 \end{pmatrix}, \qquad (6.43)$$

where

$$M_{11} = W_{11}(H_{24}^2 - H_{22}H_{44}) + W_{12}(H_{12}H_{44} - H_{14}H_{24}) - W_{14}(H_{12}H_{24} - H_{14}H_{22}),$$

$$M_{22} = W_{12}(H_{12}H_{44} - H_{14}H_{24}) - W_{22}(H_{11}H_{44} - H_{14}^2) - W_{24}(H_{14}H_{12} - H_{11}H_{24}),$$

$$M_{44} = W_{14}(H_{14}H_{22} - H_{12}H_{24}) - W_{24}(H_{14}H_{12} - H_{11}H_{24}) - W_{44}(H_{11}H_{22} - H_{12}^2),$$

$$M_{24} = W_{14}(H_{14}H_{24} - H_{12}H_{44}) + W_{24}(H_{11}H_{44} - H_{14}^2) + W_{44}(H_{14}H_{12} - H_{11}H_{24}),$$

$$M_{42} = W_{12}(H_{12}H_{24} - H_{14}H_{22}) + W_{22}(H_{14}H_{12} - H_{11}H_{24}) + W_{24}(H_{11}H_{22} - H_{12}^2),$$

$$M_{12} = W_{12}(H_{22}H_{44} - H_{24}^2) - W_{22}(H_{12}H_{44} - H_{14}H_{24}) + W_{24}(H_{12}H_{24} - H_{14}H_{22}),$$

$$M_{14} = W_{14}(H_{24}^2 - H_{22}H_{44}) + W_{24}(H_{12}H_{44} - H_{14}H_{24}) - W_{44}(H_{12}H_{24} - H_{14}H_{22}),$$

$$M_{21} = W_{11}(H_{12}H_{44} - H_{14}H_{24}) - W_{12}(H_{11}H_{44} - H_{14}^2) - W_{14}(H_{14}H_{12} - H_{11}H_{24}),$$

$$M_{41} = W_{11}(H_{12}H_{24} - H_{14}H_{22}) + W_{12}(H_{14}H_{12} - H_{11}H_{24}) + W_{14}(H_{11}H_{22} - H_{12}^2),$$

$$N_{11} = H_{22}H_{44} - H_{24}^2, \quad N_{22} = H_{11}H_{44} - H_{14}^2,$$

$$N_{44} = H_{11}H_{22} - H_{12}^2, \quad N_{24} = H_{11}H_{24} - H_{14}H_{12},$$

$$N_{12} = H_{12}H_{44} - H_{14}H_{24}, \quad N_{14} = H_{12}H_{24} - H_{14}H_{22}.$$